Fluorescent Detection of Homologous Recombination Reveals the Impact of Genetic, Physiological, and Environmental Factors on Genomic Stability

by

Michelle R. Sukup Jackson

B.S. Biomedical Engineering
The University of Iowa, 2006

M.S. Biomedical Engineering
The University of Iowa, 2007

SUBMITTED TO THE DEPARTMENT OF BIOLOGICAL ENGINEERING IN PARTIAL FULFILLMENT OF THE REQUIREMENTS FOR THE DEGREE OF

DOCTOR OF PHILOSOPHY IN BIOLOGICAL ENGINEERING
at the
MASSACHUSETTS INSTITUTE OF TECHNOLOGY

JUNE, 2007
[June 2013]

Signature of Author: _____
Michelle R. Sukup Jackson
Department of Biological Engineering
May 24, 2013

Certified By: _____
Dr. Bevin P. Engelward
Associate Professor of Biological Engineering
Thesis Supervisor

Accepted By: _____
Dr. Forest White
Chair, Graduate Program Committee
Associate Professor of Biological Engineering

This doctoral thesis has been examined by a committee of the Department of Biological Engineering as follows:

Professor Leona D. Samson: _____
Chairman

Professor Bevin P. Engelward: _____
Thesis Supervisor

Professor John M. Essigmann: _____

This work is dedicated to

my dear partner, John;
my loving parents, Michael and Peggy;
my encouraging siblings, Marie and Justin;
and treasured friends near and far.

Your support and encouragement made this accomplishment a reality.

Preface

This work was accomplished through collaboration with many talented individuals in the laboratory of Dr. Bevin P. Engelward at MIT and beyond. I am extremely grateful to all those who have contributed to this project.

Chapter II will be submitted as a manuscript pending data collection for the effect of KU and ERCC1 on DNA damage induced recombination in the laboratory of Dr. Laura J Niedernhofer at The Scripps Research Institute. Dr. Niedernhofer, Dr. Engelward, Dr. Dominika Wiktor-Brown, and the author initiated the experiments. Breeding of knockout mice was performed in Dr. Niedernhofer's laboratory, and data were collected and analyzed by the author with initial training from Dr. Wiktor-Brown and Dr. Werner Olipitz. The author contributed all other work.

At the time of writing, Chapter III has been submitted for publication. The pROSA26PA and pBigT plasmids were generous gifts from Dr. P. Soriano. Original development of the raDR-GFP plasmid was by Dr. Tetsuya Matsuguchi, and the original targeted ES cells were characterized by Dr. Vidya Jonnalagadda. Electroporation and embryo manipulation were performed by Dr. Aurora Burds Conner at the Mouse ES cell and Transgenic Facility of the Koch Institute for Integrative Cancer Research. Dr. Dushan N. Wadduwage, Vijay R. Singh, Dr. Jagath C Rajapakse, and Dr. Peter So of the BioSystems and Micromechanics Inter-Disciplinary Research Programme, SMART, wrote

software for automatic counting of fluorescent foci that Dr. Orsolya Kiraly and the author assisted in validating. This software was used to count foci in the pancreas and liver of all data sets of the raDR-GFP samples except the aging cohorts. Dr. Kiraly developed the protocol and collected data for exposure of FYDR mice to T3 and MNU. Dr. Laura Collier at The University of Wisconsin generously provided positive control raDR-GFP mice. The author collected data for frequency of raDR-GFP recombinant cells and the number of fluorescent foci with technical support from Elizabeth A. Rowland, Danielle N. Chow, Jennifer E. Kay, and Kelly E. Winther. The author contributed all other work.

Chapter IV, while unpublished at the time of writing, represents the combined efforts of several people. Dr. Susan E. Erdman, Dr. Engelward, Jennifer E. Kay, and the author contributed to the inception of the project. Dr. Erdman and Dr. James G. Fox generously provided original Rag2 and IL10 deficient mice that the author used to establish the experimental lines. Dr. Amy Yu of Dr. Leona D. Samson's laboratory at MIT provided support in DSS dosing and tissue harvest. Under the direction of Dr. Erdman, Tatiana Levkovich and Jessica Lakritz of the Division of Comparative Medicine provided technical support in *H. hepaticus* infections. Data collection and analysis of *H. hepaticus* infected mice was done in collaboration with Jennifer Kay. Under the direction of Dr. Fox, Christian Kaufman and Lenzie Cheaney of the Division of Comparative Medicine provided technical support in *H. trogontum* infection and harvest. The author contributed all other work with technical support from Elizabeth A. Rowland and Danielle N. Chow.

This work was primarily supported by National Institutes of Health grant P01-CA026731 (to BPE). Partial support was provided by NIH grants 2-R01-CA079827-05A1 and R33-CA112151-01A2 (to BPE) and from the Kimmel Foundation (to LSC). The author was supported, in part, by the National Institute of Environmental Health Sciences (NIEHS) Toxicology Training Grant (T32-ES007020), by the Medtronic Foundation Fellowship, by the Robert A. Brown Fellowship, by the P.E.O. Presidential Fellowship, and by the National Science Foundation Graduate Research Fellowship. The Koch Institute Core facilities are supported by NCI CCSG P30-CA14051 and The Center for Environmental Health Sciences at MIT is supported by NIEHS P30-ES002109.

Acknowledgements

With sincerity and admiration I thank my advisor, Dr. Bevin Engelward, for her guidance and support while helping me mature scientifically, professionally, and personally. Her enthusiasm for discovery is inspiring. She encourages her students to think globally while staying grounded. It is with deep gratitude that I thank my thesis committee members, Dr. Leona Samson and Dr. John Essigmann for their many insights and guidance through my graduate work. As my committee chair and leader in the field, Professor Samson shared her expertise and wisdom by suggesting avenues for further investigation. Her high standards and scientific rigor encouraged me to grow further as a scientist. Professor Essigmann provided invaluable mechanistic understanding of the various DNA repair processes and his ability to bring talented people together from around the globe is admirable.

I am also grateful for the Department of Biological Engineering for giving me the opportunity to pursue cutting edge research with incredibly talented students and faculty. In addition to the incredible insights of my professors, the assistance and encouragement of my fellow students and researchers were integral in completion of my graduate work. I am also thankful for the fruitful collaborations with others in the Biological Engineering Department and Department of Comparative Medicine, especially those among the Engelward, Wogan, Essigmann, Fox, Samson, and Erdman research

groups, that enable first-rate science and learning opportunities. Many thanks to the staff of the MIT Flow Cytometry Core Facility and the MIT Department of Comparative Medicine, especially Glenn Paradis, Tatiana Levkovich, Jessica Lakritz, and Dr. Susan Erdman. I also want to recognize the contributions of the numerous people behind the scenes that enable animal research to continue on our campus.

I thank the members of the Engelward laboratory, Dr. David Wood, Dr. James Mutamba, Dr. David Weingeist, Jing Ge, Dwight Chambers, Marcus Parrish, Jenny Kay, Ian Tay, and Kathy Reposa, for contributing to a congenial and collaborative environment that engenders good science and enabled my personal and professional growth. I am particularly grateful to Dr. Werner Olipitz, Dr. Dominika Wiktor-Brown, and Dr. Orsolya Kiraly for their instruction and guidance, especially early in my graduate work. The willing help and lively discussions of my labmates contribute to the companionable environment that invites helpful questioning and critiques of each other's work. I would also like to thank the members of the Engelward Laboratory that came before us whose legacy is integral to the continued success of our work.

I am particularly thankful for the talented undergraduates that I have had the pleasure of working with. The insightful and careful work of Kelly Winther, Elizabeth Rowland, and Danielle Chow during countless hours of sample processing and flow cytometry directly contributed to the success of this work. Working with them helped me grow as a member and leader of a team and I am incredibly thankful for their

patience. Their enthusiasm for learning new techniques and biology helped me retain my enthusiasm for the scientific process.

I am eternally grateful for my professional and personal mentors, Dr. Gina Schatteman, Rev. Janie Donohue, and Rev. Karie Jo Verhulst, whose counsels have been invaluable. Most of all, I am especially thankful for my loving and supportive family. I am forever grateful to my parents for instilling in me the value of hard work, the thirst for knowledge, and the independence to strike out on my own. Their unconditional love and support has given me the confidence to try, the strength to fail, and the humility to succeed. To my siblings, Justin and Marie, thank you for keeping me grounded while encouraging me through the tough times. I am also grateful for the friends who have been my second family throughout my education. Lastly, I am exceptionally thankful for the unwavering support of my partner, John, for his love, encouragement, and humor through many late nights and working weekends. Together, we will go far.

Use and Development of Recombomice to Visualize the Effects of Endogenous and Exogenous Factors on DNA Repair *In Vivo*

by

Michelle R. Sukup Jackson

Submitted to the Department of Biological Engineering
on May 24, 2013 in partial fulfillment
of the requirements for the
Degree of Doctor of Philosophy

Abstract

Unless repaired correctly, DNA double strand breaks (DSBs) can cause the loss of millions of base pairs of information and can induce cellular toxicity. DSBs are repaired via mitotic homologous recombination (HR), non-homologous end-joining (NHEJ) or microhomology-mediated end-joining (MMEJ).

Here we use the Fluorescent Yellow Direct Repeat (FYDR) mouse to examine these pathways. Specifically, we crossed FYDR mice with mice lacking an essential NHEJ protein. Consistent with *in vitro* studies, we observed an increase in HR in the NHEJ deficient mice, indicating a shift from one pathway to another. Additionally, FYDR mice deficient in ERCC1, a protein involved in several pathways including nucleotide excision repair and MMEJ, showed an increase in HR. We describe a possible model for this observation.

HR is presumed to be largely limited to replicating cells; however, little is known about differences in HR rates between tissues. Thus, we engineered the Rosa26 Direct Repeat-GFP (raDR-GFP) mouse that enables study of HR in many tissues in response to endogenous and exogenous factors. The raDR-GFP mouse harbors two truncated EGFP genes integrated at the *ROSA26* locus. HR at the locus yields a full-length EGFP gene and a fluorescent cell. In adult raDR-GFP mice, differences in frequency of recombinant cells among tissues of challenged and unchallenged mice demonstrate the utility of raDR-GFP mice in measuring exposure-induced HR and the importance of multi-tissue studies. We also observed the progressive accumulation of recombinant cells in the pancreas, liver, and colon with age. These data are consistent with the finding that cancer is an age-related disease requiring time to accumulate tumorigenic mutations.

To test the hypothesis that chronic inflammation promotes the induction of DSBs, we bred raDR-GFP mice deficient in an anti-inflammatory cytokine. These mice showed an increase in spontaneous HR in the pancreas. Interestingly, 10 week-infection of *RAG2*$^{-/-}$ *raDR-GFP* mice with *H. hepaticus*, and longer-term 20-week infection with *H. trogontum* did not have the same effect on HR in the pancreas, liver, or colon. Further studies of large-scale sequence rearrangements, point mutations, and small deletions in multiple tissues in response to environmentally-induced inflammation are planned.

Thesis Supervisor: Bevin P. Engelward
Title: Associate Professor of Biological Engineering

Preface 4

Acknowledgements 7

Abstract 10

Table of Contents 12

List of Figures 17

List of Tables 19

List of Abbreviations 20

Chapter I: Introduction **25**

1.1 Mutation Accumulation in Aging and Cancer 26

1.2 Consequences of DNA Damage and DSB Repair 26

1.3 Mechanisms of DNA Damage Repair in Mammalian Cells 30

Non-Homologous End Joining (NHEJ) 31

Homology Directed DNA Repair 31

Gene Conversion – Synthesis Dependent Strand Annealing (SDSA) 32

Gene Conversion – Double Holliday Junction 34

Break-Induced Replication (BIR) 34

Single Strand Annealing (SSA) 35

Microhomology-Mediated End-Joining (MMEJ) 36

1.4 Exogenous Damage Requiring Homology Directed Repair 37

1.5 Detection of DNA Damage 40

In vitro Eukaryote Assays 40

In vivo Mouse Assays 41

Detection of Loss of Heterozygosity 41

Detection of Point Mutations and Small Deletions 44

Direct Detection of Homologous Recombination *in vivo* 47

1.6 Specific Aims 49

1.7 References 54

Chapter II: Deficiencies in KU and ERCC1 Increases Susceptibility to Homologous Recombination in FYDR 78

2.1 Abstract 79

2.2 Introduction 80

KU Protein is Necessary for NHEJ 82

ERCC1 Protein Plays a Role in Many Pathways 83

DNA Damage is Linked to Progeria 84

2.3 Materials and Methods 86

Experimental Animals 87

Whole Tissue Imaging 88

Flow Cytometry 89

Statistical Analysis 89

2.4 Results 90

Ku$^{-/-}$ *FYDR*$^{Y/Y}$ Mice show Increased HR 90

Ercc1$^{-/-}$*FYDR*$^{Y/+}$ Mice Show Increased HR 90

2.5 Discussion 92

HR Increases in NHEJ Deficient Cells 92

Defects in ERCC1 Lead to an Increase in HR 93

2.6 Acknowledgements 96

2.7 References 97

Chapter III: *ROSA26*-GFP Direct Repeat-GFP (raDR-GFP) Mice Reveal Tissue-, Age-, and Exposure-Dependence of Homologous Recombination _____ 108

3.1 Abstract 109

3.2 Introduction 111

3.3 Materials and Methods 114

Construction of the raDR-GFP Substrate 114

Creation of raDR-GFP Transgenic Mouse 114

PCR Analysis 115

Southern Blot Analysis 116

Positive Control Mouse 116

Isolation of Ear Fibroblasts 116

Flow Cytometry 117

In situ Imaging of Recombinant Foci 117

DNA Damage Induced Recombination 118

Statistical Analysis 119

3.4 Results 119

Creation of the raDR-GFP Mouse 119

HR Yields a Fluorescent Signal in raDR-GFP Mice 121

HR Reporter is Broadly Expressed in raDR-GFP Mice 122

Spontaneous HR is Detectable in Various Tissues 123

HR is Detectable *in situ* in the Pancreas, Liver, and Colon 124

DNA Damage Induces HR in raDR-GFP Mice 126

Recombinant Cells Accumulate with Age in the Pancreas, Liver, and Colon 127

3.5 Discussion 128

3.6 Acknowledgements 134

3.7 References 136

Chapter IV: Studies of Inflammation and its Impact on Homologous Recombination in Proximal and Distal Tissues *in vivo* 159

4.1 Abstract 160

4.2 Introduction 162

Chronic Inflammation Increases Cancer Risk 162

Inflammation Induces DNA Damage Through ROS and RON 163

Bacterial Infection Induces Tumorgenesis 163

Innate and Adaptive Immunity 165

4.3 Materials and Methods 166

Experimental Animals 166

Chronic DSS Exposure 167

Experimental *H. hepaticus* Inoculation 167

Experimental *H. trogontum* Inoculation 168

Fluorescent Foci Imaging 168

Fluorescent Cell Analysis by Flow Cytometry 169

Histological Evaluation 170

Statistical Evaluation of Data 170

4.4 Results 171

Pro-Inflammatory Environment Induces Recombination 171

Chemically Induced Inflammation Does Not Induce Detectable Distal HR 171

H. hepaticus Infection Does Not Lead To Detectable Increase HR *in vivo* 172

H. trogontum Infection Does Not Lead To Detectable Increase HR 173

4.5 Discussion 174

4.6 Acknowledgements 178

4.7 References 180

Chapter V: Conclusions and Future Work 194

5.1 Conclusions and Future Work 180

5.2 References 201

List of Figures

Figure 1-1 Basic Mechanisms of Double-Strand Break Repair 70

Figure 1-2 Replication Fork Collapse Leading to One-Ended Double-Strand Break..... 72

Figure 1-3 Nonhomologous End-Joining (NHEJ) Repair 73

Figure 1-4 Subpathways of Homology Directed Repair 74

Figure 1-5 Homologous Recombination (HR) Repair 75

Figure 1-6 FYDR HR Reporter System *in vivo* 76

Figure 2-1 ERCC1 is a Structure Specific Endonuclease 104

Figure 2-2 HR Increases in NHEJ Deficient Mice 105

Figure 2-3 HR Increases in ERCC1 Deficient Mice 106

Figure 3-1 Arrangement of raDR-GFP Direct Repeat Transgene and Recombinant raDR-GFP Cells 143

Figure 3-2 Arrangement of the DNA Targeted to the *ROSA26* Locus of raDR-GFP Mice 144

Figure 3-3 Analysis of Cells from raDR-GFP Mice..... 145

Figure 3-4 Expression of EGFP in Various Tissues of Positive Control raDR-GFP Mice 146

Figure 3-5 Spontaneous Recombination in Various Tissues of Heterozygous raDR-GFP (2 mo old) 148

Figure 3-6 Recombinant Foci in Various Tissues of FYDR and raDR-GFP Mice 149

Figure 3-7 Effect of Aging on the Frequency of Recombinant Foci in the Pancreas, Liver, and Colon 150

Figure 3-8 Effect of MNU/T3 Treatment on Frequency of Recombinant Cells in the Pancreas, Liver, and Colon..... 151

Figure 3-S1 Outline of the Major HR Pathways Resulting in a Fluorescent Cell in the raDR-GFP Construct 153

Figure 3-S2 The Δ*3egfp* and Δ*5egfp* Cassettes are Created from the pCX-NNX-EGFP Plasmid 154

Figure 3-S3 Recombinant Foci per Square Centimeter in the Pancreata of FYDR and raDR-GFP 2-month-old Heterozygous Mice 155

Figure 3-S4 Comparison of the Response to MNU/T3 treatment in FYDR and raDR-GFP Mice 156

Figure 3-S5 Tissue Response to MNU/T3 treatment 157

Figure 4-1 Spontaneous HR Increases in Pancreata of *RAG2*$^{-/-}$*IL10*$^{-/-}$*raDR-GFP* Mice . 185

Figure 4-2 Histology of the Pancreas of *H. hepaticus* Infected Mice 186

Figure 4-3 DSS-Induced Colitis Has No Apparent Impact on Distal HR 187

Figure 4-4 Inflammation Increased in the Colon Following *H. hepaticus* Infection 188

Figure 4-5 HR in the Colon Following *H. hepaticus* Infection 189

Figure 4-6 HR in the Pancreas Following *H. hepaticus* Infection 190

Figure 4-7 HR in the Liver Following *H. hepaticus* Infection 191

Figure 4-8 HR in the Colon, Pancreas, and Liver Following *H. trogontum* Infection ... 192

List of Tables

Table 1-1 DNA Repair Proteins 71

Table 3-1 Recombination Rate and Expression in raDR-GFP C57BL/6 Mice 141

List of Abbreviations

3MeA	3-methladenine
3MeG	3-methlyguanine
5-Cl-dC	5-chloro-2'-deoxycytidine
5'dRP	5' deoxyribose phosphate
7MeA	7-methyladenine
7MeG	7-methylguanine
8-oxoG	8-oxo-guanine
AAG	alkyladenine-DNA glycosylase
AP	apurinic / apyrimidinic
BER	base excision repair
BIR	break-induced repair
BLM	Bloom helicase
bp	base pair
CDT	cytolethal distending toxin
DBA	*Doichos biflorus* agglutinin
DMEM	Dulbecco's modified eagle medium
DNA	deoxyribonucleic acid
DNA-PK	DNA-dependent protein kinase
DNA-PK_{CS}	DNA-dependent protein kinase catalytic subunit

DR	direct reversal
DSB	double-strand break
dsDNA	double-stranded DNA
DSS	dextran sulfate sodium
EGFP	enhanced green fluorescent protein
EYFP	enhanced yellow fluorescent protein
FYDR	Fluorescent Yellow Direct Repeat
GPI	glycosylphosphatidylinisotol
GC	gene conversion
HR	homologous recombination
IBS	irritable bowl syntrome
Ig	immunoglobulin
IP	intraperitoneal
Iz	imidazolone
kb	kilobase
LIGIIIa	DNA ligaseIIIa
LIG4	DNA ligaseIV
LOH	loss of heterozygosity
MEF	mouse embryonic fibroblast
MGMT	O^6-methylguanine-DNA methyltransferase
MMEJ	microhomology-mediated end-joining
MMR	mismatch repair

MNU	*N*-methyl-*N*-nitrosourea
MRN	MRE11/RAD50/NBS1 complex
NER	nucleotide excision repair
NHEJ	nonhomologous end-joining
$NO^{\bullet}$	nitric oxide
$O_2^{\bullet}$	superoxide
O^6MeG	O^6-methylguanine
$ONOO^-$	peroxynitrite
Ox	oxaluric acid
PBS	phosphate buffered saline
PCR	polymerase chain reaction
Pig-a	phosphatidylinositol glycan, Class A
p^{un}	pink-eyed ustable
raDR-GFP	*ROSA26*-GFP Direct Repeat
RPA	replication protein A
RT	room temperature
SCE	sister chromatid exchange
SDSA	synthesis dependent strand annealing
Sp	spiroiminodihydantoin
ssDNA	single-strand DNA
T3	thyroid hormone
TCR	T-cell receptor

UV	ultraviolet
WT	wild type
X-gal	5-bromo-4-chloro-3-indol-β-D-galactopyranoside
XP	xeroderma pigmentosum
β-gal	β-galactosidase

Chapter I

Introduction and Motivation

Chapter I

1.1 Mutation Accumulation in Aging and Cancer

DNA repair is critical for maintaining genomic integrity. As DNA damage can lead to mutations, DNA repair is important for preventing mutations that contribute to cancer and aging (1, 2). The link between genomic fidelity and aging is evidenced by the progeria symptoms of patients deficient in DNA repair genes (2-5), and the link between repair deficiencies and cancer is well-established (6-12). Age and the associated accumulation of mutations is also a contributing risk factor in the development of cancer as genetic analysis of tumors often shows mutations in oncogenes and tumor suppressors within a tumor (1, 13-15).

1.2 Consequences of DNA Damage and DSB Repair

Approximately ten spontaneous DSBs per cell division occur due to environmental or endogenous factors or as a result DNA repair processing (16-22). Double-stranded breaks (DSBs) are both cytotoxic and mutagenic (23), and can result in the irreparable loss of over 100 million base pairs upon loss of an entire arm of a chromosome. These breaks can be repaired through homologous recombination (HR), non-homologous end-joining (NHEJ), or microhomology-mediated end-joining (MMEJ)

(24), but incorrect repair of DSBs can lead to large-scale and potentially toxic chromosomal rearrangements (25). The importance of DSB repair is further illustrated in studies of deficiencies in DSB repair, such as mutations in *BRCA1* and *BRCA2,* that convey an increased risk of tumorgenesis, likely through chromosomal instability (26-30). For example, 30-50% of patients with mutations in *BRCA1* and *BRCA2* develop breast and/or ovarian cancer by age 50 (31). In spontaneous breast and ovarian tumors, 50-70% are deficient in BRCA1, while 30-50% are deficient in BRCA2 (32). Similar DNA repair disregulation is seen in nearly all accelerated aging diseases, such as Bloom syndrome (33, 34) and Fanconi anemia (34, 35).

Mitotic HR plays in integral role in maintaining genomic integrity by repairing DNA DSBs and interstrand cross-links, and many proteins involved in HR (i.e. RAD51 and BRCA2) are also essential during embryogenesis (36-39). To properly repair DSBs, HR utilizes homologous sequences on the sister chromatid or homologous chromosome as a template, thereby repairing DSBs with high fidelity. Thus, HR is crucial in maintaining genetic integrity in the presence of DSBs. Rather than utilize homologous sequences as a template for repair, NHEJ directly ligates the double-stranded ends, regardless of the sequence (40, 41). MMEJ, on the other hand, utilizes sequences of microhomology (5-25 bp) along the damaged DNA strand to enable annealing (Figure 1-1).

While HR is vital for repair of DSBs, misapplication of DNA repair mechanisms can be detrimental. For instance, some deficiencies in HR are embryonic lethal and can lead to translocations, and convey an increased cancer risk. Similarly, excess HR can lead

to translocations, insertions, deletions, and loss of heterozygosity (LOH), also with an increased cancer risk. The balance among the various DSB repair processes HR, NHEJ, and MMEJ, is important for accurate repair as each DSB repair pathway is preferentially utilized at different phases of the cell cycle. NHEJ is the preferred pathway during G_0, G_1, and early S phase, while Lieber, *et. al*, show that MMEJ occurs most frequently in G_2 (40, 42). HR, on the other hand, is utilized efficiently in late S and G_2, when the newly synthesized sister chromatid is available as a repair template (21).

While a mechanism which brings together double-strand ends in a sequence-independent fashion may sound problematic, NHEJ, and to some extent MMEJ, do serve to prevent large-scale sequence rearrangements. When the cell is not replicating under non-stressed conditions, in most cell types, there are very few DSBs in proximity to each other with one DSB occurring every 10^8 bp, thus the correct ends are rapidly rejoined 95% of the time (43-45). If multiple double-stranded DNA fragments are present due to damage, the likelihood of translocations and chromosomal rearrangements increases dramatically (46). DSBs repaired via the MMEJ pathway are more likely to result in large deletions, insertions, and translocations when compared with DSBs repaired via NHEJ, possibly because this pathway can be active following replication fork breakdown, when a double-stranded end does not have an appropriate partner (43). By definition, both NHEJ and MMEJ are error-prone with regard to point mutations and small deletions since damaged bases are not restored, thus there is a loss of genetic information from direct ligation (NHEJ) or processing prior to ligation (MMEJ).

In contrast to NHEJ and MMEJ, HR is often referred to as an error-free repair pathway, since HR between sister chromatids can repair a DSB without any associate point mutations or small deletions. Furthermore, HR is the only DNA repair pathway that can correctly repair a broken replication fork (Figure 1-2). Unrepaired double-stranded ends from fork breakdown can act as a signal for apoptosis, making HR essential for vertebrate life (20, 47, 48). Furthermore, if DSBs resulting from replication fork breakdown are instead processed by NHEJ or MMEJ, ends from individual collapsed forks can be joined, leading to large-scale rearrangements. While a deficiency in HR is problematic, excess HR can also be detrimental. If the sister chromatid is not available (in G_0/G_1) and an area of homology is used on a nearby chromosome, it is likely to result in sequence misalignment, since 40% of the genome is composed of repeated sequences, and recombination between one functional and one nonfunctional allele can lead to LOH (49).

As HR has been shown to lead to deletions and tumorigenic LOH, it follows that increased susceptibility to HR is often associated with increased risk of cancer. For instance, most patients inherit two functional copies of tumor suppressor genes, one from each parent, thus an inactivating mutation in one allele carries no detrimental effect in a cell. However, in a cell that carries one mutated allele and one functional allele, LOH in the functioning allele may result in initiation of tumorgenesis (50-52). Indeed, in essentially all cancers, there is loss of function of a tumor suppressor gene. It is now known that HR causes a significant portion, if not most, of the LOH events observed in cancers (9, 53-55).

1.3 Mechanisms of DNA Damage Repair in Mammalian Cells

The DNA repair process is initiated by a series of complex signaling cascades that involve identification of damage and recruitment of appropriate DNA processing machinery. Pathway choice during DSB repair is carefully regulated, primarily to allow for preferential use of HR at broken replication forks (since NHEJ or MMEJ of broken ends can lead to large scale sequence rearrangements) and to suppress HR during G_1 (since there is not a sister chromatid available for repair, and HR between repeat sequences will promote deleterious sequence rearrangements). If repair via HR is unsuccessful, the DSB can be repaired by MMEJ as this pathway requires end processing similar to HR (43, 56). Therefore, the type of damage, e.g. DSBs versus double-stranded ends, in addition to the timing of damage influences pathway selection.

The initiation of DSB repair follows a competitive binding model involving a number of proteins, a subset of which are outlined in Table 1-1. Upon detection of a DSB, the histone H2AX is phosphorylated to form γH2AX, which signals and recruits repair machinery that it then links to the chromatin surrounding the break (57). MDC1 then binds γH2AX and promotes binding of RNF8 and the MRN complex (58). The RNF8 is a mediator that ubiquitylates proteins and histones at the DSB and mediates 53BP1 and BRCA1 interactions (59). It has been suggested that 53BP1 acts on the DSB to inhibit resection and tether ends together, thereby promoting NHEJ (23). Furthermore, in G_1 phase, 53BP1 interferes with HR protein BRCA1 binding directly or indirectly, which

inhibits HR (59-63). If bound, BRCA1 enables binding of CtIP, which further suppresses NHEJ during S/G_2 (61).

Non-Homologous End Joining (NHEJ)

A deficiency in NHEJ results in the persistence of DSBs into G_2/S phase which may induce apoptosis during replication (16). NHEJ repairs DSBs in G_1 by direct ligation to restore chromosomal integrity as seen in Figure 1-3 (40, 64, 65). Upon detection and binding of a DSB by the MRE11/RAD50/NBS1 (MRN) complex, the Ku70 and Ku80 proteins form a heterodimer (Ku) at the double-stranded end, protecting it from further processing (66, 67). The MRN complex also keeps the double-stranded ends in proximity to each other, thus enabling the formation of the DNA protein kinase (DNA-PK), comprised of Ku and the DNA protein kinase catalytic subunit (DNA-PK_{CS}), which is capable of end-joining (56, 68). DNA-PK also recruits Artemis to allow for end processing which is generally necessary in order to ligate the double-stranded ends (23, 69, 70). Ku is required for recruitment of DNA ligase IV (LIG4) and accessory proteins XRCC4 and XLF (70, 71), which together complete the repair of the DSB.

Homology Directed DNA Repair

While NHEJ repairs DSBs in G_1, HR repairs double-strand DNA damage largely in G_2/S through a number of subpathways: gene conversion (GC), break-induced repair (BIR), single strand annealing (SSA), and translation-induced fork breakdown (Figure 1-4) (16, 17, 72-74).

To initiate HR, CtIP signals to MRN to initiate the nucleolytic degredation of the 5′ strand to yield a 3′ overhang of single-stranded DNA (ssDNA). All subpathways of homology-directed repair are initiated by this 5′→3′ resection at the DSB end (Figure 1-5). ssDNA has high affinity for replication protein A (RPA), which rapidly binds to the ssDNA to prevent further degradation and to prevent premature annealing (18, 75).

Gene Conversion – Synthesis Dependent Strand Annealing (SDSA)

Synthesis dependent strand annealing (SDSA) is thought to be the predominant mechanism of homology directed repair of DSBs (16). As with initiation of all homology directed repair pathways, the SDSA pathway is initiated by 5′→3′ resection of the double-stranded ends to create ssDNA that is bound to RPA. When other DNA strands are involved in homology directed repair, RAD51 displaces RPA with assistance from BRCA2 and RAD52 and other mediator proteins (RAD51B, RAD51C, RAD51D, XRCC2, XRCC3). BRCA2 has binding modalities for ssDNA, dsDNA, and RAD51, thus it binds to the dsDNA/ssDNA junction at the resected end and loads RAD51 onto the ssDNA (76). BRCA2 deficient cells are deficient in their ability to load RAD51 onto the ssDNA, resulting in an inability to repair (76). Further illustrating the importance of these proteins, mice deficient in BRCA2 or RAD51 are embryonic lethal (36, 37, 77).

The ssDNA-bound nucleoprotein filament searches for and finds homologous sequences. The frequency of recombination with the sister chromatid is far greater than the frequency of HR with the homologous chromosome, in part due to proximity (78, 79). RAD54 facilitates strand invasion and helix unwinding and annealing of the ssDNA

to the homologous region to yield heteroduplex DNA, forming the displacement loop (D-loop). The 3' end of the invading strand is extended by DNA synthesis beyond the original break site to restore the missing sequence information at the break point (80). On the side opposite invasion of the D-loop, an 'X' shaped Holliday junction is formed at the junction of the hetero- and homoduplex DNA (Figure 1-5). A variety of proteins, including RTEL1, MUS81-EME1, SLX1-SLX4, GEN1, p53, WRN RAD54, BLAP75, hMSH2-hMSH6, and BLM-TOPIIIa, are involved in identifying and processing Holliday junctions, though the exact interactions have not yet been fully elucidated (81-85). The newly synthesized strand is displaced, likely by sliding the Holliday junction (branch migration) to the 3' end aided by BLM, RAD54, and/or WRN (16). It is unclear how these proteins direct branch migration, or if migration direction is random with strands in the middle of synthesis reannealing to the template if further synthesis is necessary. If DNA synthesis bridged the damaged portion and DNA on the other side of the break was similarly recessed, the newly synthesized 3' strand may anneal directly to the other side of the break in the original strand (Figure 1-5). Depending on the degree of extension, there may be overhangs that may be removed by structure specific endonuclease ERCC1/XPF (86-88). Final processing to fill in gaps and ligate nicks in the phosphate backbone finishes the repair process resulting in complete double-stranded DNA (dsDNA).

Gene Conversion – Double Holliday Junction

In the double Holliday junction model of DNA DSB repair, both sides of the break are resected as above and utilize complementary strands of the same template to repair the break. The resultant Holliday junctions can be resolved to yield a crossover or non-

crossover repair (Figure 1-4). It is likely that crossover and non-crossover events do not happen with the same likelihood as crossover products are rarely observed when examining induced DSB repair *in vitro* (89). Since mutations in BLM result in a substantial increase in sister chromatid exchanges, the lack of crossover products are likely the result of the ready availability of BLM and TOPIIIa to resolve the double Holliday junction (9, 33, 67, 90).

Break-Induced Replication (BIR)

While NHEJ or HR may repair two-ended DSBs, one-ended DSBs must be repaired by homology directed repair. Replication induced DSBs arise from a broken replication fork that can arise when the replication fork encounters a pre-existing nick or gap in the phosphate backbone or a bulky lesion that it is unable to bypass (Figure 1-2). Furthermore, if a replication fork encounters a transcription bubble, either or both sets of cellular machinery may dissociate, resulting in a single-sided DSB. The inability to replicate past this damage is potentially lethal to the cell if replication cannot be restarted (91).

The DSB is likely recognized with BRCA1 and the MRN complex. As before, the dsDNA is acted upon by Mre11 to cause a 3' overhang of ssDNA that is wrapped in RPA with RAD52. The ssDNA invades the intact DNA to form a Holliday junction as above (22, 29, 92, 93). BIR is initialized by HR as demonstrated by its dependence on RAD51, RAD52, RAD55, and RAD54. The invading strand primes the replication fork with DNA helicase, then Cdc45, GINS, Mcm2-7, and Cdt all contribute to the restart of replication

(8). While this process restores the integrity of the chromosome, if the original DSB occurred in one of the many repeated areas of the genome the likelihood of LOH increases with potentially tumorgenic consequences (8, 92).

Single Strand Annealing (SSA)

DSBs that occur between repeated sequences may be repaired via SSA. In this case, the DSB is processed to yield two 3' overhangs that are aligned and annealed (Figure 1-4). The genetic information between the two areas of homology are lost, thus SSA always leads to errors as it introduces potentially large deletions (94). Recalling the human genome contains approximately 10% repeated sequences with great than 10^6 Alu repeats, the potential for deleterious SSA is high, thus it is likely that SSA does not play a large role in the repair of DSBs in human mitotic cells (16, 95, 96).

In addition to the DSB recognition and HR pathway selection described above, SSA requires a number of other proteins. This repair process requires RPA and RAD52 and is RAD51-independent (16). When homology is found on the other side of the break, the RAD52 heptamer aligns complementary regions and the ssDNA anneals, leaving the non-homologous overhangs to be removed by the structure-specific endonuclease ERCC1/XPF (97). The resulting gaps are filled by DNA synthesis and the phosphate backbone is ligated, restoring continuous dsDNA (98). SSA can occur if the homologous sequences are separated by as much as 15kb, and is most efficient if the area of homology is over 400 bp (99).

Microhomology-Mediated End-Joining (MMEJ)

While similar to SSA, MMEJ is mechanistically distinct from SSA and other homology-directed repair pathways (100). While the presence of an alternative enjoining repair process has been suspected for some time (101), the exact mechanism of MMEJ remains unclear (8). The MMEJ pathway is responsible for ligating DNA ends in the absence of the classical NHEJ factors (KU, DNA-PKs, XRCC4, and LIG4) (102). Furthermore, studies in mammalian cells that lack XRCC4, LIGIV, or KU 70/80 exhibit NHEJ-independent, highly error-prone end-joining (103, 104). It is suggested that the several proteins involved in other repair processes are also utilized in MMEJ including PARP-I, MRN complex, CtIP, XRCC1, PARP, and DNA ligaseIIIa (LIGIIIa) (65, 105).

When a double-sided DSB is recognized, PARP-I binds the ends (which is competitively inhibited by KU) (106). This suggests that the MMEJ pathway is not active while the NHEJ pathway is active. The MRN complex is loaded on the DSBby CtIP and MRN is capable of limited BRCA1-independent DSB resection (5-25 bp) to yield a 3' overhang in G_1 (58). The areas of microhomology initiate SSA followed by LIGIIIa-dependent DNA ligation (107-109). The ERCC1-XPF structure-specific nuclease acts in a KU-independent end-joining pathway as evidenced by the hypersensitivity of *Ercc1*$^{-/-}$ / *Ku*$^{-/-}$ mutants relative to single-mutant cells (86, 104). *In vitro* end-joining assays have shown that joining of blunt ends is not significantly impaired in *Ercc1*$^{-/-}$ / *Ku*$^{-/-}$ mutants, but joining of ends with 3' non-complementary overhangs is significantly impaired with

a decreased use of microhomology in end-joining in *Ercc1*$^{-/-}$ compared to WT cells (86), supporting the role of ERCC1 in an alternative end-joining method.

1.4 Exogenous Damage and Homology Directed Repair

Alkylating agents are abundant in the environment (110, 111) and produced endogenously as byproducts of metabolism (112). When alkylating agents react with DNA, they can potentially form mutagenic and/or cytotoxic alkylated adducts on the oxygen and nitrogen molecules. These adducts can induce HR by creating lesions that block DNA replication if they are not first properly repaired through a more appropriate pathway (113). Many of these lesions are repaired through direct reversal (DR), base excision repair (BER), or nucleotide excision repair (NER) (111). Alkyladenine-DNA glycosylase (AAG) excises many DNA lesions, including 7-methylguanine (7MeG) and 3-methladenine (3MeA) (111). Following base removal, the resulting apurinic/apyrimidinic (AP) site is recognized by APE and XRCC1. APE1 cleaves the sugar phosphate backbone, leaving a 5'dRP that Polβ removes before inserting a replacement nucleotide and the backbone is ligated closed with DNA ligase (111, 113). Each of the BER intermediates, if they persist until G_2/S, can result in replication fork breakdown leading to HR (113).

The importance of alkylation-induced homology directed repair is likely dependent on the amount of alkylation damage and the ability of more appropriate pathways (BER, DR, NER) to repair these lesions. *N*-methyl-*N*-nitrosourea (MNU), an S_N1

alkylating agent, creates a number of methyl lesions including 7MeG (68%), 3MeA (8%), O^6-methylguanine (O^6MeG) (7.5%), 7-methyladenine (7MeA) (1.5%), 3-methlyguanine (3MeG) (0.8%), and phosphotriesters (12%) (21). While 7MeG is the most stable and most abundant adduct, it is not mutagenic; toxicity from 7MeG does not come from the lesion itself, but rather from the impact of its depurination. The two most toxic lesions are 3MeA and O^6MeG, with 3MeA being the most serious as it causes cytotoxic replication fork breakdown and O^6MeG causes mutagenic G-T mispairing during replication, which can induce mismatch-repair (MMR), futile cycling, and subsequent DSBs (Figure 1-2) (114-116). These alkyl lesions, particularly 3MeA, can induce HR directly through BER intermediates leading to DSBs or replication fork breakdowns (113, 117-120) (Figure 1-2). During mitosis, the replication fork may encounter one of the AP sites, nicks, single-strand gaps, or unrepaired lesions, leading to replication fork breakdown. As discussed, HR is the only repair pathway that is capable of replication fork repair (Figure 1-2, Figure 1-5). 3MeA is recombinogenic if it persists into replication (58), and lesions on the lagging strand may cause the replication fork to stall, leading to ssDNA that must be repaired via HR. If O^6MeG is not directly repaired by O^6-methylguanine-DNA methyltransferase (MGMT), the DNA may be replicated via translesion synthesis that may result in mispairing and mutation. Furthermore, if two lesions occur near each other on opposite strands, processing by BER repair enzymes could lead to a DSB. If this occurs during S or G_2 phase, the resulting DSB would be repaired through an HR pathway.

Inflammation, either endogenously or exogenously induced, also leads to DNA damage (121). DNA damage as a result of chronic inflammation has been shown to be a contributing factor in cancer development (122-126). Chronic inflammation and the resultant genomic instability has linked *Helicobacter pylori* infection with gastric cancer in humans (127-129). While the inflammatory response is vital in clearing infection, the reactive oxygen (ROS) and nitrogen species (RNS) coupled with the radicals and electrophilic compounds secreted by phagocytes pose a serious threat to the integrity of the host DNA (130, 131). The DNA damaging agents produced during inflammation can lead to DNA oxidation and halogenation or DNA deamination (132). Two of the most toxic products of inflammation include $NO^{\bullet}$ and $ONOO^{-}$. While the steady-state concentration of $NO^{\bullet}$ is less than 1 μM locally, the induced DNA damaged ranges from AP sites to bulky lesions including hypoxanthine, xanthine, and 2'-deoxyuridine (121). The reaction of $ONOO^{-}$ with guanine results with 8-oxoguanine (8-oxoG), which is 1000-fold more susceptible to further oxidation by $ONOO^{-}$ (132, 133). The major products of $ONOO^{-}$ oxidation of guanine and 8-oxoG are imidazolone (Iz) and oxaluric acid (Ox); 8-nitroG; Nitro-Iz; and spiroiminodihydantoin (Sp) (121, 132). Each of these adducts is problematic in that they may cause G → T mutations or result in AP sites. As discussed, the persistence of these damaged sites or AP sites into G_2 and S phase can result in fork breakdown or DSBs that necessitate homology-directed repair.

1.5 Detection of DNA Repair

Various methods have been developed for *in vitro* and *in vivo* detection of DNA damage and repair. Eukaryote assays including yeast, mammalian cell lines, and mice have provided invaluable insight into the role of individual proteins involved in DNA repair. While there is strength in the flexibility of choice of model system, the field is still lacking an ideal model that enables *in vivo* detection of recombinant cells in a variety of tissues and is a source of somatic cells for *in vitro* studies.

In vitro Eukaryote Assays

A number of *in vitro* assays have been used to discover the mechanistic pathways responsible for DNA damage and repair. In the *his3* complementation system, *S. cerevisiae* contains two non-functional *his3* alleles that, upon HR, enable growth in the absence of histidine, thus providing a measurement of mutation frequency in simple eukaryotes (134, 135). Similar mammalian cell direct-repeat systems have offered a straightforward way to look at homology-directed repair in a variety of genetic and treatment situations, but are still indirect measurements of organismal biology (136-139). These systems have demonstrated that recombination is dependent on the amount of shared homology as well as the location in the genome (139-141). In fact, Hellgren, *et al.* found that recombination frequency varied as much as 24-fold depending on locus of incorporation (140).

In vivo Mouse Assays

There are now many approaches for studying genetic change *in vivo*. In addition to FYDR recombomice mouse and p^{un} mice that detect HR (142-144), there are also mice that have been used to study LOH ($Aprt^{+/-}$, $Tk^{+/-}$, p^{un}, Dbl-1 (50, 143, 145, 146)) and point mutations/small deletions (Hprt, Pig-a, Muta^{TM}Mouse, Big Blue$^{©}$, *gpt-Δ* (147-153)). Most *in vivo* mutation assays require the disaggregation of cells for analysis, obfuscating information about individual recombination events. The systems that enable visualization of HR events *in situ* are limited in the tissues available for study. The ability to detect individual mutation events in a wide range of tissues is a powerful tool for determining the effects of genetic, environmental, and endogenous factors on DNA damage.

Detection of Loss of Heterozygosity (LOH)

In vivo LOH studies have been instrumental in defining parameters that lead to loss of genetic information (44, 152, 154-160). Without extensive additional analysis, though, the underlying mechanism is not known.

$Aprt^{-/+}$ and $Tk^{-/+}$ Mice

The $Aprt^{-/+}$ mouse can be used to study point mutations, frameshifts, and small deletions as well as LOH events resulting from large deletions, mitotic nondisjunction, mitotic recombination, and gene conversion (50, 161-163). The mouse *Aprt* gene is

located on chromosome 8 and encodes for adenine phosphoribosyltransferase that catalyzes the conversion of adenine to AMP in the purine salvage pathway (50, 162, 164). Consequently, if cells lose all *Aprt* functionality, they are not able to convert purine analogs (9-azaadenine or 2,6-diaminopurine) into cytotoxic by-products and survive in selection media containing purine analogs (50, 162, 164). To determine mutagenic effects of an exposure or genetic condition, $Aprt^{-/+}$ mice are treated and cells, such as splenic T-lymphocytes, are harvested and cultured with or without selection media. The mutation frequency is determined from the ratio of mutant (9-azaadenine selected) vs nonmutant (grown without selection) colonies. The detected spontaneous mutation frequency at the *Aprt* locus in heterozygous mice is approximately 8.7×10^{-6} (116). The loss of *Aprt* eliminates the ability of a cell to process purine analogs, thus, there may be negative selection pressures on mutant cells *in vivo* (164, 165). Furthermore, the detection of *Aprt* mutant cells is limited to tissues that may be subcultured *in vitro*, thus tissues of particular interest, such as liver hepatocytes, cannot be readily studied with this model.

The $Tk^{-/+}$ mice are a similarly constructed mouse line that can also measure indirectly LOH in addition to point mutations, frameshifts, and small deletions. The *Tk* reporter is located on the distal portion of mouse chromosome 11 and encodes thymine kinase, which is involved in pyrimidine salvage. *Tk* is generally expressed in mitotically active cells. Similar to the $Aprt^{-/-}$ cells, mutated $Tk^{-/-}$ cells are identified *in vitro* in the presence of pyrimidine analog BrdU, while unmutated $Tk^{-/+}$ are unable to grow. As with the *Aprt* assay, mice are commonly exposed to a mutagen, then splenic T-lymphocytes

are removed and cultured with and without selection media (145). The mutation frequency is determined by comparing the number of selected and unselected mutants and the spontaneous mutant frequency is reported to be 2×10^{-5} (125). Similar limitations regarding the necessity of subcultured cells and the potential for negative selection against mutant cells *in vivo*. Unfortunately, selection pyrimidine analog BrdU is mutagenic, leading to the possibility that the assay itself is introducing further mutations (145).

Dlb-I Mice

The *Dlb-I* assay measures *in vivo* mutations occurring in the small intestine of *Dlb-I* heterozygotic mice (146, 166). *Dlb-I* is a bi-allelic locus on chromosome 11 that determines the expression of binding sites for lectin *Dolichos biflorus* agglutinin (DBA) in the intestinal epithelium (146). Heterozygous *Dlb-I* mice may develop a mutation in an intestinal stem cell that results in loss of the functional DBA binding sits is detected via staining, and the number of unstained and stained crypts are compared to determine the mutation frequency. While the *Dlb-I* assay can be used to study animals of any age, this assay does not yield any information about the mechanism of LOH. While fewer *Dlb-I* than p^{un} animals are necessary for the same analysis, this assay is limited to colonic epithelial cells (167).

Detection of Point Mutations and Small Deletions

HPRT Assay

The HPRT assay detects point mutations, frameshifts, and small insertions/deletions. HPRT is on the X-chromosome and codes for hypoxanthine-guanine phosphoribosyltransferase, which transforms purines (ie 6-thioguanine) to a cytotoxic monophosphate. The effects of exposure or genetics on HPRT mutation can be determine by removing cells of interest (often splenic T-lymphocytes), culturing these cells with and without selection agent 6-thioguanine, which is toxic to non-mutant cells (153, 166). The mutation frequency is determined from the frequency of mutant (6-thioguanine selected) vs nonmutant (no selection) colonies. The HPRT assay is readily performed on any mice as HPRT is a transcriptionally active endogenous gene (thus is subject to transcription-coupled DNA repair, but is limited to cells that can be cultured (117)).

Pig-a Assay

The *Pig-a* assay (phosphatidylinositol glycan, Class A) takes advantage of a naturally occurring marker on the outside of cells. In its natural state, *Pig-a* (phosphatidylinositol glycan, Class A) is involved in glycosylphosphatidylinisotol (GPI) anchors of CD59 markers to the surface of a cell. While there are other proteins involved in the anchoring process, they are all autosomal, while *Pig-a* is X-linked (147). In males, defects in both alleles of these other genes would be necessary to disrupt GPI anchors, which is unlikely; thus, all cells not exhibiting CD59 are classified as having a

mutated *Pig-a* gene (147, 168). Harvested cells are analyzed for immunohistochemical tagging of CD59 markers and the total mutated cell frequency is calculated, though individual mutation events cannot be uncovered. *Pig-a* is naturally occurring, thus there is no expense or time associated with breeding transgenic animals and the assay can be performed in conjunction with any other genotype. Though this assay is limited to peripheral blood erythrocytes and reticulocytes, this cell-type allows rapid and repeated sampling (169).

Muta™Mouse

The Muta™Mouse transgenic mouse system is based on the lambda/*lacZ* reporter system (148). The Muta™Mouse contains approximately 150 copies of a lambda gt10-*lacZ* shuttle vector integrated into chromosome 3 (165). The reporter carries a functional bacterial *lacZ* gene, from the Lac operon, that is responsible for the synthesis of β-galactosidase (β-gal). When expressed in bacteria, β-gal can be detected by 5-bromo-4-chloro-3-indol-β-D-galactopyranoside (X-gal) (170). An unmutated phage from Muta™Mouse produces β-gal, which produces a blue phenotype in the presence of X-gal, while mutated phages produce little or no β-gal, resulting in a white plaque.

In practice, a Muta™Mouse is treated, tissues are collected, and DNA is extracted from cells. The reporter DNA is isolated and packaged into a lambda::lacZ phage that infects *E. coli lac⁻ galE⁻*, which is then streaked on agar for X-gal identification (or, more recently, P-gal, that selects for mutant plaques, rather than resulting in a color change). Mutation frequency is determined by counting the number of white (mutated)

compared with the number of blue (wild-type) plaques. Since the DNA inserted in the genome is not expressed *in vivo*, there is no opportunity for transcription-induced damage transcription-coupled repair. The indirect measurement of mutations using the Muta™Mouse is laborious, expensive, and slow. Moreover, significant expertise in performing the assay is required in order to obtain reliable data, which, taken together, together severely limit the utility of this model.

Big Blue© Mice

Similar to Muta™Mouse, the BigBlue© transgenic reporter system contains a bacterial operon that is harvested and transferred into bacteria that are grown under selection conditions that yield a color-change or survival advantage. The 45 kb lambda phage contains approximately 40 copies of the vector incorporated into chromosome 4 (148). The *lacI* gene that codes for a monomeric repressor of the lac operator, which prevents transcription of β-gal precursors, thus mutation in *lacI* causes β-gal to be produced. White plaques will arise from phases bearing wild-type (unmutated) *lacI* when the SCS-8 bacteria are grown on X-gal containing medium. Dark blue plaques will form when mutations in *lacI* result in a Lac repressor that cannot bind to the Lac operator; thus β-gal will be produced, resulting in cleavage of X-gal and a blue plaque. The proportion of blue plaques is a measure of the mutation frequency. The limitations with BigBlue© are the same as with Muta™Mouse: the expense and time required for the assay.

gpt-Δ Mice

The *gpt*-Δ mouse is used to detect point mutations (6-thioguanine) or deletions (Spi^-) depending on the selection method. The *gpt*-Δ mouse carries approximately 80 copies of the 456 bp *gpt*-Δ transgene on chromosome 17 that is used as a reporter (152). Like Muta™Mouse and BigBlue©, the *gpt*-Δ DNA must be recovered and packaged into lambda-phage to transfer DNA to bacteria for analysis. The *gpt* gene of *E. coli* is responsible for guanine phosphoribosyltransferase, thus if bacteria are grown in the presence of 6-thioguanine, only plaques with a mutated *gpt* gene will thrive (165). The mutation frequency is calculated as the number of mutant (growing in 6-thioguanine selection) vs. non-mutants (no selection). DNA from mutant plaques can be sequenced to determine specific point mutations or deletions. Accurate data analysis requires an experienced technician, a large number of plates, and a significant amount of time to indirectly detect mutants in the mouse. The processing required for analysis enables an indirect measurement of total mutation load, but cannot parse the total number of *de novo* events as opposed to clonal expansion. Furthermore, as the transgene is not expressed *in vivo* in the mouse, the DNA is not subject to the same types of transcription and repair interactions as endogenous expressed genes.

Direct Detection of Homologous Recombination *in vivo*

A method of detecting HR is by analyzing changes in direct repeats resulting from homology-directed repair *in vivo.* Recombined cells result in a detectable phenotypic

change; in the case of p^{un} mice, deletion of one of the direct repeats results in melanin production; in FYDR mice, reconstitution of a fluorescent gene cassette results in detectable fluorescence. These mice enable direct detection of DNA repair that is subjected to the same transcriptional and physiological effects as native DNA *in situ*.

p^{un} Mice

The pink-eyed unstable (p^{un}) mice carry a naturally occurring 70 kb duplication the *p* locus that prohibits the production of melanin, resulting in a mouse with grey fur and pink eyes (171-173). Loss of one of the duplications as a result of HR enables the production of melanin, resulting in black spots on the grey fur and retinal epithelium of adult mice (143, 171, 174). Since clonal expansion of melanin-producing recombinant cells is required to visually detect dark spots, only recombination events *in utero* undergo clonal expansion to yield detectable spots. The large biological variation even in inbred animals necessitates a large number of animals for single variable studies, rendering these experiments costly and time intensive. While the p^{un} mice have been used to show the effects of various genetic and environmental factors on recombination in early development (175-180), it is impossible to gather information about HR in adult animals.

FYDR Mice

Our laboratory has previously developed the Fluorescent Yellow at a Direct Repeat (FYDR) mouse that allows direct detection of homology-directed DNA repair (181, 182). The FYDR mouse contains a direct repeat of two fluorescent yellow gene

cassettes with unique deletions that render them non-functional (Figure 1-6). When the transgene is damaged and repaired via HR, a functional, full-length EYFP gene cassette results (142, 182-184). EYFP expressing cells are directly observed *in situ* using fluorescence microscopy or as disaggregated cells via flow cytometry (142, 181, 182). This allows measurement of total mutated cells as well as individual HR events. The FYDR mouse has been invaluable in understanding the complex genetic and environmental interactions involved in HR; furthermore, since the transgene is expressed *in vivo* in mammals, the reporter is subject to transcription-coupled damage and repair, thus more closely representing the physiological state of the rest of the genome (142, 184, 185). The FYDR transgene is only expressed at a high level in the pancreas and skin, and is not expressed at all in some tissues (182). The construct must be expressed to enable visualization and quantification of recombination events, thus the FYDR assay cannot be used in all tissues.

1.6 Specific Aims of This Thesis

Mitotic HR is an important repair pathway that enables error-free repair of DSBs and collapsed replication forks (16). Defects in HR are particularly dangerous, and may be embryonic lethal or tumorigenic (10, 37, 38, 186-190). The ultimate goal of this work is to understand the role of HR in a variety of tissues with genetic and environmental pressures.

To examine the impact of deficiencies in proteins of other repair pathways on HR, we used FYDR mice to study HR in the pancreas. Ku86, one component of the KU heterodimer, is necessary for NHEJ. In *Ku*$^{-/-}$ *FYDR* mice, we are able to study the effect of removing the NHEJ pathway on HR. Without NHEJ to repair DSBs in G_1, DSBs must be repaired through another pathway, or DSBs may induce cell cycle arrest or apoptosis (191). With the *Ku*$^{-/-}$ *FYDR* mice, we see HR increases in the pancreas when NHEJ is unavailable. While Rockwood, *et. al*, hinted at this relationship *in vivo* by showing a decrease in *lacZ* mutations in *Ku86*$^{-/-}$ mice, likely due to increased HR (192). We show direct evidence that HR increases *in vivo* in response to unavailability of NHEJ.

The importance of DSB repair is evidence by the multiple pathways for repair. In addition to NHEJ and HR, MMEJ is capable of repairing DSBs. We examine the effect of deficiencies in repair protein ERCC1, which recognizes a structural bend in DNA formed in bulky lesions and non-homologous 3' flaps, and is a factor in both NER and MMEJ. *Ercc1*$^{-/-}$ *FYDR* mice exhibit an increase in HR in the pancreas similar to that of the *Ku*$^{-/-}$ FYDR mice.

It is well-documented that there are tissue-specific differences in mutation accumulation (183, 193). Due to limitations in the expression of the FYDR transgene, we were limited in our ability to study the impact of exposures on HR susceptibility in many tissues (182, 183). To enable study of DNA repair in multiple tissues, we developed an *in vivo* method of examining HR in a variety of tissues by targeting an EGFP direct repeat reporter system to the *ROSA26* locus which interrupts two transcripts that encode

nuclear RNA. We targeted this particular locus on chromosome 6 because other genes inserted here have been shown to be universally expressed (194). To compare the frequency of HR across tissues, the transgene must be expressed at similar levels to enable visualization of the fluorescent marker of HR. The *ROSA26* Direct Repeat-GFP (raDR-GFP) positive control, which expresses a fluorescent protein at the same locus and promoter as the raDR-GFP transgene, demonstrates high expression of the transgene in all 11 tissues examined, enabling studies in many different tissues. The spontaneous recombination rate between tissues is variable. Consistent with age as a risk for developing cancer, the number ofmbinant foci increases with age in the pancreas, liver, and colon, but at different rates that do not necessarily correlate to the proliferation profile associated with each tissue.

While age and genetic factors contribute to tumorgenesis, environmentally-induced DNA damage can lead to mutations and cancer (112, 195-197). With the raDR-GFP mouse, we show that HR increases in response to environmentally-induced alkylation damage. Alkylation damage is dangerous and mutagenic, and is usually repaired via BER, but BER intermediates that persist to G_2 and S phase can cause mutation and fork breakdown that must be repaired via HR (117-119, 198). We show that the raDR-GFP mouse is a valuable tool for studying environmentally-induced alkylation damage.

It has long been suggested that inflammation-induced DNA damage induces cancer, and recently it was demonstrated for the first time that indeed induced DNA

damage in the colon induces cancer (125, 126, 197, 199-209). Chronic inflammation associated with irritable bowl syndrome (IBS) conveys an increased cancer risk both locally and distally (210-212); in fact, we saw the distal effects of long-term *H. hepaticus* infection-induced inflammation in the colon led to pre-neoplastic lesions in the pancreas. Consistent with an inflamed environment inducing DNA damage, we see an increase in HR in the absence of RAG2 and anti-inflammatory cytokine IL10 in the raDR-GFP pancreas. When we examine the effect of repeated bouts of chemically-induced inflammation in the colon on the level of HR in the FYDR pancreas, we saw no difference in the level of HR, which is consistent with parallel studies in this laboratory showing that inflammation must occur in conjunction with proliferation in order to induce HR (Kiraly, manuscript in preparation). Our studies of chronic infection of *Rag2*$^{-/-}$ *raDR-GFP* mice show no consistent change in HR among the colon, liver, and pancreas. While the colon and the pancreas show no change in HR with *H. hepaticus* or *H. trogontum* infection, surprisingly the liver showed a decrease in the number of recombinant foci with *H. hepaticus* infection. These data provide further motivation for investigation into the impact of inflammation and particularly infection-induced inflammation on the initiation of DNA damage and the subsequent development of cancer.

While the importance of HR in maintenance of genomic integrity and the link between DNA damage and cancer is well-established, we aim to understand the connection between different DNA repair processes *in vivo* to better illustrate the

importance of environmental and genetic factors that can contribute to cancer in a variety of tissues.

1.7 References

1. DePinho RA (2000) The age of cancer. *Nature* 408:248–254.

2. Musich PR, Zou Y (2009) Genomic instability and DNA damage responses in progeria arising from defective maturation of prelamin A. *Aging (Albany NY)* 1:28–37.

3. Saintigny Y, Makienko K, Swanson C, Emond MJ, Monnat RJ (2002) Homologous recombination resolution defect in werner syndrome. *Mol Cell Biol* 22:6971–6978.

4. Niedernhofer LJ (2008) Nucleotide excision repair deficient mouse models and neurological disease. *DNA Repair (Amst)* 7:1180–1189.

5. Moraes MCS, Neto JBC, Menck CFM (2012) DNA repair mechanisms protect our genome from carcinogenesis. *Front Biosci* 17:1362–1388.

6. Dollé MET et al. (2006) Increased genomic instability is not a prerequisite for shortened lifespan in DNA repair deficient mice. *Mutat Res* 596:22–35.

7. Friedberg EC (2003) DNA damage and repair. *Nature* 421:436–440.

8. Kasparek TR, Humphrey TC (2011) DNA double-strand break repair pathways, chromosomal rearrangements and cancer. *Semin Cell Dev Biol* 22:886–897.

9. Wu L, Hickson ID (2003) The Bloom's syndrome helicase suppresses crossing over during homologous recombination. *Nature* 426:870–874.

10. Digweed M, Sperling K (2004) Nijmegen breakage syndrome: clinical manifestation of defective response to DNA double-strand breaks. *DNA Repair (Amst)* 3:1207–1217.

11. LaRocque JR et al. (2011) Interhomolog recombination and loss of heterozygosity in wild-type and Bloom syndrome helicase (BLM)-deficient mammalian cells. *Proc Natl Acad Sci USA* 108:11971–11976.

12. Gray MD et al. (1997) The Werner syndrome protein is a DNA helicase. *Nat Genet* 17:100–103.

13. Sidransky D et al. (1992) Clonal expansion of p53 mutant cells is associated with brain tumour progression. *Nature* 355:846–847.

14. Powell SM et al. (1992) APC mutations occur early during colorectal

tumorigenesis. *Nature* 359:235–237.

15. Almoguera C et al. (1988) Most human carcinomas of the exocrine pancreas contain mutant c-K-ras genes. *Cell* 53:549–554.

16. Helleday T, Lo J, van Gent DC, Engelward BP (2007) DNA double-strand break repair: from mechanistic understanding to cancer treatment. *DNA Repair (Amst)* 6:923–935.

17. Helleday T (2003) Pathways for mitotic homologous recombination in mammalian cells. *Mutat Res* 532:103–115.

18. West SC (2003) Molecular views of recombination proteins and their control. *Nat Rev Mol Cell Biol* 4:435–445.

19. McHugh PJ, Spanswick VJ, Hartley JA (2001) Repair of DNA interstrand crosslinks: molecular mechanisms and clinical relevance. *Lancet Oncol* 2:483–490.

20. Michel B et al. (2001) Rescue of arrested replication forks by homologous recombination. *Proc Natl Acad Sci USA* 98:8181–8188.

21. Friedberg EC et al. (2005) *DNA Repair and Mutagenesis* (Amer Society for Microbiology). 2nd Ed.

22. Haber JE (1999) DNA recombination: the replication connection. *Trends Biochem Sci* 24:271–275.

23. Chapman JR, Taylor MRG, Boulton SJ (2012) Playing the end game: DNA double-strand break repair pathway choice. *Mol Cell* 47:497–510.

24. Gregory SG et al. (2006) The DNA sequence and biological annotation of human chromosome 1. *Nature* 441:315–321.

25. Ferguson DO, Alt FW (2001) DNA double strand break repair and chromosomal translocation: lessons from animal models. *Oncogene* 20:5572–5579.

26. Venkitaraman AR (2002) Cancer susceptibility and the functions of BRCA1 and BRCA2. *Cell* 108:171–182.

27. Bishop AJ, Schiestl RH (2001) Homologous recombination as a mechanism of carcinogenesis. *Biochim Biophys Acta* 1471:M109–21.

28. Bishop AJR, Schiestl RH (2002) Homologous Recombination and Its Role in Carcinogenesis. *J Biomed Biotechnol* 2:75–85.

29. Moynahan ME, Chiu JW, Koller BH, Jasin M (1999) Brca1 controls homology-

directed DNA repair. *Mol Cell* 4:511–518.

30. Sonoda E (1998) Rad51-deficient vertebrate cells accumulate chromosomal breaks prior to cell death. *EMBO J* 17:598–608.

31. Rahman N, Stratton MR (1998) THE GENETICS OF BREAST CANCER SUSCEPTIBILITY. *Annu Rev Genet* 32:95–121.

32. Welcsh PL (2001) BRCA1 and BRCA2 and the genetics of breast and ovarian cancer. *Hum Mol Genet* 10:705–713.

33. Chaganti RS, Schonberg S, German J (1974) A manyfold increase in sister chromatid exchanges in Bloom's syndrome lymphocytes. *Proc Natl Acad Sci USA* 71:4508–4512.

34. Thompson LH, Schild D (2002) Recombinational DNA repair and human disease. *Mutat Res* 509:49–78.

35. Niedzwiedz W et al. (2004) The Fanconi anaemia gene FANCC promotes homologous recombination and error-prone DNA repair. *Mol Cell* 15:607–620.

36. Sharan SK et al. (1997) Embryonic lethality and radiation hypersensitivity mediated by Rad51 in mice lacking Brca2. *Nature* 386:804–810.

37. Tsuzuki T et al. (1996) Targeted disruption of the Rad51 gene leads to lethality in embryonic mice. *Proc Natl Acad Sci USA* 93:6236–6240.

38. Lim DS, Hasty P (1996) A mutation in mouse rad51 results in an early embryonic lethal that is suppressed by a mutation in p53. *Mol Cell Biol* 16:7133–7143.

39. Pittman DL, Schimenti JC (2000) Midgestation lethality in mice deficient for the RecA-related gene, Rad51d/Rad51l3. *Genesis* 26:167–173.

40. Lieber MR, Ma Y, Pannicke U, Schwarz K (2003) Mechanism and regulation of human non-homologous DNA end-joining. *Nat Rev Mol Cell Biol* 4:712–720.

41. Weterings E, van Gent DC (2004) The mechanism of non-homologous end-joining: a synopsis of synapsis. *DNA Repair (Amst)* 3:1425–1435.

42. Lieber MR (2010) NHEJ and its backup pathways in chromosomal translocations. *Nat Struct Mol Biol* 17:393–395.

43. Li L, Robert C, Rassool FV The Role of Error-Prone Alternative Non-Homologous End-Joining in Genomic Instability in Cancer. *cdnintechopencom*

44. Kolomietz E, Meyn MS, Pandita A, Squire JA (2002) The role of Alu repeat clusters

as mediators of recurrent chromosomal aberrations in tumors. *Genes Chromosomes Cancer* 35:97–112.

45. Vilenchik MM, Knudson AG (2003) Endogenous DNA double-strand breaks: production, fidelity of repair, and induction of cancer. *Proc Natl Acad Sci USA* 100:12871–12876.

46. Pluth JM et al. (2008) DNA double-strand break and chromosomal rejoining defects with misrejoining in Nijmegen breakage syndrome cells. *DNA Repair (Amst)* 7:108–118.

47. Rich T, Allen RL, Wyllie AH (2000) Defying death after DNA damage. *Nature* 407:777–783.

48. Huang LC, Clarkin KC, Wahl GM (1996) Sensitivity and selectivity of the DNA damage sensor responsible for activating p53-dependent G1 arrest. *Proc Natl Acad Sci USA* 93:4827–4832.

49. Lander ES et al. (2001) Initial sequencing and analysis of the human genome. *Nature* 409:860–921.

50. Gupta PK et al. (1994) Analysis of in vivo somatic mutations at the APRT locus. *Adv Exp Med Biol* 370:653–656.

51. Morley AA, Grist SA, Turner DR, Kutlaca A, Bennett G (1990) Molecular nature of in vivo mutations in human cells at the autosomal HLA-A locus. *Cancer Res* 50:4584–4587.

52. Zhu J, Petersen S, Tessarollo L, Nussenzweig A (2001) Targeted disruption of the Nijmegen breakage syndrome gene NBS1 leads to early embryonic lethality in mice. *Curr Biol* 11:105–109.

53. Wan R, Crowe DL (2012) Haploinsufficiency of the Nijmegen breakage syndrome 1 gene increases mammary tumor latency and metastasis. *Int J Oncol* 41:345–352.

54. Ha G et al. (2012) Integrative analysis of genome-wide loss of heterozygosity and monoallelic expression at nucleotide resolution reveals disrupted pathways in triple-negative breast cancer. *Genome Res* 22:1995–2007.

55. Abkevich V et al. (2012) Patterns of genomic loss of heterozygosity predict homologous recombination repair defects in epithelial ovarian cancer. *Br J Cancer* 107:1776–1782.

56. Shibata A et al. (2011) Factors determining DNA double-strand break repair pathway choice in G2 phase. *EMBO J* 30:1079–1092.

57. Lukas J, Lukas C, Bartek J (2011) More than just a focus: The chromatin response to DNA damage and its role in genome integrity maintenance. *Nat Cell Biol* 13:1161–1169.

58. Ciccia A, Elledge SJ (2010) The DNA damage response: making it safe to play with knives. *Mol Cell* 40:179–204.

59. Giunta S, Belotserkovskaya R, Jackson SP (2010) DNA damage signaling in response to double-strand breaks during mitosis. *J Cell Biol* 190:197–207.

60. Kolas NK et al. (2007) Orchestration of the DNA-damage response by the RNF8 ubiquitin ligase. *Science* 318:1637–1640.

61. Escribano-Díaz C et al. (2013) A cell cycle-dependent regulatory circuit composed of 53BP1-RIF1 and BRCA1-CtIP controls DNA repair pathway choice. *Mol Cell* 49:872–883.

62. Stewart GS (2009) Solving the RIDDLE of 53BP1 recruitment to sites of damage. *Cell Cycle* 8:1532–1538.

63. Mailand N et al. (2007) RNF8 ubiquitylates histones at DNA double-strand breaks and promotes assembly of repair proteins. *Cell* 131:887–900.

64. Daley JM, Palmbos PL, Wu D, Wilson TE (2005) Nonhomologous end joining in yeast. *Annu Rev Genet* 39:431–451.

65. Lieber MR (2010) The mechanism of double-strand DNA break repair by the nonhomologous DNA end-joining pathway. *Annu Rev Biochem* 79:181–211.

66. Dynan WS, Yoo S (1998) Interaction of Ku protein and DNA-dependent protein kinase catalytic subunit with nucleic acids. *Nucleic Acids Res* 26:1551–1559.

67. Wu D, Topper LM, Wilson TE (2008) Recruitment and dissociation of nonhomologous end joining proteins at a DNA double-strand break in Saccharomyces cerevisiae. *Genetics* 178:1237–1249.

68. Reliene R, Bishop AJR, Li G, Schiestl RH (2004) Ku86 deficiency leads to reduced intrachromosomal homologous recombination in vivo in mice. *DNA Repair (Amst)* 3:103–111.

69. O'Driscoll M, Jeggo PA (2006) The role of double-strand break repair - insights from human genetics. *Nat Rev Genet* 7:45–54.

70. Symington LS, Gautier J (2011) Double-strand break end resection and repair pathway choice. *Annu Rev Genet* 45:247–271.

71. Zhang Y et al. (2007) Role of Dnl4-Lif1 in nonhomologous end-joining repair complex assembly and suppression of homologous recombination. *Nat Struct Mol Biol* 14:639–646.

72. Liang F, Han M, Romanienko PJ, Jasin M (1998) Homology-directed repair is a major double-strand break repair pathway in mammalian cells. *Proc Natl Acad Sci USA* 95:5172–5177.

73. Gottipati P, Helleday T (2009) Transcription-associated recombination in eukaryotes: link between transcription, replication and recombination. *Mutagenesis* 24:203–210.

74. Arnaudeau C, Lundin C, Helleday T (2001) DNA double-strand breaks associated with replication forks are predominantly repaired by homologous recombination involving an exchange mechanism in mammalian cells. *J Mol Biol* 307:1235–1245.

75. Heyer W-D, Ehmsen KT, Liu J (2010) Regulation of homologous recombination in eukaryotes. *Annu Rev Genet* 44:113–139.

76. Moynahan ME, Pierce AJ, Jasin M (2001) BRCA2 is required for homology-directed repair of chromosomal breaks. *Mol Cell* 7:263–272.

77. Shu Z, Smith S, Wang L, Rice MC, Kmiec EB (1999) Disruption of muREC2/RAD51L1 in mice results in early embryonic lethality which can Be partially rescued in a p53(-/-) background. *Mol Cell Biol* 19:8686–8693.

78. Richardson C, Moynahan ME, Jasin M (1998) Double-strand break repair by interchromosomal recombination: suppression of chromosomal translocations. *Genes Dev* 12:3831–3842.

79. Stark JM, Jasin M (2003) Extensive loss of heterozygosity is suppressed during homologous repair of chromosomal breaks. *Mol Cell Biol* 23:733–743.

80. Maloisel L, Fabre F, Gangloff S (2008) DNA polymerase delta is preferentially recruited during homologous recombination to promote heteroduplex DNA extension. *Mol Cell Biol* 28:1373–1382.

81. Muñoz-Galván S et al. (2012) Distinct roles of Mus81, Yen1, Slx1-Slx4, and Rad1 nucleases in the repair of replication-born double-strand breaks by sister chromatid exchange. *Mol Cell Biol* 32:1592–1603.

82. Barber LJ et al. (2008) RTEL1 maintains genomic stability by suppressing homologous recombination. *Cell* 135:261–271.

83. Ehmsen KT, Heyer W-D (2008) Saccharomyces cerevisiae Mus81-Mms4 is a

catalytic, DNA structure-selective endonuclease. *Nucleic Acids Res* 36:2182–2195.

84. Wechsler T, Newman S, West SC (2011) Aberrant chromosome morphology in human cells defective for Holliday junction resolution. *Nature* 471:642–646.

85. Ellis NA et al. (1995) The Bloom's syndrome gene product is homologous to RecQ helicases. *Cell* 83:655–666.

86. Ahmad A et al. (2008) ERCC1-XPF endonuclease facilitates DNA double-strand break repair. 28:5082–5092.

87. Adair GM et al. (2000) Role of ERCC1 in removal of long non-homologous tails during targeted homologous recombination. *EMBO J* 19:5552–5561.

88. Niedernhofer LJ et al. (2004) The structure-specific endonuclease Ercc1-Xpf is required to resolve DNA interstrand cross-link-induced double-strand breaks. *Mol Cell Biol* 24:5776–5787.

89. Johnson RD, Jasin M (2000) Sister chromatid gene conversion is a prominent double-strand break repair pathway in mammalian cells. *EMBO J* 19:3398–3407.

90. Raynard SS, Bussen WW, Sung PP (2006) A double Holliday junction dissolvasome comprising BLM, topoisomerase IIIalpha, and BLAP75. *J Biol Chem* 281:13861–13864.

91. Ward JD, Barber LJ, Petalcorin MI, Yanowitz J, Boulton SJ (2007) Replication blocking lesions present a unique substrate for homologous recombination. *EMBO J* 26:3384–3396.

92. Smith CE, Llorente B, Symington LS (2007) Template switching during break-induced replication. *Nature* 447:102–105.

93. Agmon N, Pur S, Liefshitz B, Kupiec M (2009) Analysis of repair mechanism choice during homologous recombination. *Nucleic Acids Res* 37:5081–5092.

94. Lin Y, Lukacsovich T, Waldman AS (1999) Multiple pathways for repair of DNA double-strand breaks in mammalian chromosomes. *Mol Cell Biol* 19:8353–8360.

95. Schmid CW (1996) Alu: structure, origin, evolution, significance and function of one-tenth of human DNA. *Prog Nucleic Acid Res Mol Biol* 53:283–319.

96. Batzer MA, Deininger PL (2002) Alu repeats and human genomic diversity. *Nat Rev Genet* 3:370–379.

97. Vasileva A, Jessberger R (2005) Precise hit: adeno-associated virus in gene

targeting. *Nat Rev Microbiol* 3:837–847.

98. Li X, Heyer W-D (2008) Homologous recombination in DNA repair and DNA damage tolerance. *Cell Res* 18:99–113.

99. Pâques F, Haber JE (1999) Multiple pathways of recombination induced by double-strand breaks in Saccharomyces cerevisiae. *Microbiol Mol Biol Rev* 63:349–404.

100. Bennardo N, Cheng A, Huang N, Stark JM (2008) Alternative-NHEJ is a mechanistically distinct pathway of mammalian chromosome break repair. *PLoS Genet* 4:e1000110.

101. Roth DB, Wilson JH (1986) Nonhomologous recombination in mammalian cells: role for short sequence homologies in the joining reaction. *Mol Cell Biol* 6:4295–4304.

102. Fattah F et al. (2010) Ku regulates the non-homologous end joining pathway choice of DNA double-strand break repair in human somatic cells. *PLoS Genet* 6:e1000855.

103. Jolly CJ, Cook AJL, Manis JP (2008) Fixing DNA breaks during class switch recombination. *J Exp Med* 205:509–513.

104. Yan CT et al. (2007) IgH class switching and translocations use a robust non-classical end-joining pathway. *Nature* 449:478–482.

105. Khanna KK et al. (1998) ATM associates with and phosphorylates p53: mapping the region of interaction. *Nat Genet* 20:398–400.

106. Khanna KK, Shiloh Y (2009) *The DNA Damage Response* (Springer).

107. You Z, Bailis JM (2010) DNA damage and decisions: CtIP coordinates DNA repair and cell cycle checkpoints. *Trends Cell Biol* 20:402–409.

108. Yun MH, Hiom K (2009) CtIP-BRCA1 modulates the choice of DNA double-strand-break repair pathway throughout the cell cycle. *Nature* 459:460–463.

109. Yun MH, Hiom K (2009) Understanding the functions of BRCA1 in the DNA-damage response. *Biochem Soc Trans* 37:597–604.

110. Singer B, Grunberger D (1983) *Molecular biology of mutagens and carcinogens* (Plenum Pub Corp).

111. Fu D, Calvo JA, Samson LD (2012) Balancing repair and tolerance of DNA damage caused by alkylating agents. *Nat Rev Cancer* 12:104–120.

112. Friedberg EC, McDaniel LD, Schultz RA (2004) The role of endogenous and exogenous DNA damage and mutagenesis. *Curr Opin Genet Dev* 14:5–10.

113. Hendricks CA et al. (2002) The S. cerevisiae Mag1 3-methyladenine DNA glycosylase modulates susceptibility to homologous recombination. *DNA Repair (Amst)* 1:645–659.

114. Larson K, Sahm J, Shenkar R, Strauss B (1985) Methylation-induced blocks to in vitro DNA replication. *Mutat Res* 150:77–84.

115. Loechler EL, Green CL, Essigmann JM (1984) In vivo mutagenesis by O6-methylguanine built into a unique site in a viral genome. *Proc Natl Acad Sci USA* 81:6271–6275.

116. Nowosielska A, Marinus MG (2008) DNA mismatch repair-induced double-strand breaks. *DNA Repair (Amst)* 7:48–56.

117. Drabløs F et al. (2004) Alkylation damage in DNA and RNA--repair mechanisms and medical significance. *DNA Repair (Amst)* 3:1389–1407.

118. Beranek DT (1990) Distribution of methyl and ethyl adducts following alkylation with monofunctional alkylating agents. *Mutat Res* 231:11–30.

119. Maher VM et al. (1990) Alkylation damage, DNA repair and mutagenesis in human cells. *Mutat Res* 233:235–245.

120. Schiestl RH, Gietz RD, Mehta RD, Hastings PJ (1989) Carcinogens induce intrachromosomal recombination in yeast. *Carcinogenesis* 10:1445–1455.

121. Lonkar P, Dedon PC (2011) Reactive species and DNA damage in chronic inflammation: reconciling chemical mechanisms and biological fates. *Int J Cancer* 128:1999–2009.

122. Hanahan D, Weinberg RA (2011) Hallmarks of cancer: the next generation. *Cell* 144:646–674.

123. Fox JG, Ge Z, Whary MT, Erdman SE, Horwitz BH (2011) Helicobacter hepaticus infection in mice: models for understanding lower bowel inflammation and cancer. *Mucosal Immunol* 4:22–30.

124. Ohshima H, Tatemichi M, Sawa T (2003) Chemical basis of inflammation-induced carcinogenesis. *Arch Biochem Biophys* 417:3–11.

125. Balkwill F, Mantovani A (2001) Inflammation and cancer: back to Virchow? *Lancet* 357:539–545.

126. Shacter E, Weitzman SA (2002) Chronic inflammation and cancer. *Oncology (Williston Park, NY)* 16:217–26– 229– discussion 230–2.

127. Farrell RJ, Peppercorn MA (2002) Ulcerative colitis. *Lancet* 359:331–340.

128. Asaka M, Takeda H, Sugiyama T, Kato M (1997) What role does Helicobacter pylori play in gastric cancer? *Gastroenterology* 113:S56–60.

129. Ebert MP, Yu J, Sung JJ, Malfertheiner P (2000) Molecular alterations in gastric cancer: the role of Helicobacter pylori. *Eur J Gastroenterol Hepatol* 12:795–798.

130. Nathan C, Shiloh MU (2000) Reactive oxygen and nitrogen intermediates in the relationship between mammalian hosts and microbial pathogens. *Proc Natl Acad Sci USA* 97:8841–8848.

131. Nathan CF (1987) Secretory products of macrophages. *J Clin Invest* 79:319–326.

132. Dedon PC, Tannenbaum SR (2004) Reactive nitrogen species in the chemical biology of inflammation. *Arch Biochem Biophys* 423:12–22.

133. Uppu RM, Cueto R, Squadrito GL, Salgo MG, Pryor WA (1996) Competitive reactions of peroxynitrite with 2"-deoxyguanosine and 7,8-dihydro-8-oxo-2-"deoxyguanosine (8-oxodG): relevance to the formation of 8-oxodG in DNA exposed to peroxynitrite. *Free Radic Biol Med* 21:407–411.

134. Fasullo M, Dave P, Rothstein R (1994) DNA-damaging agents stimulate the formation of directed reciprocal translocations in Saccharomyces cerevisiae. *Mutat Res* 314:121–133.

135. Schiestl RH (1993) Nonmutagenic carcinogens induce intrachromosomal recombination in dividing yeast cells. *Environ Health Perspect* 101 Suppl 5:179–184.

136. Lambert IB, Singer TM, Boucher SE, Douglas GR (2005) Detailed review of transgenic rodent mutation assays. *Mutat Res* 590:1–280.

137. Hellgren D (1992) Mutagen-induced recombination in mammalian cells in vitro. *Mutat Res* 284:37–51.

138. Pierce AJ, Johnson RD, Thompson LH, Jasin M (1999) XRCC3 promotes homology-directed repair of DNA damage in mammalian cells. *Genes Dev* 13:2633–2638.

139. Liskay RM, Letsou A, Stachelek JL (1987) Homology requirement for efficient gene conversion between duplicated chromosomal sequences in mammalian cells. *Genetics* 115:161–167.

140. Hellgren D, Sahlén S, Lambert B (1989) Mutagen-induced recombination between stably integrated neo gene fragments in CHO and EM9 cells. *Mutat Res* 226:1–8.

141. Bollag RJ, Liskay RM (1991) Direct-repeat analysis of chromatid interactions during intrachromosomal recombination in mouse cells. *Mol Cell Biol* 11:4839–4845.

142. Hendricks CA et al. (2003) Spontaneous mitotic homologous recombination at an enhanced yellow fluorescent protein (EYFP) cDNA direct repeat in transgenic mice. *Proc Natl Acad Sci USA* 100:6325–6330.

143. Reliene R, Bishop AJR, Aubrecht J, Schiestl RH (2004) In vivo DNA deletion assay to detect environmental and genetic predisposition to cancer. *Methods Mol Biol* 262:125–139.

144. Melvold RW (1971) Spontaneous somatic reversion in mice. Effects of parental genotype on stability at the p-locus. *Mutat Res* 12:171–174.

145. Dobrovolsky VN, Casciano DA, Heflich RH (1999) Tk+/- mouse model for detecting in vivo mutation in an endogenous, autosomal gene. *Mutat Res* 423:125–136.

146. Vomiero-Highton G, Heddle JA (1995) An assay for loss of heterozygosity in vivo at the Dlb-1 locus. *Mutagenesis* 10:381–384.

147. Bryce SM, Bemis JC, Dertinger SD (2008) In vivo mutation assay based on the endogenous Pig-a locus. *Environ Mol Mutagen* 49:256–264.

148. Gossen JA et al. (1989) Efficient rescue of integrated shuttle vectors from transgenic mice: a model for studying mutations in vivo. *Proc Natl Acad Sci USA* 86:7971–7975.

149. Stiegler GL, Stillwell LC (1993) Big Blue transgenic mouse lacI mutation analysis. *Environ Mol Mutagen* 22:127–129.

150. Dollé ME, Martus HJ, Gossen JA, Boerrigter ME, Vijg J (1996) Evaluation of a plasmid-based transgenic mouse model for detecting in vivo mutations. *Mutagenesis* 11:111–118.

151. Swiger RR et al. (1999) The cII locus in the MutaMouse system. *Environ Mol Mutagen* 34:201–207.

152. Nohmi T et al. (1996) A new transgenic mouse mutagenesis test system using Spi- and 6-thioguanine selections. *Environ Mol Mutagen* 28:465–470.

153. Jones IM, Burkhart-Schultz K, Carrano AV (1985) A method to quantify spontaneous and in vivo induced thioguanine-resistant mouse lymphocytes. *Mutat Res* 147:97–105.

154. Thybaud V et al. (2003) In vivo transgenic mutation assays. *Mutat Res* 540:141–151.

155. Hsu C-H, Stedeford T (2010) *Cancer Risk Assessment* (Wiley).

156. Hill KA et al. (2004) Spontaneous mutation in Big Blue mice from fetus to old age: tissue-specific time courses of mutation frequency but similar mutation types. *Environ Mol Mutagen* 43:110–120.

157. Stuart GR, Oda Y, Boer JG, Glickman BW (2000) No change in spontaneous mutation frequency or specificity in dietary restricted mice. *Carcinogenesis* 21:317–319.

158. Stuart GR, Oda Y, de Boer JG, Glickman BW (2000) Mutation frequency and specificity with age in liver, bladder and brain of lacI transgenic mice. *Genetics* 154:1291–1300.

159. Ono T et al. (2000) Age-associated increase of spontaneous mutant frequency and molecular nature of mutation in newborn and old lacZ-transgenic mouse. *Mutat Res* 447:165–177.

160. Dollé ME, Snyder WK, Gossen JA, Lohman PH, Vijg J (2000) Distinct spectra of somatic mutations accumulated with age in mouse heart and small intestine. *Proc Natl Acad Sci USA* 97:8403–8408.

161. Wijnhoven SW et al. (1998) Carcinogen-induced loss of heterozygosity at the Aprt locus in somatic cells of the mouse. *Proc Natl Acad Sci USA* 95:13759–13764.

162. Vrieling H et al. (1999) Heterozygous Aprt mouse model: detection and study of a broad range of autosomal somatic mutations in vivo. *Environ Mol Mutagen* 34:84–89.

163. Ponomareva ON, Rose JA, Lasarev M, Rasey J, Turker MS (2002) Tissue-specific deletion and discontinuous loss of heterozygosity are signatures for the mutagenic effects of ionizing radiation in solid tissues. *Cancer Res* 62:1518–1523.

164. Van Sloun PP et al. (1998) Determination of spontaneous loss of heterozygosity mutations in Aprt heterozygous mice. *Nucleic Acids Res* 26:4888–4894.

165. Jacobson-Kram D, Keller KA (2006) *Toxicological Testing Handbook* (CRC Pressl Llc).

166. Heddle JA et al. (2000) In vivo transgenic mutation assays. *Environ Mol Mutagen* 35:253–259.

167. Okayasu I et al. (2006) Significant increase of colonic mutated crypts correlates with age in sporadic cancer and diverticulosis cases, with higher frequency in the left- than right-side colorectum. *Cancer Sci* 97:362–367.

168. Brown AD, Claybon AB, Bishop AJR (2011) A conditional mouse model for measuring the frequency of homologous recombination events in vivo in the absence of essential genes. *Mol Cell Biol* 31:3593–3602.

169. Weeda G et al. (1997) Disruption of mouse ERCC1 results in a novel repair syndrome with growth failure, nuclear abnormalities and senescence. *Curr Biol* 7:427–439.

170. Myhr BC (1991) Validation studies with Muta Mouse: a transgenic mouse model for detecting mutations in vivo. *Environ Mol Mutagen* 18:308–315.

171. Brilliant MH, Gondo Y, Eicher EM (1991) Direct molecular identification of the mouse pink-eyed unstable mutation by genome scanning. *Science* 252:566–569.

172. Gondo Y et al. (1993) High-frequency genetic reversion mediated by a DNA duplication: the mouse pink-eyed unstable mutation. *Proc Natl Acad Sci USA* 90:297–301.

173. Rosemblat S et al. (1994) Identification of a melanosomal membrane protein encoded by the pink-eyed dilution (type II oculocutaneous albinism) gene. *Proc Natl Acad Sci USA* 91:12071–12075.

174. Searle AG (1977) The use of pigment loci for detecting reverse mutations in somatic cells of mice. *Arch Toxicol* 38:105–108.

175. Bishop AJ, Barlow C, Wynshaw-Boris AJ, Schiestl RH (2000) Atm deficiency causes an increased frequency of intrachromosomal homologous recombination in mice. *Cancer Res* 60:395–399.

176. Bishop AJ, Kosaras B, Sidman RL, Schiestl RH (2000) Benzo(a)pyrene and X-rays induce reversions of the pink-eyed unstable mutation in the retinal pigment epithelium of mice. *Mutat Res* 457:31–40.

177. Aubrecht J, Secretan MB, Bishop AJ, Schiestl RH (1999) Involvement of p53 in X-ray induced intrachromosomal recombination in mice. *Carcinogenesis* 20:2229–2236.

178. Jalili T, Murthy GG, Schiestl RH (1998) Cigarette smoke induces DNA deletions in the mouse embryo. *Cancer Res* 58:2633–2638.

179. Schiestl RH, Khogali F, Carls N (1994) Reversion of the mouse pink-eyed unstable mutation induced by low doses of x-rays. *Science* 266:1573–1576.

180. Bishop AJR et al. (2003) Atm-, p53-, and Gadd45a-deficient mice show an increased frequency of homologous recombination at different stages during development. *Cancer Res* 63:5335–5343.

181. Wiktor-Brown DM, Hendricks CA, Olipitz W, Engelward BP (2006) Age-dependent accumulation of recombinant cells in the mouse pancreas revealed by in situ fluorescence imaging. *Proc Natl Acad Sci USA* 103:11862–11867.

182. Wiktor-Brown DM, Hendricks CA, Olipitz W, Rogers AB, Engelward BP (2006) Applications of fluorescence for detecting rare sequence rearrangements in vivo. *Cell Cycle* 5:2715–2719.

183. Wiktor-Brown DM, Olipitz W, Hendricks CA, Rugo RE, Engelward BP (2008) Tissue-specific differences in the accumulation of sequence rearrangements with age. *DNA Repair (Amst)* 7:694–703.

184. Wiktor-Brown DM, Sukup-Jackson MR, Fakhraldeen SA, Hendricks CA, Engelward BP (2011) p53 null fluorescent yellow direct repeat (FYDR) mice have normal levels of homologous recombination. *DNA Repair (Amst)* 10:1294–1299.

185. Niu Y et al. (2010) Irradiated esophageal cells are protected from radiation-induced recombination by MnSOD gene therapy. *Radiat Res* 173:453–461.

186. Ludwig T, Chapman DL, Papaioannou VE, Efstratiadis A (1997) Targeted mutations of breast cancer susceptibility gene homologs in mice: lethal phenotypes of Brca1, Brca2, Brca1/Brca2, Brca1/p53, and Brca2/p53 nullizygous embryos. *Genes Dev* 11:1226–1241.

187. Thompson D, Easton DF, Breast Cancer Linkage Consortium (2002) Cancer Incidence in BRCA1 mutation carriers. *J Natl Cancer Inst* 94:1358–1365.

188. Hahn SA et al. (2003) BRCA2 germline mutations in familial pancreatic carcinoma. *J Natl Cancer Inst* 95:214–221.

189. Couch FJ et al. (2005) Germ line Fanconi anemia complementation group C mutations and pancreatic cancer. *Cancer Res* 65:383–386.

190. Ford D et al. (1998) Genetic heterogeneity and penetrance analysis of the BRCA1 and BRCA2 genes in breast cancer families. The Breast Cancer Linkage Consortium. *Am J Hum Genet* 62:676–689.

191. Difilippantonio MJ et al. (2000) DNA repair protein Ku80 suppresses chromosomal aberrations and malignant transformation. *Nature* 404:510–514.

192. Rockwood LD, Nussenzweig A, Janz S (2003) Paradoxical decrease in mutant frequencies and chromosomal rearrangements in a transgenic lacZ reporter gene in Ku80 null mice deficient in DNA double strand break repair. *Mutat Res* 529:51–58.

193. Hill KA et al. (2005) Tissue-specific time courses of spontaneous mutation frequency and deviations in mutation pattern are observed in middle to late adulthood in Big Blue mice. *Environ Mol Mutagen* 45:442–454.

194. Soriano P (1999) Generalized lacZ expression with the ROSA26 Cre reporter strain. *Nat Genet* 21:70–71.

195. Covo S, Ma W, Westmoreland JW, Gordenin DA, Resnick MA (2012) Understanding the origins of UV-induced recombination through manipulation of sister chromatid cohesion. *Cell Cycle* 11:3937–3944.

196. Mangerich A et al. (2012) Infection-induced colitis in mice causes dynamic and tissue-specific changes in stress response and DNA damage leading to colon cancer. *Proc Natl Acad Sci USA* 109:E1820–9.

197. Lisiane B Meira JMBSLGC-WLBPDBBHRABRCAM-EJLMDBSPCDJGFLDS (2008) DNA damage induced by chronic inflammation contributes to colon carcinogenesis in mice. *J Clin Invest* 118:2516.

198. Wyatt MD, Pittman DL (2006) Methylating agents and DNA repair responses: Methylated bases and sources of strand breaks. *Chem Res Toxicol* 19:1580–1594.

199. Erdman SE et al. (2009) Nitric oxide and TNF-alpha trigger colonic inflammation and carcinogenesis in Helicobacter hepaticus-infected, Rag2-deficient mice. *Proc Natl Acad Sci USA* 106:1027–1032.

200. Erdman SE et al. (2003) CD4+ CD25+ regulatory T lymphocytes inhibit microbially induced colon cancer in Rag2-deficient mice. *Am J Pathol* 162:691–702.

201. Tomczak MF et al. (2006) Inhibition of Helicobacter hepaticus-induced colitis by IL-10 requires the p50/p105 subunit of NF-kappa B. *J Immunol* 177:7332–7339.

202. Rao VP, Poutahidis T, Fox JG, Erdman SE (2007) Breast cancer: should gastrointestinal bacteria be on our radar screen? *Cancer Res* 67:847–850.

203. García A et al. (2002) Hepatobiliary inflammation, neoplasia, and argyrophilic bacteria in a ferret colony. *Vet Pathol* 39:173–179.

204. Ge Z et al. (2005) Cytolethal distending toxin is essential for Helicobacter hepaticus colonization in outbred Swiss Webster mice. *Infect Immun* 73:3559–3567.

205. Coussens LM, Werb Z (2002) Inflammation and cancer. *Nature* 420:860–867.

206. Farrow B, Evers BM (2002) Inflammation and the development of pancreatic cancer. *Surg Oncol* 10:153–169.

207. Itzkowitz SH, Yio X (2004) Inflammation and cancer IV. Colorectal cancer in inflammatory bowel disease: the role of inflammation. *Am J Physiol Gastrointest Liver Physiol* 287:G7–17.

208. Levin B (1992) Ulcerative colitis and colon cancer: biology and surveillance. *J Cell Biochem Suppl* 16G:47–50.

209. Wiseman H, Halliwell B (1996) Damage to DNA by reactive oxygen and nitrogen species: role in inflammatory disease and progression to cancer. *Biochem J* 313 (Pt 1):17–29.

210. Loftus EV (2004) Clinical epidemiology of inflammatory bowel disease: Incidence, prevalence, and environmental influences. *Gastroenterology* 126:1504–1517.

211. Harpaz N, Polydorides AD (2010) Colorectal Dysplasia in Chronic Inflammatory Bowel Disease: Pathology, Clinical Implications, and Pathogenesis.

212. Danese S (2011) Ulcerative colitis: a cinderella story. *Curr Drug Targets* 12:1372.

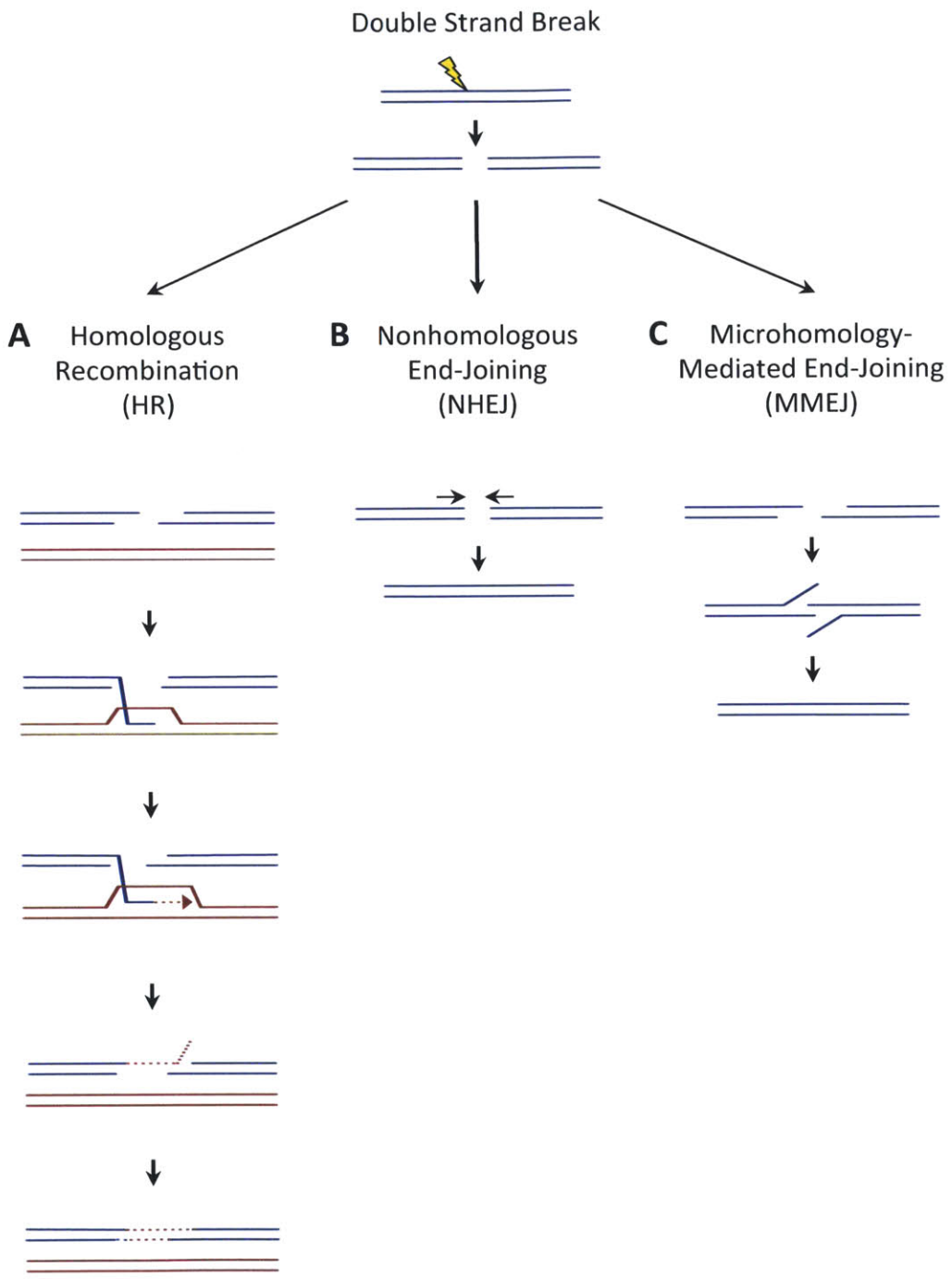

Figure 1-1. Basic Mechanisms of DSB Repair. (A) HR utilizes homologous sequences on the sister chromatid or homologous chromosome as templates for repair. (B) NHEJ directly ligates the two double-stranded ends, while (C) MMEJ utilizes small areas of homology on the damaged strand to initiate repair of the DSB.

Table 1-1. A Subset of DNA Repair Proteins

	Protein	Activity	Repair Function
	ATM	Recognizes double strand breaks	Phosphorylates resection proteins
	ATR	Recognizes double strand breaks	Phosphorylates resection proteins
Upstream Regulator			
NHEJ	53BP1	Mediator protein	Limits dsDNA end resection and promoted NHEJ
Damage-response	γH2AX	H2A/H2AX isoform formed after DSB signaling	Mediates retention of DSB-responsive proteins on DSB associated chromatin
	BLM	Multiple roles of DNA damage signaling and HR; 3'→5' helicase	Part of the BRCA1-associated genome surveillance complex; required for Rad51 focus formation
	MDC1	Mediator protein; cell-cycle arrest in response to DNA damage	Binds γH2AX; promotes RNF8/168 MRN binding
	RNF8	Ubiquitin ligase	Ubiquitinates proteins at DSBs; mediates BRCA1/53BP1 recruitment to DSBs
HR	BRCA1	Mediator and enzymatic activities	Antagonizes 53BP1; interactions with CtIP
Repair Machinery			
NHEJ	Ku	Ku70-Ku80 heterodimer; dsDNA binding	Tethers DSB ends and protects from resection
	DNA-PK_{cs}	Binds to DSB with Ku to form DNA-PK	Activated by Ku-dsDNA complexes to promote NHEJ
	Artemis	Required for V(D)J recombination, may be used for DSB end processing prior to NHEJ	May stimulate endonucleolytic activity on 5' and 3' hairpins and overhangs
	LIG4	DNA ligase	DSB end ligation activity during NHEJ and is dependent on DNA-PK assembly
	XRCC4	Scaffold protein that enhances LIG4 activity	Structural facilitators of NHEJ by binding DNA and LIG4
	XLF	Scaffold proteins	Enables XRCC4 access to DNA at DSB
HR	MRN	Enzymatic (MRE11), structural (RAD50), and adaptor/checkpoint (NBS1)	MRE11, endonuclease; 3'→5' exonuclease; RAD50, structural maintenance of chromosomes; NBS1, ATM kinase interactions
	CtIP		Cooperates with MRN to initiate DSB resection and associated with BRCA1
	EXO1	5'→3' exonuclease	Mediates DSB resection
	RPA	Stabilizes and protects ssDNA	Binds ssDNA to prevent degradation and annealing
	BRCA2	Recombination mediator	Assists RAD51 loading onto RPA-coated ssDNA
	PALB2	Scaffold	Facilitates BRCA1-BRCA2 interactions; promotes BRCA2 recruitment to DSB
	RAD51	Recombinase	Homology searching and DNA nucleoprotein filaments
FA Pathway	FANCC	Subunit of FA core complex (E3 ligase)	Promotes HR-dependent repair of DNA ICLs; suppresses toxic NHEJ events in S-phase
HR Regulators			
Regulators of HR Execution	PARI	Helicase	Prevents HR by RAD51-ssDNA filament disruption
	FBH1	Helicase	Prevents harmful HR
	RECQL5	RecQ family helicase	Prevents harmful HR by RAD51-ssDNA filament disruption; recognizes strand break with 3'OH
	ERCC1/XPF	Structure-specific endonuclease	Removes ssDNA overhangs after SSA or SDSA, responsible for 5' incision
	RTEL1	Iron-sulfur helicase	Promotes SDSA and suppresses crossing over by disrupting D-loops
	MUS81-EME1/EME2	Structure-specific endonuclease	Produces crossovers by D-loop cleavage, and processes Holliday junctions
	GEN1	Structure-specific endonuclease	Holliday junction dissolution (with/without crossover)
	BLM-TOPIIIα	RecQ helicase and topoisomerase	Holliday junction dissolution (no crossover)
	CDK enzymes	Cyclin-dependent protein kinases	S/G_2 phase phosphorylation event promote DSB resection and mediates protein-protein interactions through the cell cycle

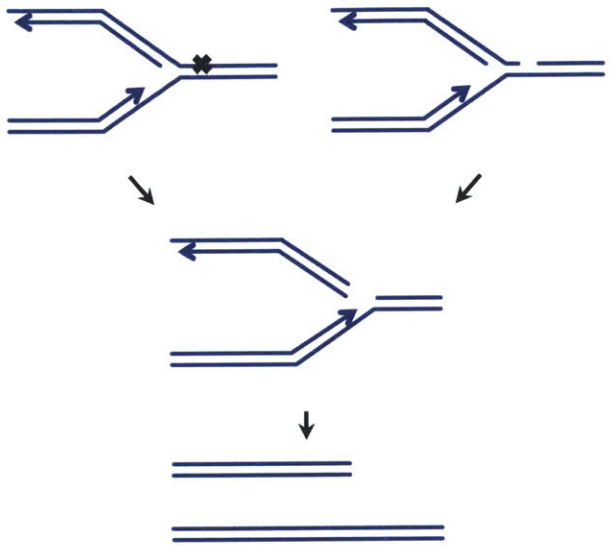

Figure 1-2. Replication Fork Collapse Leading to One-ended Double-Strand Break. When a replication fork encounters a replication blocking lesion or single-strand gap, a double-stranded break forms that can only be repaired through HR.

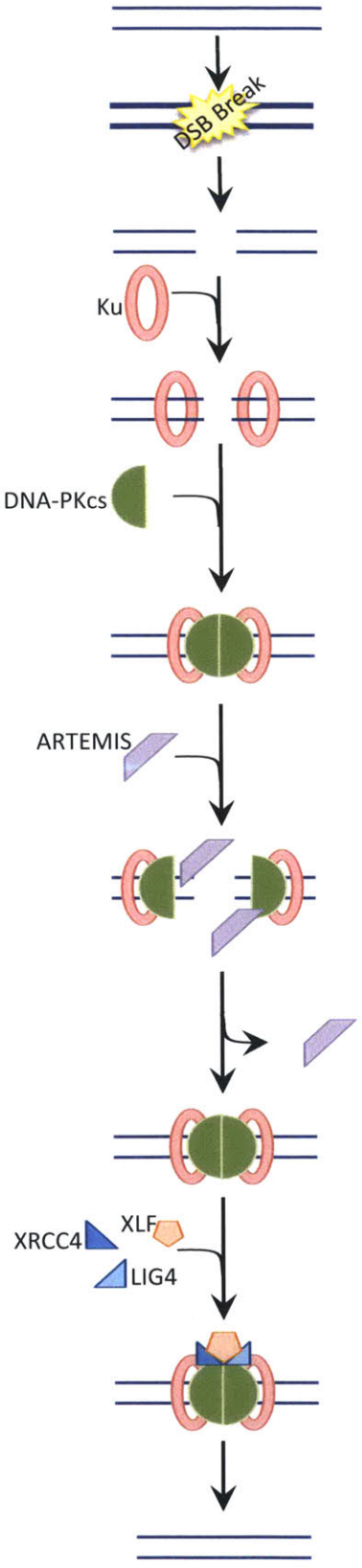

Figure 1-3. Nonhomologous End-Joining (NHEJ) Pathway. The double strand break is recognized, processed, and directly ligated in the NHEJ pathway with the aid of many repair proteins. The action of select proteins is outlined.

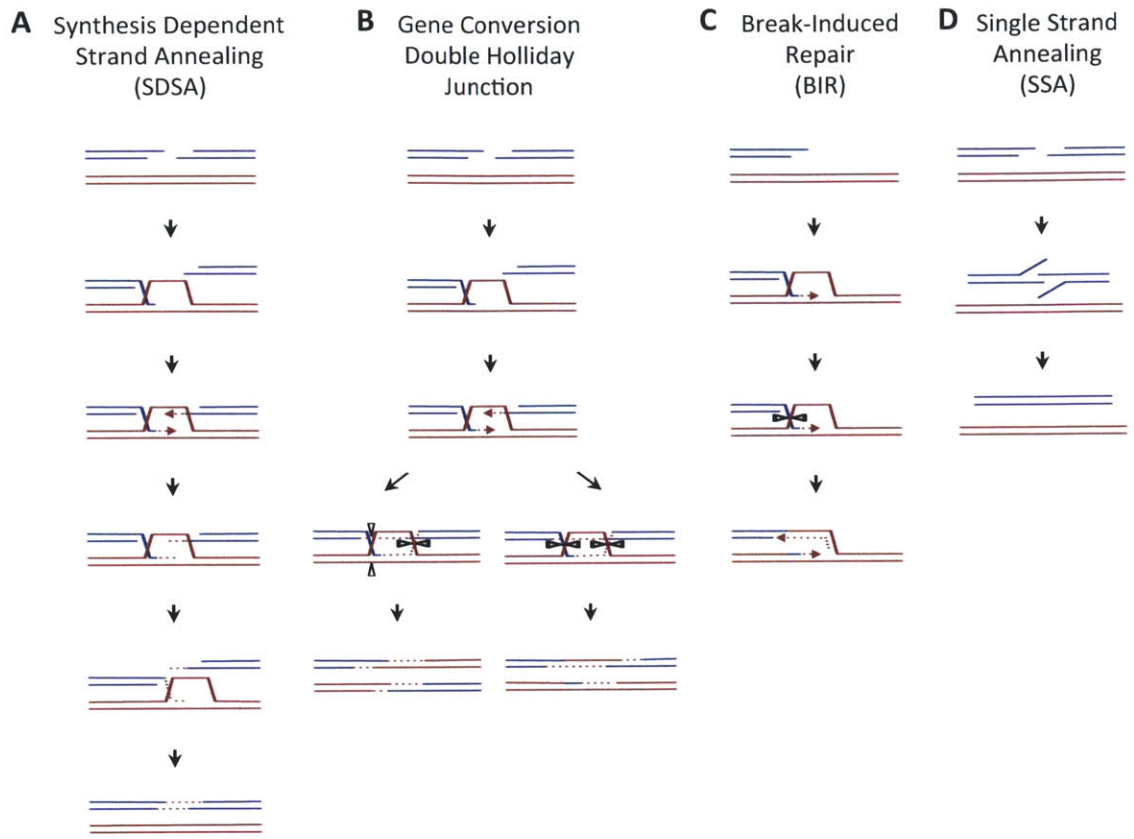

Figure 1-4. Subpathways of Homology Directed Repair. (A) Synthesis Dependent Strand Annealing: Double stranded ends undergo resection to yield a 3' overhang followed by homology searching and strand invasion to enable DNA synthesis and the formation of a Holliday Junction. Branch migration enables further DNA synthesis and leads to release of the newly synthesized DNA and subsequent annealing to fully repair the DSB. (B) Gene Conversion with Double Holliday Junction: Double stranded ends undergo resection to yield a 3' overhang followed by homology searching and strand invasion to enable DNA synthesis and the formation of a Holliday Junction for one DNA end, then the other. The two resultant Holliday Junctions can be cleaved to yield a crossover or a non-crossover product. (C) Break Induced Repair: Double stranded ends undergo resection to yield a 3' overhang followed by homology searching and strand invasion to enable DNA synthesis and the formation of a Holliday Junction. Resolution of the Holliday Junction restores the broken replication fork. (D) Single Strand Annealing: Double stranded ends undergo resection to yield a 3' overhang followed by homology searching across the DSB gap. Annealing of DNA ends repairs the DSB.

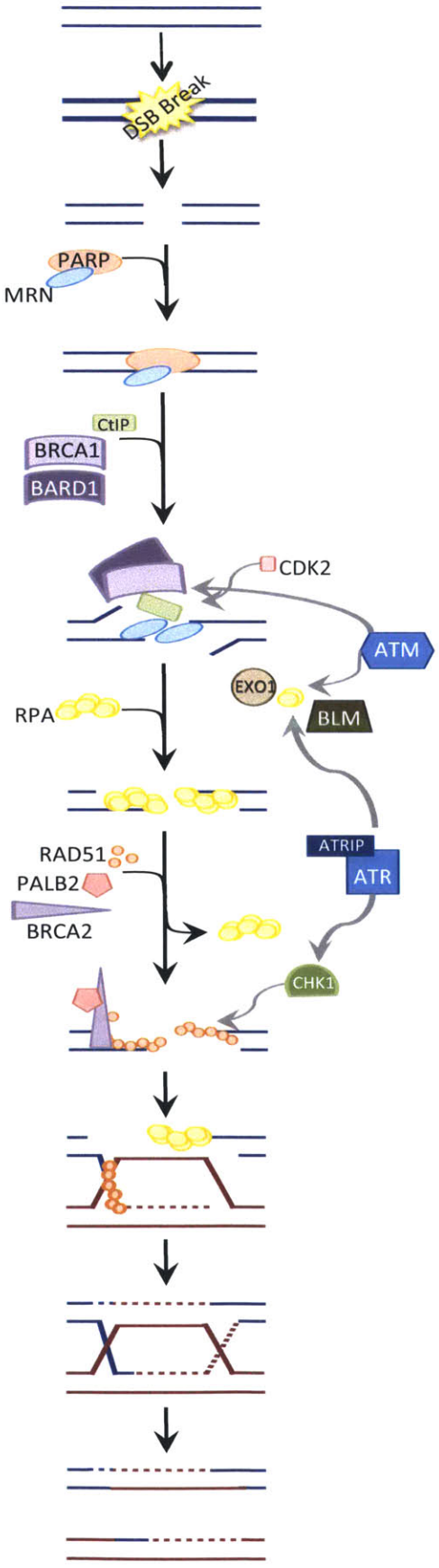

Figure 1-5. Homologous Recombination (HR) Pathway. The double strand break is recognized, process, and repaired. The action of select proteins is outlined.

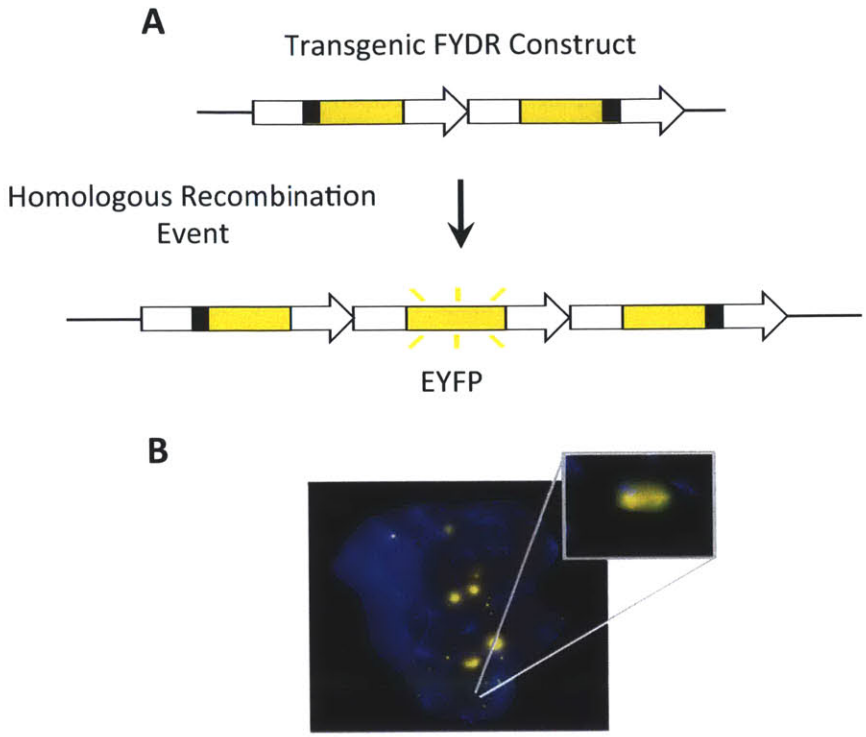

Figure 1-6. FYDR HR Reporter System *In Vivo*. (A) Arrangement of the FYDR direct repeat recombination substrate. Large arrows indicate expression cassettes; yellow boxes indicate EYFP coding sequences with black boxes show positions of deleted sequences (deletion sizes not to scale). (B) Image for representative FYDR pancreas and an individual fluorescent cell. Yellow fluorescent foci image complied with image of nuclei stained with Hoechst.

Chapter II

Deficiencies in KU and ERCC1 Increase Susceptibility to Homologous Recombination in FYDR mice

Chapter II

2.1 Abstract

Cellular mechanisms have evolved to repair particular DNA damage through a variety of pathways. While HR, NHEJ, and MMR all repair DSBs, each pathway preferentially repairs certain DNA damage at particular points in the cell cycle. When one of these repair pathways is unavailable, we show that another DNA repair pathway can repair the damage. Utilizing the FYDR HR reporter mice, we show deficiencies in Ku86, a vital NHEJ repair protein, leads to a dramatic increase in HR.

While ERCC1 is a protein known to play a part in NER, we investigated its effect on DSB repair through MMEJ. Though our results support the role of ERCC1 in MMEJ, unrepaired lesions that require NER may induce replication fork breakdown, which requires homology directed repair to restart the replication fork. Our model for MMEJ utilizes ERCC1 in clipping the 3' overhangs resulting from joining areas of microhomology (~6 bp) in single-stranded DNA. Deficiencies in ERCC1 and MMEJ results in more DSBs to repaired by HR. We see this shift in repair pathway reflected in an increase in HR events in *Ercc1*$^{-/\Delta}$ *FYDR*$^{Y/+}$ mice.

2.2 Introduction

The genome is under constant stress from endogenous and exogenous factors that cause damage thought to contribute to the detrimental effects of aging (1); as a result, many different DNA repair pathways have evolved to combat this damage. Bulky, helix-distorting lesions such as thymine dimers resulting from UV-induced damage (linked to skin cancer) are removed individually through NER that occurs during G_0 and G_1 (2). Defects in the NER pathway are associated with a dramatic increase in skin cancer seen in patients with Xeroderma pigmentosum (XP) (3-5). Improper DNA repair via NER can lead to nicks or incomplete removal of the damaged nucleotide, which causes replication fork breakdown during cell division (6). These single-ended double-stranded ends are dangerous because they may induce chromosomal translocations or deletions if they are repaired improperly via NHEJ, HR, SSA, or MMEJ (7-10). DSBs are particularly dangerous during cell division since mitosis is unable to progress without repair.

The two major mechanisms of DSB repair in eukaryotes are HR and NHEJ (11). HR is an error-free mechanism where lost genetic information is usually recovered from a homologous sequence on the sister chromatid. As a consequence, HR is usually restricted to the S and G_2 phases of the cell cycle. Collapsed replication forks are repaired during replication as homology directed repair is used to reinsert the partially replicated double-stranded end. Alternatively, NHEJ ligates the double-stranded ends of a break without regard to sequence, thus it is not restricted to proliferating cells (12).

Since NHEJ does not use a template to guide repair, damaged bases cannot be replaced and inappropriate ends may be rejoined, causing a chromosomal translocation (13, 14). Despite the potential for translocations and deletions as a result of repair, NHEJ is primarily error-free (15, 16).

Alternative error-prone mechanisms for DNA repair include SSA and MMEJ that align broken ends by using homologous sequences near the DSB. The SSA repair process utilizes areas of homology of 25 bp or greater, while MMEJ can utilize as little as 6 bp of homology (17, 18). After the complementary portions are aligned, the ERCC1-XPF endonuclease removes extraneous 3' flaps of nonhomologous sequences from the ends, enabling DNA synthesis and ligation or repair completion. These repair mechanisms automatically result in a genetic deletion. While SSA and MMEJ are similar mechanistically, they both require a different set of proteins to complete repair. In *S. cerevisiae*, SSA is Rad52-dependent while MMEJ is Rad52-independent and both require ERCC1-XPF homologue, Rad10-Rad1. MMEJ also requires Mre11-Rad50-XRS2, flap endonuclease Sae2, and mismatch repair proteins Msh2 and Pms1 (19-21). SSA is utilized in mammalian cells to repair DSBs (22), however mammalian cells that are deficient in NHEJ are still able to undergo end-joining, suggesting an alternative end-joining pathway (23). Mammalian NHEJ deficient cells are able to support end-joining by utilizing microhomology at the broken ends (18, 24). The exact pathway requirements of MMEJ are not yet known in mammalian cells.

KU Protein is Necessary for NHEJ

The KU heterodimeric protein mediates a number of cellular processes including DNA repair, telomere maintenance, V(D)J recombination, transcription, and apoptosis (25, 26). When involved in DNA repair, the KU protein binds double-stranded DNA to initiate the NHEJ pathway in G_0 and G_1. Though KU is most often implicated in the binding of blunt-ended double-stranded DNA, it is also capable of binding double-stranded DNA with 3′ overhangs, 5′ overhangs (27-31).

Homologues of the KU protein are conserved evolutionarily in bacteria (32), yeast (33), and mammalian cells (34). Eukaryotic KU is a heterodimer of Ku70 and Ku80, so named for their molecular weights, that attaches to both blunt ends of a double-stranded DNA break and is essential for NHEJ repair (35). KU has been shown to translocate along double-stranded DNA, thus allowing multiple KU proteins to bind the DNA (29). Once bound to the DNA, KU enables the binding of DNA-PK_{CS} to form DNA-PK, which is necessary to phosphorylate proteins downstream of the NHEJ pathway (25).

The early binding of KU onto double-stranded breaks may maintain the DNA ends in proximity to each other to prevent gross translocations (13, 15, 25). In *S. cerevisiae*, the rate of 5′→3′ resection is dramatically increased at a DSB in the absence of KU (36). These data indicate that KU may protect the broken DNA ends from unnecessary resection, in addition to its function of attracting other proteins to the damage and providing a scaffold for stable binding (25). The consequence of KU readily binding to DSBs is that the damage is shunted to the NHEJ pathway, rather than further

processed for repair via HR. *In vitro* studies using cell lines deficient in various repair processes have shown competition and compensation between NHEJ and HR (37, 38). Strikingly, cell lines deficient in KU showed a greater increase in HR than cell lines with defects in other downstream NHEJ proteins, supporting KU's role in directing DSB repair through NHEJ (37).

ERCC1 Protein Plays a Role in Many Pathways

The excision repair cross-complementation group 1 (ERCC1) is a structure specific endonuclease that plays a part in a number of DNA repair pathways (4, 39). Since this protein is involved in multiple repair mechanisms, mutations in this gene convey an increased risk of cancer (5). ERCC1 recognizes a bend in DNA as seen in Figure 2-1. This type of bend occurs when the DNA bows outwards due to bulky lesions, as 3' nonhomologous flaps form when ssDNA is repaired via SSA or MMEJ, or in a variety of other situations. Once ERCC1 attaches to the specific DNA structure, XPF (also known as ERCC4) binds to it to form the ERCC1-XPF complex (40).

The ERCC1-XPF complex forms a nuclease that is necessary for NER (4, 39). NER removes helix-distorting DNA lesions from the genome through the coordinated action of over 30 proteins (2, 4, 39). The ERCC1-XPF complex cuts the DNA 5' of the damaged DNA base while another protein (XPG) cuts the 3' backbone on the 3' side of the damaged DNA base. The damaged nucleotide, along with approximately 30 bp surrounding it, is removed and DNA polymerases and ligases repair the gap and

backbone. If ERCC1 fails to incise the DNA, the damage will persist, causing replication fork breakdown during mitosis which can only be repaired via HR (41).

Ahmad, *et al.,* have shown that ERCC1 deficient primary mouse embryonic fibroblasts (MEFs) exhibit dramatically decreased survival when exposed to DSB-inducing ionizing radiation *in vitro* (4). Cell survival was rescued by transfection of a plasmid containing functioning human *ERCC1* cDNA, suggesting that ERCC1 plays a role in a direct repair of DSBs (4). When compared to ERCC1 deficient cells, KU deficient MEF cells senesce prematurely, with $Ercc1^{-/-}Ku^{-/-}$ cells showing even earlier senesce (4). In an attempt to investigate the interplay between KU and ERCC1 functions in DSB repair *in vivo*, Niedernhofer and colleagues attempted to breed mice lacking both *Ku* and *Ercc1* (4). While both $Ku^{-/-}$ and $ERCC1^{-/+}$ mice are born with Mendellian frequency, no double mutant pups were recovered. These data suggest a role for ERCC1 in a KU-independent mechanism of DSB repair (4).

DNA Damage is Linked to Progeria

Many human progeroid syndromes are caused by defects in genome maintenance mechanisms. Werner syndrome (i.e. defect in WRN helicase that acts in 3'→5' direction), ataxia telangiectasia (i.e. defect in ATM used in dsDNA break signalling), Cockayne syndrome (i.e. defect in ERCC6 or ERCC8 used in transcription-coupled NER), and trichothiodystrophy (i.e. defect in ERCC2 or ERCC3 in transcription coupled-NER) are examples of segmented progeria diseases associated with defects in DNA repair (42). Deficiencies in these repair pathways allow damage to persist or to be

repaired by an alternative pathway that may result in cancer inducing mutations. The correlation between progeria and DNA repair defects suggests a relationship between the maintenance of genomic integrity and aging.

Mice deficient in KU exhibit progeroid symptoms associated with a profound defect in NHEJ with a lifespan of approximately 10 weeks (43, 44). *Ku80*$^{-/-}$ mice are approximately half the size of WT littermates and MEF cells derived from these mice demonstrate premature senescence (43, 44). The link between the inability to repair DNA damage and growth inhibition is further elucidated in the sensitivity of *Ku80*$^{-/-}$ to DSB inducing ionizing radiation (43). Irradiated *Ku80*$^{-/-}$ mice show dramatic growth retardation compared to un-irradiated *Ku80*$^{-/-}$ mice as well as irradiated WT mice (43).

ERCC1 deficient mice also have a dramatically shortened lifespan (32 vs 100+ weeks), and exhibit aging associated changes to epidermal, hematopoietic, endocrine, hepatobiliary, renal, nervous, and musculoskeletal systems (45). ERCC1 has been effectively silenced via hypomorphic mutations in the *mErcc1* locus in *Ercc1*$^{-/\Delta}$ mice (46). Neuropathy observed in 27-33 month old aged mice is mirrored in 5 month-old *Ercc1*$^{-/\Delta}$ mice (47). Previous studies have shown that associated neuropathy is likely the result of DNA repair deficiency as chemotherapeutic agent cisplatin causes interstrand crosslinking with resultant peripheral neuropathy (47, 48). Additional factors contributing to premature aging may include apoptosis (i.e. seen in liver tissue) (49), decreased replication frequency (i.e. seen in ERCC1 deficient ES cells and primary ear fibroblasts) (50), as well as depletion of hematopoietic stem cells (51).

The progeroid effects of ERCC1 deficiency support its role in DNA repair, but do not directly implicate it in MMEJ. If ERCC1 is active in MMEJ, we hypothesize that HR will repair the dsDNA damage that would have otherwise been repaired by MMEJ. As the main role of KU is NHEJ repair, knocking out this protein and pathway results in more dsDNA damage that persists until G_2 and S phase when it can be repaired by HR. This increase in HR can be visualized FYDR reporter mice that enable detection of HR. Confounding the FYDR HR signal are the unrepaired NER lesions that induce replication fork breakdown and subsequent homology directed repair. While the FYDR substrate detects replication fork repair, we have shown that a majority of recombination events leading to a fluorescent cell are the result of gene conversion *in vitro* in a similar reporter substrate (22).

2.3 Materials and Methods

All experiments involving mice were approved by the University of Pittsburgh (Pittsburgh, PA) Institutional Care and Use Committee and in accord with the National Institutes of Health guidelines for the humane care of animals.

Experimental Animals

The FYDR mouse model was developed to visualize HR *in vivo* and have been described in detail previously (52). Briefly, the FYDR mice harbor two tandem copies of

EYFP that contain unique deletions rendering them non-fluorescent. Damage of the FYDR substrate and subsequent repair via HR can yield a fluorescent cell.

Ku$^{-/-}$*FYDR*$^{Y/Y}$ mice were the result of breeding of heterozygous mice of different inbred backgrounds to yield isogenic f1 hybrids (*Ku*$^{+/-}$ *FYDR*$^{Y/Y}$ FBV/n x *Ku*$^{+/-}$ *FYDR*$^{+/+}$ C57Bl/6). *Ku*$^{+/+}$*FYDR*$^{Y/Y}$ and *Ku*$^{+/-}$*FYDR*$^{Y/Y}$ littermates were used as controls. Animals were humanely euthanized at 9 weeks of age, when *Ku*$^{-/-}$*FYDR*$^{Y/Y}$ animals began to develop progeria-associated morbidity.

All *Ercc1*$^{-/\Delta}$*FYDR*$^{Y/+}$ mice are the result of mating heterozygous mice of two different inbred backgrounds to yield isogenic f1 hybrids (*Ercc1*$^{+/\Delta}$ FVB/n x *ERCC1*$^{+/-}$ *FYDR*$^{Y/Y}$ C57Bl/6). Littermates with at least one wild-type *Ercc1* allele (*Ercc1*$^{+/\Delta}$, *Ercc1*$^{+/+}$, *and Ercc1*$^{+/-}$) were used as controls. Genotype determination was performed as described (4, 40, 47). Animals were humanely euthanized and pancreata harvested when the mice were 17-20 weeks old. The expression of ERCC1 in *Ercc1*$^{-/\Delta}$ ES cells is approximately 15% of that of that of WT cells (50).

Ercc1$^{-/-}$*FYDR*$^{Y/+}$ mice were bred from heterozygous mice of different inbred backgrounds to yield isogenic f1 hybrids (*Ercc1*$^{+/-}$ FBV/n x *Ercc1*$^{+/-}$ *FYDR*$^{+/+}$ C57Bl/6). *Ercc1*$^{+/+}$*FYDR*$^{Y/+}$ littermates were used as controls. The *Ercc1*$^{-/-}$ *FYDR*$^{Y/+}$ mice developed morbidity within 3 weeks of birth due to chronic hepatic insufficiency, thus animals were humanely euthanized, and pancreata harvested between 18 and 22 days of age.

Whole Tissue Imaging

Pancreata were imaged as described previously for foci analysis with a Nikon80i microscope (53, 54). Tissues were held in 1% trypsin inhibitor (Sigma-Aldrich) on ice overnight. Briefly, whole organs were compressed to 0.5 mm and imaged using a fixed exposure time (1x Nikon objective). Composite images were taken with TRITC filter (Excitation: 540/25 nm, Emission: 605/55 nm) and FITC (Excitation: 500/20 nm, Emission: 535/30 nm). Nikon Elements was used to automatically pseudocolor black and white images.

Images were compiled manually to cover the entire visible area of the pancreas. Adobe Photoshop CS3 (Adobe Systems, San Jose, CA) was used to optimally adjust brightness and contrast of all images identically. Images were taken under the TRITC filter and inverted to create negatives that were merged with images taken under the FITC filter. Any focus in the FITC image obscured by a focus in the TRITC image was not counted as a fluorescent foci. All counting was completed manually. The area of compiled pancreata images was determined by using Image J by manually tracing the pancreas edge (National Institutes of Health, Bethesda, MD, USA).

Flow Cytometry

Tissues were minced and incubated in 5 ml 2 mg/ml collagenase V in Hank's Balanced Salt Solution (Sigma) at 37 °C for 45 min shaken at approximately 150 cycles per minute. Triturated samples were filtered through a 70 μm filter into equal volume of

DMEM with 20% FBS (Atlanta Biologicals, Lawrenceville, GA) on ice. Cells were pelleted at 1500 rpm for 10 minutes and resuspended in OptiMEM (GIBCO) and passed through a cell strainer filter for flow cytometry analysis (Falcon).

Cells were analyzed with a Becton Dickinson FACScan flow cytometer (excitation 488 nm argon laser) or sorted with a Cytomation MoFlo cytometer (excitation 488 nm argon laser; emission 580/30 nm) (Fort Collins, Co). Live cells were gated using forward and side scatter and then examined for fluorescence.

Statistical Analysis

Fluorescent cell frequency follows a non-normal distribution, thus significance was calculated using a two-tailed Mann-Whitney test for both flow cytometry and foci data. For all other normally distributed data, a two-tailed Student's t-test was used to determine significance. A p values less than 0.05 was considered significant with further significance indicated.

2.4 Results

Ku$^{-/-}$ *FYDR*$^{Y/Y}$ Mice Show Increased HR

The *Ku*$^{-/-}$*FYDR*$^{Y/Y}$ mice have decreased body weight compared to control littermates (11.5 ± 2.4 g vs 25.4 ± 1.9 g, $p<10^{-13}$) that is reflected in the size of pancreata

(0.10 ± 0.07 g vs 0.20 ± 0.04 g, $p<0.05$). *Ku*$^{-/-}$*FYDR*$^{Y/Y}$ mice exhibit progeroid symptoms and develop morbidity by 9 weeks of age (55, 56). The number of recombinant fluorescent foci per square centimeter in the NHEJ deficient pancreata of *Ku*$^{-/-}$*FYDR*$^{Y/Y}$ is increased significantly over that of NHEJ competent animals as seen in Figure 2-2 (median 148 vs 83, $p<0.001$). While individual recombinant foci totals provide a more sensitive measurement than the total number of recombinant cells per million when examined via flow cytometry (54), the percentage of fluorescent cells also reflected the increase in recombination events in *Ku*$^{-/-}$*FYDR*$^{Y/Y}$ mice (median 270 vs 52, $p<0.005$). Since the only DNA repair pathway that KU has been implicated in is NHEJ, these data show that, *in vivo*, DSBs not repaired by NHEJ are repaired by an alternative DSB repair pathway.

Ercc1$^{-/\Delta}$ *FYDR*$^{Y/-}$ Mice Show Increased HR

Initial experiments with *Ercc1*$^{-/-}$ *FYDR*$^{+/-}$ mice were unsuccessful as these mice developed morbidity at 3 weeks of age due to progressive hepatic insufficiency associated with segmental progeria. These *Ercc1*$^{-/-}$ *FYDR*$^{+/-}$ mice weighed significantly less than their WT littermates (4.2 ± 0.5 g vs 11.4 ± 2.8 g, $p<0.05$). The pancreata of these animals also reflected the difference in body weight (0.009 ± 0.004 g vs 0.028 ± 0.011g, $p<0.05$). At this age, an insignificant number of fluorescent cells was observed in both these and WT mice. *Ercc*$^{+/\Delta}$ and *Ercc1*$^{-/+}$ mice do not exhibit a progeroid phenotype and do not differ from the WT mice as shown by others (50, 57). *Ercc1*$^{-/\Delta}$ mice show normal development until 8 weeks of age when they exhibit progressively worsening

characteristics of old age, including dystonia, trembling, and ataxia (4, 40, 50). The *Ercc1*$^{-/\Delta}$ mice were also significantly smaller in size and weight than control littermates (12.8 g ± 1.5 g vs 36.7 g ± 6.7 g, $p<10^{-18}$) with corresponding differences seen in the size of the pancreata of these animals (0.17 g ± 0.22 g vs 0.27 g ± 0.05 g, $p<0.05$). The median recombinant foci per square centimeter in *Ercc1*$^{-/\Delta}$ mice shows a significant increase compared to WT mice as seen in Figure 2-3 (median 171 v 66, $p<0.00001$). The total number of recombinant cells per million as determined via flow cytometry also reflects the increase in recombination events in *Ercc1*$^{-/\Delta}$ mice (median 20 v 4, $p<0.001$). These data are consistent with the findings of Dollé and coworkers who showed that *Ercc1*$^{-/m}$ mice show a rapid accumulation of point mutations and rearrangements with age in the *lacZ*-reporter, but that *Ercc1*$^{-/-}$ mice do not show a significant difference in *lacZ*-reporter mutations compared with WT mice at 3 weeks of age (57).

2.5 Discussion

DNA repair pathways have evolved to repair DNA damage at nearly all points in the cell cycle. KU-dependent NHEJ repairs DSBs during G_0 and G_1 to allow direct ligation of the ends without regard to potential sequence changes, while HR is utilized in G_2 and S phase when homology is readily found on the sister chromatid during replication (58, 59). While MMEJ and SSA do not require a homologous template for repair, they both require 3' overhangs formed during DSB processing for HR. It is likely that in

unperturbed cells, MMEJ and SSA occur during G_2/S phase. If the most appropriate repair pathway is not able or available to repair damage, the application of repair pathways may shift causing the damage to be repaired by an alternative and possibly disadventageous pathway. Inappropriate pathway selection may result in an increase in mutations, translocations, deletions, or duplications that may lead to apoptosis at best and unchecked growth and cancer at worst.

HR Increases in NHEJ Deficient Cells

The KU complex localizes to the ends of DSBs both to keep the ends in proximity to each other and to initiate NHEJ repair (15, 32). When KU is unavailable, the dsDNA is susceptible to nuclease and helicase processing that yields 3' overhangs necessary for homology-directed repair (60). Furthermore, other NHEJ repair proteins are unable to localize to the point of damage if KU does not first bind the ends of the break, leaving the DNA available for processing to initiate HR (61, 62). The lack of KU and NHEJ allows the DSBs to persist into G_2/S when it may be repaired via HR. Jasin and colleagues have shown that mouse embryonic stem cell lines deficient in *Ku70* had a six-fold increase in HR in a reporter integrated into the *hprt* locus (37). Nickoloff and colleagues showed the inverse relationship in yeast: cells with deficiencies in HR showed an increase in NHEJ (63). *Ku80*$^{-/-}$ mice harboring a *lacZ* reporter show a 32-fold decrease in chromosomal rearrangements, suggesting that DSBs are accurately repaired by HR or alternative pathways in the absence of NHEJ (64). The increase in recombinant foci seen in the *Ku*$^{-/-}$

FYDR$^{Y/Y}$ compared to *Ku*$^{+/+}$*FYDR*$^{Y/Y}$ pancreata confirms the repair of DSBs by HR in the absence of NHEJ *in vivo*.

Defects in ERCC1 Lead to an Increase in HR

The ERCC1-XPF structure-specific endonuclease cuts at the junction of dsDNA and 3' ssDNA that occur when helix-distorting lesions are removed through NER or when 3' unpaired flaps result from homology directed strand annealing (65). The ERCC1-XPF complex also initiates removal of aberrant DNA structures such as cross-linked Y structures and loops (65, 66). It has been suggested that ERCC1-XPF is also involved in resolution of Holliday junctions and D-loops in gene conversion events in HR (39, 67), though the accumulation of cross-overs in the sister chromatid exchange (SCE) assay by irradiated ERCC1-XPF deficient MEFs indicate HR is still functional in ERCC1 deficient mammalian cells, though Hagelstrom, *et al.*, did not see an increase in SCEs of unchallenged *Ercc1*$^{-/-}$ MEF cell lines (4, 68). The work of Sargent, *et. al*, supports the role of ERCC1 as a component of an error-prone homology-directed repair mechanism (41) and orthologs of ERCC1-XPF have been shown to facilitate DSB repair in model eukaryote *S. cerevisiae* (Rad10-Rad1), and fly *Drosophila melanogaster* (DmERCC1-MEI-9) (69-73).

The increase in recombinant pancreatic cells of *Ercc1*$^{-/\Delta}$ mice supports the ERCC1-independence of HR *in vivo*. Though the XPG endonuclease responsible for incision 3' to the lesion is still recruited to the lesion, cleavage does not take place without ERCC1 (74). The lesion is not repaired and may induce replication fork

breakdown during mitosis (75, 76). While the observed increase in HR may be due to increased replication fork break breakdown and repair (76), which is not dependent on ERCC1, the absence of ERCC1 also limits the repair of ssDNA through SSA and MMEJ (4, 77, 78). dsDNA that has already been processed for homology-directed repair through SSA and MMEJ might then be repaired through HR. In our experimental system, neither SSA nor MMEJ results in a fluorescent recombination product that indicates homology directed repair, but repair directed through HR may result in a full-length EYFP product and thus a fluorescent cell.

Though the two main mechanisms of DNA DSB repair (NHEJ and HR) are intact in *Ercc1*$^{-/-}$ mice, cumulative defects in NER, interstrand-crosslinking repair, and DSB repair likely contribute to the severe phenotype of ERCC1 deficient mice (3, 79). Though the ERCC1-XPF complex co-localizes with TRF2 at telomeres, the absence of ERCC1-XPF does not have a negative impact on telomere maintenance; therefore it is unlikely that *Ercc1*$^{-/-}$ associated progeria is due to telomere function (3, 80, 81). While both KU and ERCC1 deficient mice exhibit progeria, *Ku*$^{-/-}$ mice exhibit severe combined immunodeficiency, a pathognomonic feature of NHEJ deficiency, ERCC1 deficient mice do not have this characteristic NHEJ immunodeficiency, further demonstrating the disparate functions of ERCC1 and KU (24).

Providing further evidence supporting two distinct end-joining repair pathways in mammalian cells, Ahmad, *et. al*, demonstrated that double mutant *Ercc1*$^{-/-}$*Ku*$^{-/-}$ MEFs have a significantly impaired ability to join noncomplementary overhangs of a linear

plasmid *in vitro* when compared to either single mutant *Ercc1*$^{-/-}$ or *Ku*$^{-/-}$ cells (4). Furthermore, *Ercc1*$^{-/-}$ cells demonstrate decreased proficiency in repairing 3' non-complementary overhangs, resulting in very large deletions, without affecting proficiency in repairing complementary 5' overhangs or blunt ends (4). While ERCC1-XPF is a factor in a variety of DNA repair pathways, our data are consistent with both a) unrepaired NER substrates causing replication fork breakdown and subsequent ERCC1-independent fork reinsertion, and b) ERCC1-XPF participating in an error-prone, microhomology mediated, KU-independent end-joining pathway *in vivo*.

The existence of multiple DSB repair pathways underscores the importance of repairing DSBs to ensure genomic fidelity. As we have shown, DSB damage that may be best repaired by one pathway may be repaired by an alternative pathway if necessary. The redundancy of DSB repair mechanisms helps ensure dangerous DSBs are repaired to prevent cell-cycle arrest, apoptosis, mutation, or cancer.

2.6 Acknowledgements

This work was done in collaboration with the laboratory of Dr. Laura J. Niedernhofer. The author would also like to recognize the technical help and training from previous Engelward Laboratory members, Dr. Dominika Wiktor-Brown and Dr. Werner Olipitz for training and assistance with experiment inception. Breeding of animals and tissue harvest was performed in Dr. Niedernhofer's laboratory and the

author was responsible for data collection and analysis. The author is also grateful to Dr. Leona D. Samson and Dr. John M. Essigmann for helpful suggestions in planning experiments and preparing this text.

The author thanks the Koch Institute Flow Cytometry Facility core, particularly G. Paradis for assistance in data collection. The Koch Institute Core facilities are supported by NCI CCSG P30-CA14051. This work was supported by National Institutes of Health T32 Training Grant in Environmental Toxicology ES007020 and by a National Science Foundation Graduate Research Fellowship. This work is funded by NIH grant 2-RO1-Ca079827-05A1 and by NIH/NCI grant T32-ES07020

2.7 References

1. Vilenchik MM, Knudson AG (2003) Endogenous DNA double-strand breaks: production, fidelity of repair, and induction of cancer. *Proc Natl Acad Sci USA* 100:12871–12876.

2. Friedberg EC et al. (2005) *DNA Repair and Mutagenesis* (Amer Society for Microbiology). 2nd Ed.

3. Gregg SQ, Robinson AR, Niedernhofer LJ (2011) Physiological consequences of defects in ERCC1-XPF DNA repair endonuclease. *DNA Repair (Amst)* 10:781–791.

4. Ahmad A et al. (2008) ERCC1-XPF endonuclease facilitates DNA double-strand break repair. 28:5082–5092.

5. Goode EL, Ulrich CM, Potter JD (2002) Polymorphisms in DNA repair genes and associations with cancer risk. *Cancer Epidemiol Biomarkers Prev* 11:1513–1530.

6. Cox MM et al. (2000) The importance of repairing stalled replication forks. *Nature* 404:37–41.

7. Essers J et al. (2000) Homologous and non-homologous recombination differentially affect DNA damage repair in mice. *EMBO J* 19:1703–1710.

8. Bishop AJR, Schiestl RH (2002) Homologous Recombination and Its Role in Carcinogenesis. *J Biomed Biotechnol* 2:75–85.

9. Kasparek TR, Humphrey TC (2011) DNA double-strand break repair pathways, chromosomal rearrangements and cancer. *Semin Cell Dev Biol* 22:886–897.

10. Li L, Robert C, Rassool FV The Role of Error-Prone Alternative Non-Homologous End-Joining in Genomic Instability in Cancer. *cdnintechopencom*.

11. Brugmans L, Kanaar R, Essers J (2007) Analysis of DNA double-strand break repair pathways in mice. *Mutat Res* 614:95–108.

12. Karran P (2000) DNA double strand break repair in mammalian cells. *Curr Opin Genet Dev* 10:144–150.

13. Difilippantonio MJ et al. (2000) DNA repair protein Ku80 suppresses chromosomal aberrations and malignant transformation. *Nature* 404:510–514.

14. Walker JR, Corpina RA, Goldberg J (2001) Structure of the Ku heterodimer bound to DNA and its implications for double-strand break repair. *Nature* 412:607–614.

15. Guirouilh-Barbat J et al. (2004) Impact of the KU80 pathway on NHEJ-induced genome rearrangements in mammalian cells. *Mol Cell* 14:611–623.

16. van Heemst D, Brugmans L, Verkaik NS, van Gent DC (2004) End-joining of blunt DNA double-strand breaks in mammalian fibroblasts is precise and requires DNA-PK and XRCC4. *DNA Repair (Amst)* 3:43–50.

17. Venkitaraman AR (2002) Cancer susceptibility and the functions of BRCA1 and BRCA2. *Cell* 108:171–182.

18. Kuhfittig-Kulle S et al. (2007) The mutagenic potential of non-homologous end joining in the absence of the NHEJ core factors Ku70/80, DNA-PKcs and XRCC4-LigIV. *Mutagenesis* 22:217–233.

19. Haber JE (1999) DNA recombination: the replication connection. *Trends Biochem Sci* 24:271–275.

20. Decottignies A (2007) Microhomology-mediated end joining in fission yeast is repressed by pku70 and relies on genes involved in homologous recombination. *Genetics* 176:1403–1415.

21. Lee K, Lee SE (2007) Saccharomyces cerevisiae Sae2- and Tel1-dependent single-strand DNA formation at DNA break promotes microhomology-mediated end joining. *Genetics* 176:2003–2014.

22. Jonnalagadda VS, Matsuguchi T, Engelward BP (2005) Interstrand crosslink-induced homologous recombination carries an increased risk of deletions and insertions. *DNA Repair (Amst)* 4:594–605.

23. Kabotyanski EB, Gomelsky L, Han JO, Stamato TD, Roth DB (1998) Double-strand break repair in Ku86- and XRCC4-deficient cells. *Nucleic Acids Res* 26:5333–5342.

24. Yan CT et al. (2007) IgH class switching and translocations use a robust non-classical end-joining pathway. *Nature* 449:478–482.

25. Downs JA, Jackson SP (2004) A means to a DNA end: the many roles of Ku. *Nat Rev Mol Cell Biol* 5:367–378.

26. Jeggo P, Singleton B, Beamish H, Priestley A (1999) Double strand break rejoining by the Ku-dependent mechanism of non-homologous end-joining. *C R Acad Sci III, Sci Vie* 322:109–112.

27. Mimori T, Hardin JA (1986) Mechanism of interaction between Ku protein and DNA. *J Biol Chem* 261:10375–10379.

28. Falzon M, Fewell JW, Kuff EL (1993) EBP-80, a transcription factor closely

resembling the human autoantigen Ku, recognizes single- to double-strand transitions in DNA. *J Biol Chem* 268:10546–10552.

29. Paillard S, Strauss F (1991) Analysis of the mechanism of interaction of simian Ku protein with DNA. *Nucleic Acids Res* 19:5619–5624.

30. Ono M, Tucker PW, Capra JD (1994) Production and characterization of recombinant human Ku antigen. *Nucleic Acids Res* 22:3918–3924.

31. Pang D, Yoo S, Dynan WS, Jung M, Dritschilo A (1997) Ku proteins join DNA fragments as shown by atomic force microscopy. *Cancer Res* 57:1412–1415.

32. Pastwa E, Błasiak J (2003) Non-homologous DNA end joining. *Acta Biochim Pol* 50:891–908.

33. Dudásová Z, Dudás A, Chovanec M (2004) Non-homologous end-joining factors of Saccharomyces cerevisiae. *FEMS Microbiol Rev* 28:581–601.

34. Fattah F et al. (2010) Ku regulates the non-homologous end joining pathway choice of DNA double-strand break repair in human somatic cells. *PLoS Genet* 6:e1000855.

35. Postow L (2011) Destroying the ring: Freeing DNA from Ku with ubiquitin. *FEBS Lett* 585:2876–2882.

36. Lee SE et al. (1998) Saccharomyces Ku70, mre11/rad50 and RPA proteins regulate adaptation to G2/M arrest after DNA damage. *Cell* 94:399–409.

37. Pierce AJ, Hu P, Han M, Ellis N, Jasin M (2001) Ku DNA end-binding protein modulates homologous repair of double-strand breaks in mammalian cells. *Genes Dev* 15:3237–3242.

38. Allen C, Kurimasa A, Brenneman MA, Chen DJ, Nickoloff JA (2002) DNA-dependent protein kinase suppresses double-strand break-induced and spontaneous homologous recombination. *Proc Natl Acad Sci USA* 99:3758–3763.

39. Niedernhofer LJ et al. (2004) The structure-specific endonuclease Ercc1-Xpf is required to resolve DNA interstrand cross-link-induced double-strand breaks. *Mol Cell Biol* 24:5776–5787.

40. Niedernhofer LJ et al. (2006) A new progeroid syndrome reveals that genotoxic stress suppresses the somatotroph axis. *Nature* 444:1038–1043.

41. Sargent RG et al. (1997) Recombination-dependent deletion formation in mammalian cells deficient in the nucleotide excision repair gene ERCC1. *Proc Natl Acad Sci USA* 94:13122–13127.

42. Hasty P, Campisi J, Hoeijmakers J, van Steeg H, Vijg J (2003) Aging and genome maintenance: lessons from the mouse? *Science* 299:1355–1359.

43. Nussenzweig A, Sokol K, Burgman P, Li L, Li GC (1997) Hypersensitivity of Ku80-deficient cell lines and mice to DNA damage: the effects of ionizing radiation on growth, survival, and development. *Proc Natl Acad Sci USA* 94:13588–13593.

44. Nussenzweig A et al. (1996) Requirement for Ku80 in growth and immunoglobulin V(D)J recombination. *Nature* 382:551–555.

45. Niedernhofer LJ (2008) Tissue-specific accelerated aging in nucleotide excision repair deficiency. *Mech Ageing Dev* 129:408–415.

46. Dollé MET et al. (2011) Broad segmental progeroid changes in short-lived Ercc1(-/Δ7) mice. *Pathobiol Aging Age Relat Dis* 1.

47. Goss JR et al. (2011) Premature aging-related peripheral neuropathy in a mouse model of progeria. *Mech Ageing Dev* 132:437–442.

48. Krarup-Hansen A et al. (1993) Examination of distal involvement in cisplatin-induced neuropathy in man. An electrophysiological and histological study with particular reference to touch receptor function. *Brain* 116 (Pt 5):1017–1041.

49. Kirschner K, Singh R, Prost S, Melton DW (2007) Characterisation of Ercc1 deficiency in the liver and in conditional Ercc1-deficient primary hepatocytes in vitro. *DNA Repair (Amst)* 6:304–316.

50. Weeda G et al. (1997) Disruption of mouse ERCC1 results in a novel repair syndrome with growth failure, nuclear abnormalities and senescence. *Curr Biol* 7:427–439.

51. Prasher JM et al. (2005) Reduced hematopoietic reserves in DNA interstrand crosslink repair-deficient Ercc1-/- mice. *EMBO J* 24:861–871.

52. Hendricks CA et al. (2003) Spontaneous mitotic homologous recombination at an enhanced yellow fluorescent protein (EYFP) cDNA direct repeat in transgenic mice. *Proc Natl Acad Sci USA* 100:6325–6330.

53. Wiktor-Brown DM, Hendricks CA, Olipitz W, Engelward BP (2006) Age-dependent accumulation of recombinant cells in the mouse pancreas revealed by in situ fluorescence imaging. *Proc Natl Acad Sci USA* 103:11862–11867.

54. Wiktor-Brown DM, Hendricks CA, Olipitz W, Rogers AB, Engelward BP (2006) Applications of fluorescence for detecting rare sequence rearrangements in vivo. *Cell Cycle* 5:2715–2719.

55. Didier N, Hourdé C, Amthor H, Marazzi G, Sassoon D (2012) Loss of a single allele for Ku80 leads to progenitor dysfunction and accelerated aging in skeletal muscle. *EMBO Mol Med* 4:910–923.

56. Li H, Vogel H, Holcomb VB, Gu Y, Hasty P (2007) Deletion of Ku70, Ku80, or both causes early aging without substantially increased cancer. *Mol Cell Biol* 27:8205–8214.

57. Dollé MET et al. (2006) Increased genomic instability is not a prerequisite for shortened lifespan in DNA repair deficient mice. *Mutat Res* 596:22–35.

58. Johnson RD, Jasin M (2000) Sister chromatid gene conversion is a prominent double-strand break repair pathway in mammalian cells. *EMBO J* 19:3398–3407.

59. Johnson RD, Jasin M (2001) Double-strand-break-induced homologous recombination in mammalian cells. *Biochem Soc Trans* 29:196–201.

60. Sun J, Lee K-J, Davis AJ, Chen DJ (2012) Human Ku70/80 protein blocks exonuclease 1-mediated DNA resection in the presence of human Mre11 or Mre11/Rad50 protein complex. *J Biol Chem* 287:4936–4945.

61. Dynan WS, Yoo S (1998) Interaction of Ku protein and DNA-dependent protein kinase catalytic subunit with nucleic acids. *Nucleic Acids Res* 26:1551–1559.

62. Wu D, Topper LM, Wilson TE (2008) Recruitment and dissociation of nonhomologous end joining proteins at a DNA double-strand break in Saccharomyces cerevisiae. *Genetics* 178:1237–1249.

63. Clikeman JA, Khalsa GJ, Barton SL, Nickoloff JA (2001) Homologous recombinational repair of double-strand breaks in yeast is enhanced by MAT heterozygosity through yKU-dependent and -independent mechanisms. *Genetics* 157:579–589.

64. Rockwood LD, Nussenzweig A, Janz S (2003) Paradoxical decrease in mutant frequencies and chromosomal rearrangements in a transgenic lacZ reporter gene in Ku80 null mice deficient in DNA double strand break repair. *Mutat Res* 529:51–58.

65. de Laat WL, Appeldoorn E, Jaspers NG, Hoeijmakers JH (1998) DNA structural elements required for ERCC1-XPF endonuclease activity. *J Biol Chem* 273:7835–7842.

66. Tian M, Alt FW (2000) Transcription-induced cleavage of immunoglobulin switch regions by nucleotide excision repair nucleases in vitro. *J Biol Chem* 275:24163–24172.

67. Sargent RG et al. (2000) Role of the nucleotide excision repair gene ERCC1 in formation of recombination-dependent rearrangements in mammalian cells. *Nucleic Acids Res* 28:3771–3778.

68. Hagelstrom RT, Blagoev KB, Niedernhofer LJ, Goodwin EH, Bailey SM (2010) Hyper telomere recombination accelerates replicative senescence and may promote premature aging. *Proc Natl Acad Sci USA* 107:15768–15773.

69. Fishman-Lobell J, Haber JE (1992) Removal of nonhomologous DNA ends in double-strand break recombination: the role of the yeast ultraviolet repair gene RAD1. *Science* 258:480–484.

70. Ivanov EL, Haber JE (1995) RAD1 and RAD10, but not other excision repair genes, are required for double-strand break-induced recombination in Saccharomyces cerevisiae. *Mol Cell Biol* 15:2245–2251.

71. Pâques F, Haber JE (1999) Multiple pathways of recombination induced by double-strand breaks in Saccharomyces cerevisiae. *Microbiol Mol Biol Rev* 63:349–404.

72. Gamo S, Megumi T, Nakashima-Tanaka E (1990) Sensitivity to ether anesthesia and to gamma-rays in mutagen-sensitive strains of Drosophila melanogaster. *Mutat Res* 235:9–13.

73. Radford SJ, Goley E, Baxter K, McMahan S, Sekelsky J (2005) Drosophila ERCC1 is required for a subset of MEI-9-dependent meiotic crossovers. *Genetics* 170:1737–1745.

74. Volker M et al. (2001) Sequential assembly of the nucleotide excision repair factors in vivo. *Mol Cell* 8:213–224.

75. Ward JD, Barber LJ, Petalcorin MI, Yanowitz J, Boulton SJ (2007) Replication blocking lesions present a unique substrate for homologous recombination. *EMBO J* 26:3384–3396.

76. Arnaudeau C, Lundin C, Helleday T (2001) DNA double-strand breaks associated with replication forks are predominantly repaired by homologous recombination involving an exchange mechanism in mammalian cells. *J Mol Biol* 307:1235–1245.

77. Rahn JJ, Adair GM, Nairn RS (2010) Multiple roles of ERCC1-XPF in mammalian interstrand crosslink repair. *Environ Mol Mutagen* 51:567–581.

78. Bennardo N, Cheng A, Huang N, Stark JM (2008) Alternative-NHEJ is a mechanistically distinct pathway of mammalian chromosome break repair. *PLoS*

Genet 4:e1000110.

79. Niedernhofer LJ (2008) Nucleotide excision repair deficient mouse models and neurological disease. *DNA Repair (Amst)* 7:1180–1189.

80. Capper R et al. (2007) The nature of telomere fusion and a definition of the critical telomere length in human cells. *Genes Dev* 21:2495–2508.

81. Zhu X-D et al. (2003) ERCC1/XPF removes the 3' overhang from uncapped telomeres and represses formation of telomeric DNA-containing double minute chromosomes. *Mol Cell* 12:1489–1498.

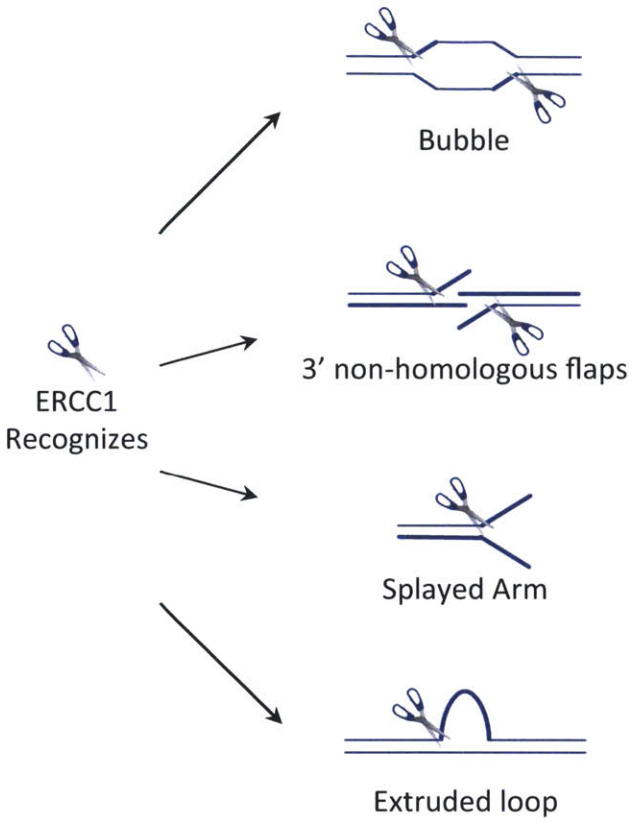

Figure 2-1. ERCC1 is a Structure Specific Endonuclease. The ERCC1-XPF endonuclease recognizes the 5'→3' bend in ssDNA that is found in bubbles and stem loops, 3' non-homologous flaps, splayed arms and extruded ssDNA loops, among others, and incises 5' to the site.

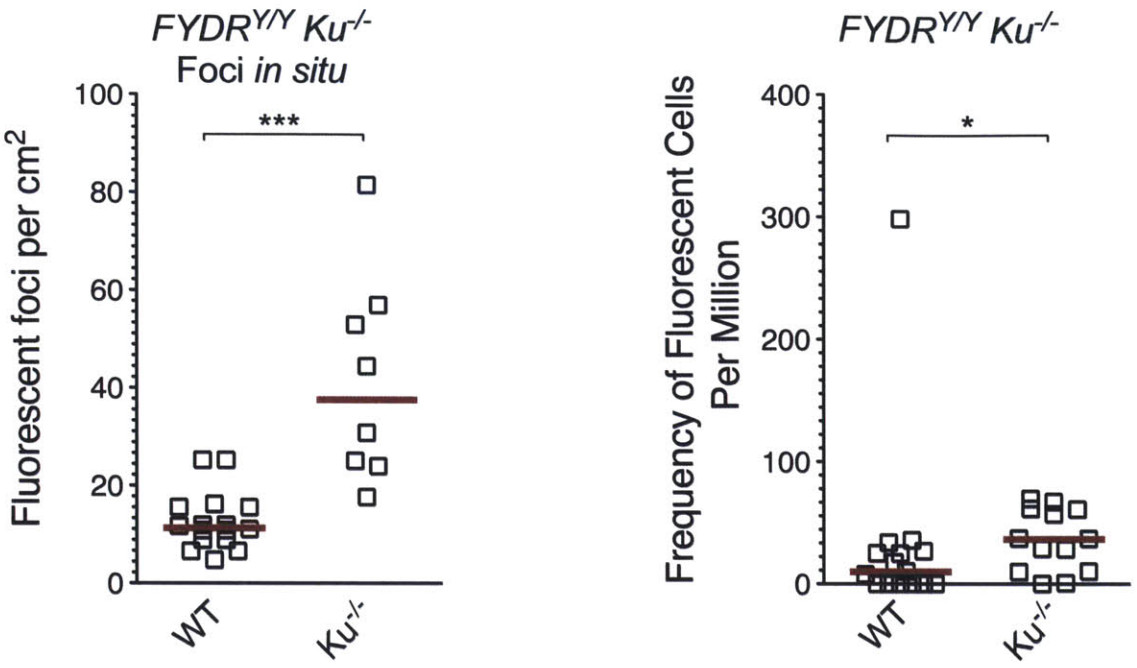

Figure 2-2. HR Increases in NHEJ Deficient Mice. FYDR mice deficient in Ku86, an essential NHEJ repair protein, show an increase in the number of recombinant foci per square centimeter in the pancreata of 9 week-old $Ku^{-/-}$ $FYDR^{Y/Y}$mice compared to $FYDR^{Y/Y}$ WT mice. The frequency of recombinant cells per million as determined by flow cytometry also showed a significant increase in the $Ku^{-/-}$ $FYDR^{Y/+}$ mice. Medians are indicated by red bars. Points on the X-axis indicate individual mice with 0 recombinant cells.

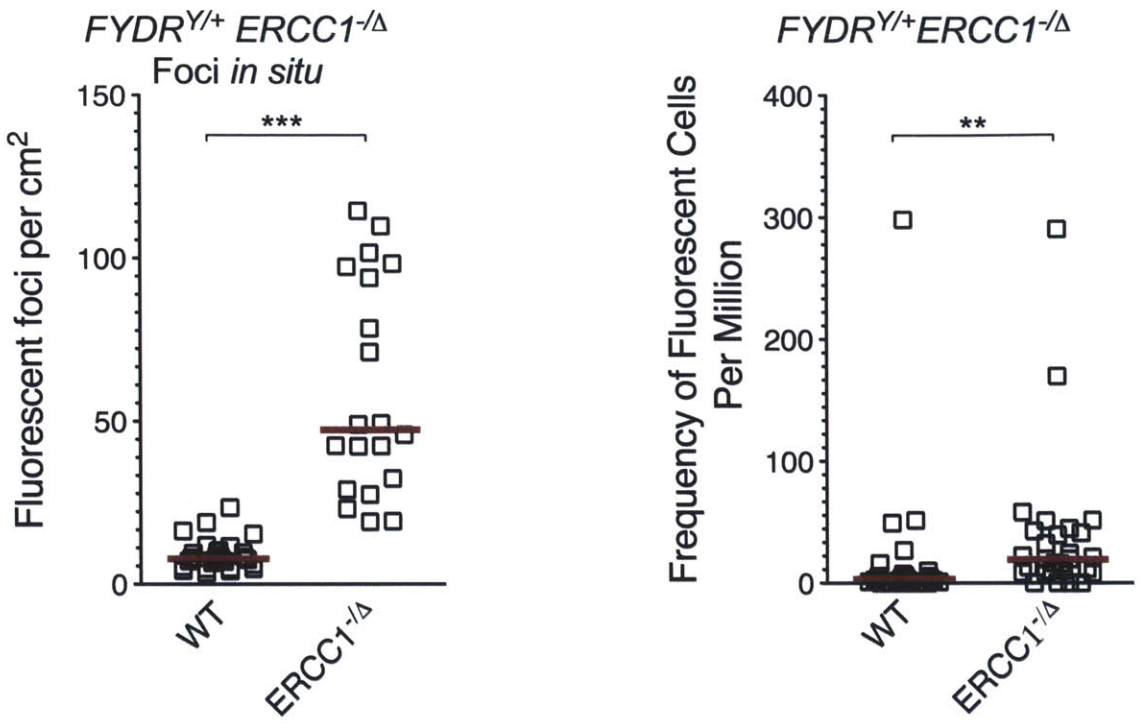

Figure 2-3. HR Increases in ERCC1 Deficient Mice. The number of spontaneous recombinant foci per square centimeter in the pancreas of 17-20 week-old *Ercc1*$^{-/\Delta}$ *FYDR*$^{Y/+}$ was significantly increased over *FYDR*$^{Y/+}$ WT mice. The frequency of recombinant cells per million as determined by flow cytometry also showed a significant increase in the *Ercc11*$^{-/\Delta}$ *FYDR*$^{Y/+}$ mice. Medians are indicated by red bars. Points on the X-axis indicate individual mice with 0 recombinant cells.

Chapter III

ROSA26 Direct Repeat-GFP (raDR-GFP) Mice Reveal Tissue-, Age-, and Exposure- Dependence of Homologous Recombination

Chapter III

3.1 Abstract

HR is critical for the repair of double-strand breaks and broken replication forks during S and G_2. Although mostly accurate, HR can lead to oncogenic sequence changes such as insertions, deletions, and loss of heterozygosity. Despite its importance in carcinogenesis, little is known about HR in different tissues due to limitations in detection. To detect HR in virtually all mammalian tissues, we developed a mouse harboring an HR reporter targeted to the ubiquitously expressed Rosa26 locus. Here we describe the Rosa26 Direct Repeat-GFP (raDR-GFP) mice in which HR between two truncated EGFP genes yields a fluorescent signal. In raDR-GFP mice, recombinant cells can be detected in all eleven tissues tested, revealing a wide variation in frequencies among tissues. Remarkably, HR is virtually undetectable in the brain, consistent with its low proliferative index. Additionally, we developed *in situ* imaging methods that enable quantification of recombination events. We show that the model alkylating agent MNU induces HR in the pancreas, colon, and liver, demonstrating that raDR-GFP mice can be used to study the impact of carcinogens and chemotherapeutics on HR in multiple tissues. Finally, quantification of HR in the pancreas, colon, and liver at 3, 6, and 12 months of age revealed a clear increase in the frequency of recombination with age in these tissues. Taken together, the raDR-GFP mice reveal the impact of tissue type and

age on HR, provide new insights into HR *in vivo* and enable studies of genetic and environmental factors that potentially impact HR.

3.2 Introduction

DNA is continuously exposed to environmental and endogenous DNA damaging agents that can lead to toxicity, mutations, and ultimately disease (1-4). Maintaining genomic stability in the face of thousands of lesions (e.g., base lesions, AP sites, single strand breaks, and DSBs) poses a major challenge, especially in the case of DSBs, which are both acutely toxic and have the potential to lead to the loss of millions of base pairs of information if they are not repaired correctly (5-10). The two major pathways used by cells to repair DSBs are to directly rejoin the ends via NHEJ, which is the dominant pathway during G_1, and to use HR to restore DSBs and broken replication forks during S and G_2 (9, 11, 12).

HR is essential for vertebrate life (1-4, 11), and the correct balance of NHEJ and HR is essential for preventing cancer. If there is a deficiency in HR, cells can suffer misrepair of DSBs, resulting in translocations that promote cancer and aging (5-10, 13, 14). Ironically, despite the fact that it is essential, too much HR can also be detrimental, since HR carries with it the risk of misalignments that can cause insertions, deletions, and LOH (9, 11, 12, 15, 16). It is likely that HR events contribute to sequence changes in virtually all cancers, since loss of function of most tumor suppressor genes requires LOH, and 30-60% of LOH events are caused by HR (17-19). Indeed, sequence changes generated by HR have been found in multiple cancers (20-22), and exposures and genetic factors that promote HR are known to promote cancer (e.g., exposure to UV

light (23, 24) and benzo[*a*]pyrene (25-29) and mutations in BLM (30, 31) and Ku80 (32, 33)).

Key insights into the role of HR in mammals have resulted from studies using mouse models that enable detection of HR in a subset of tissues. In the first studies of this kind, starting in the 1990s, the p^{un} mice (which carry a natural duplication wherein a change in pigmentation indicates an HR event) have been used to study how genes and exposures impinge on HR (34-36). Additionally, mice that are heterozygous at the *Aprt* locus have been used to show that LOH is often driven by HR *in vivo* (18, 37). More recently, our laboratory developed the FYDR mice which carry a direct repeat substrate wherein HR can lead to the reconstitution of the full-length coding sequence of the EYFP gene (38). This mouse model made it possible to detect HR events that arise in several tissues of adult animals, and thus enabled a series of studies identifying environmental and genetic factors that drive HR *in vivo* (39-41). Furthermore, the development of techniques to visualize recombinant fluorescent cells within intact tissue provided a sensitive assay for detecting conditions that induce HR (42), making it possible to delineate the relative importance of *de novo* sequence changes versus clonal expansion (42) and to reveal interactions between environmental and physiological factors acting on HR *in vivo* (manuscripts in preparation). These studies highlight the usefulness of studying HR *in vivo* to learn about early steps of carcinogenesis and warrant further studies using other tissues and exposures. However, only a limited number of tissues can be studied in the FYDR mice, due to limitations in expression of the transgene (41).

Specifically, the FYDR mouse line contains an EYFP HR reporter driven by the CAG promoter and was generated by standard transgenesis which resulted in random integration of a single reporter into chromosome 1 at a locus that enables strong expression in the pancreas, but is silenced in many other tissues (42). We therefore set out to generate a recombination reporter mouse with a broad reporter expression.

In order to create a mouse model in which HR can be studied in virtually any cell type, we targeted the recombination reporter to the *ROSA26* locus, which was originally identified for its nearly ubiquitous expression (43). Here we describe the generation and characterization of this mouse strain, termed *ROSA26* Direct Repeat-Green Fluorescent Protein (raDR-GFP). The cells in the raDR-GFP mouse harbor two uniquely truncated EGFP gene cassettes in tandem (Figure 3-1). In the event of HR in the construct, a full-length EGFP gene cassette can result, giving rise to a fluorescent cell. The construct allows detection of replication fork repair, unequal sister chromatid exchange, and gene conversion where both the *Δ3egfp* and the *Δ5egfp* cassettes can act as either a donor or recipient (Figure 3-S1) (44). Here we show that the integration of the recombination reporter into the Rosa26 locus enables the detection of cells that have undergone HR in all examined tissues, thus enabling a broad range of studies of HR in mammals. Fluorescent recombinant cells can be detected by flow cytometry after the tissue has been disaggregated, and can also be visualized *in situ* within several intact organs. Importantly, we show that recombinant fluorescent cells accumulate with age in the pancreas, liver, and colon, demonstrating that HR is active in these tissues in adult animals, as well as enabling studies of long-term exposures that can lead to

accumulation of recombinant cells. The raDR-GFP mice thus open doors to studies of exposures and genetic factors that modulate susceptibility to HR events in cancer-relevant tissues.

3.3 Materials and Methods

Construction of the raDR-GFP Substrate

Plasmid construction was described previously (44). Briefly, truncated EGFP coding sequences (Δ5*egfp* lacking 15 bases at the 5' end and Δ3*egfp* lacking 81 bases at the 3' end) were amplified by PCR from plasmid pCX-EGFP, using primers containing unique sequences. PCR products were cloned in a tandem orientation (Δ5*egfp* followed by Δ3*egfp*) into the pCX-NNX backbone to form the direct repeat HR substrate, yielding plasmid pCX-NNX-ΔGF. The HR substrate was then cloned into pBigT-TpA, released together with the neomycin resistance gene and cloned into pROSA26PA (43) (a kind gift from Dr. P. Soriano, Mount Sinai School of Medicine) to yield the targeting plasmid pROSA26-ΔGF.

Creation of raDR-GFP Transgenic Mouse

The pROSA26-ΔGF targeting plasmid was linearized by digestion with *Xho*I (New England Biolabs) and electroporated into mouse 129 embryonic stem (ES) cells. Clones were selected for resistance to neomycin by growing in selective media (40% DMEM + glucose, 40% EmbryoMax DMEM, 1% β-mercaptoethanol, 15% FBS, penicillin,

streptomycin, glutamine, nonessential amino acids, LIF, G418) and screened for correct targeting by PCR and Southern blot. Cells from clones with correct targeting were injected into the blastocoel of 3.5-day-old C57Bl/6 blastocysts, which were implanted into pseudopregnant female mice. All ES cell manipulations and transgenic mouse development were performed by the ES Cell and Transgenics Facility at the Swanson Biotechnology Center of the Koch Institute for Integrative Cancer Research at MIT. All procedures involving mice were approved by the Massachusetts Institute of Technology Committee on Animal Care and in accordance with the National Institutes of Health guidelines for the humane care of animals.

PCR Analysis

To identify clones with correct targeting of the raDR-GFP substrate, we used a forward primer annealing 5' to the targeted locus and a reverse primer landing in the neomycin resistance gene within the construct, yielding a 1.24 kb PCR product (Figure 3-2A, lower panel, T). In the absence of insertion, the forward primer yields a 1.16 kb PCR product with a reverse primer landing within the *ROSA26* locus (Figure 3-2A, upper panel, WT). Primer sequences are available upon request. PCR detection of the Δ5*egfp*, Δ3*egfp*, and full-length *EGFP* sequences was performed as described previously (44).

Southern Blot Analysis

The EGFP probing sequence was ^{32}P-labeled by random priming (NEBlot, New England Biolabs). Genomic DNA was isolated from candidate clones and digested with

HindIII (New England Biolabs). DNA fragments were resolved by electrophoresis and transferred to a nylon membrane (Hybond-XL, GE Healthcare). The blot was incubated at 65 °C in ExpressHyb (BD Biosciences/Clontech) with the ^{32}P-labeled EGFP probe. The probed blot was visualized on a Storm 840 PhosphorImager (Molecular Dynamics).

Positive Control Mouse

B6.Cg-Gt(ROSA)26Sor$^{tm6(CAG-ZsGreen1)Hze}$/J mice (Jackson Laboratory) carry the green fluorescent protein gene ZsGreen1 at the *ROSA26* locus driven by the CAG promoter, with an upstream STOP codon flanked by *loxP* sites and a downstream WPRE mRNA stabilizer. These mice were crossed with B6.C-Tg(CMV-cre)1Cgn/J mice (Jackson Laboratory) that carry the Cre recombinase gene driven by the CMV promoter, resulting in the deletion of *loxP*-flanked genes in all tissues. F_1 mice expressing ZsGreen1 under the CAG promoter at the *ROSA26* locus were used to determine the reporter expression profile.

Isolation of Ear Fibroblasts

Cells were isolated as described (45). Briefly, ear tissue was minced with scalpel blades and digested with 4 mg/ml collagenase/dispase (Sigma) dissolved in Hanks' Balanced Salt Solution (Invitrogen) for 45-60 minutes at 37 °C. Five volumes of warmed fibroblast medium (DMEM, 15% FBS, 100 units/ml penicillin, 100 units/ml streptomycin, 5 ug/ml fungizone, glutamine, non-essential amino acids) were added and cells were

incubated overnight at 37°C with 5% CO_2. Cells were resuspended, strained through a 70 μm filter (BD Falcon), and seeded into gelatinized dishes for expansion.

Flow Cytometry

Tissues were kept in 0.01% trypsin inhibitor (Sigma) on ice for up to 16 hours before analysis. Tissues were minced with scalpel blades or with a gentleMACS tissue dissociator (Miltenyi Biotec) and digested with 2 mg/ml collagenase V (Sigma) in Hanks' Balanced Salt Solution (Invitrogen) at 37 °C for 45 minutes. After digestion, the cell suspension was triturated and filtered through a 70 μm cell strainer (BD Biosciences) into an equal volume of DMEM with 20% FBS on ice. Cells were pelleted at 1500 rpm for 10 minutes, resuspended in OptiMEM (Invitrogen) and passed through a 35 μm cell strainer (BD Falcon) before flow cytometry. Cells were analyzed with a FACScan flow cytometer (Becton Dickinson) or sorted with a MoFlo cell sorter (Cytomation). Live cells were gated using forward and side scatter and then examined for fluorescence (excitation 488 nm, emission 580/30 nm).

In Situ Imaging of Recombinant Foci

Whole organs were processed for imaging by compressing between coverslips to a thickness of 0.5 mm. The colon was cut lengthwise and laid open. Tissues were imaged with a Nikon 80i microscope (1× objective) in the FITC channel using a fixed exposure time. Serial images scanning the entire tissue surface were captured using an automated stage. Images were automatically compiled using NIS Elements software

(Nikon) or Adobe Photoshop (Adobe Systems). Brightness and contrast of all images were adjusted identically in Adobe Photoshop. Fluorescent foci were counted manually in a blinded fashion or with an in-house program written in MATLAB (The Mathworks). Tissue surface area was determined using ImageJ (NIH) by manually tracing the tissue outlines. Frozen sections (5 μm) were imaged with a 60× objective in the FITC channel, stained with hematoxylin and eosin, and imaged again under visible light. Images were then overlaid manually.

DNA Damage Induced Recombination

Five- to seven-week-old heterozygous raDR-GFP mice (C57BL/6 background) were used. DNA damage was elicited by combined treatment with MNU (Sigma) and thyroid hormone (Sigma). Details will be published separately. Briefly, thyroid hormone (T3) was administered in the diet (prepared by TestDiet) at 4 ppm according to Ledda-Columbano *et al.* (46). MNU was administered at 25 mg/kg as an intraperitoneal injection at the time of peak cell proliferation in the pancreas induced by T3. Control mice were fed an identical diet without T3 and received PBS injections. Feeding of T3 continued for 2 days after MNU injection. 3.5 weeks after MNU injection, mice were humanely euthanized and organs were harvested for the raDR-GFP assay.

Statistical Analysis

Recombination frequencies do not follow a normal distribution and were compared with a two-tailed Mann–Whitney test. A p value less than 0.05 was considered statistically significant.

3.4 Results

Creation of the raDR-GFP Mouse

To study recombination *in vivo*, we previously created a direct repeat substrate in which two EGFP expression cassettes are positioned in tandem (44). Essential sequences were deleted from each of the EGFP cassettes to create *Δ5egfp*, which lacks 15 bp at the 5' end, and *Δ3egfp*, which lacks 81bp at the 3' end. Recombination between the non-functional expression cassettes can reconstitute the full-length coding sequence, which would then be expressed under a strong promoter (CMV enhancer/chicken beta-actin promoter (CAG)) (Figure 3-2A) (44, 47). The promoter, intron, and polyadenylation signal sequences were chosen for their efficacy in the already established FYDR mouse (48).

To enable broad expression, we elected to target the *ROSA26* locus, which was originally identified for its nearly ubiquitous expression (43). Using a previously

developed targeting construct (43) (a kind gift from Dr. P. Soriano), we created a targeting vector that includes a short arm, a positive selection marker (neoR), the direct repeat HR substrate, a long arm, and a negative selection cassette (diptheria toxin) (Figure 3-2A and Figure 3-S2) (43, 44). The linearized targeting construct was electroporated into mouse 129S4/SvJae (129 background) ES cells (49) which were grown under selective conditions, and resulting colonies were screened by a diagnostic PCR reaction that yields a unique 1.24 kb fragment present in the targeted allele (T). A parallel PCR reaction for the wild-type genomic allele (WT) yields a unique 1.16 kb fragment (Figure 3-2). PCR analysis of 100 candidates revealed that 7 candidates contained, at a minimum, the 5' portion of the insert at the *ROSA26* locus. Proper targeting of the raDR-GFP construct to the *ROSA26* locus in these seven candidates was further assessed by Southern blot. Correct incorporation was tested by the appearance of an 8.2 and a 2.3 kb *HindIII* fragment by Southern blotting and probing with EGFP (a representative clone is shown in Figure 3-2C). The presence of both of these unique bands and no others is consistent with a single and complete raDR-GFP construct incorporated into the *ROSA26* locus. Of the seven clones first identified by PCR, five were confirmed correctly targeted by Southern blot.

Healthy cells (10-14) from clones with confirmed correct insert incorporation were injected into the blastocoel of 3.5-day-old C57Bl/6 blastocysts, which were then implanted into pseudopregnant female mice. The resultant chimeric males were bred with 129 females to establish the raDR-GFP mouse line. While the 129 background was maintained, the transgene was also backcrossed into the C57BL/6 background for 10

generations. The transgene follows Mendelian inheritance with 49.5% of offspring of heterozygous/wildtype parents inheriting the transgene (n=99).

HR Yields a Fluorescent Signal in raDR-GFP Mice

To initiate studies of HR in the raDR-GFP mice, we first analyzed primary ear fibroblasts. Cells were harvested, expanded in culture, and examined by flow cytometry. Unstained wild-type fibroblasts show a range of natural fluorescence intensities as seen in Figure 3-3A (left panel). As a positive control for EGFP fluorescence, we analyzed primary ear fibroblasts from EGFP expressing mice (50). Gates defining 'green fluorescent' and 'autofluorescent' cells were drawn conservatively such that no wild type cells were identified as fluorescent, while capturing the majority of the EGFP expressing cells in region R2 (Figure 3-3A, middle panel). Primary ear fibroblasts isolated from raDR-GFP mice show the majority of cells to be autofluorescent with a minority population exhibiting green fluorescence, indicative of cells that have undergone an HR event at the raDR-GFP substrate (Figure 3-3A, right panel). As expected (39, 42, 44), recombinant cells are rare, presumably because only HR events at the integrated transgene can be detected.

To verify that green fluorescent cells have indeed undergone HR, we performed PCR analysis using previously created *ROSA26* targeted ES cells that harbor Δ3*egfp*, Δ5*egfp,* and full-length EGFP as controls (44). To differentiate among these three expression cassettes, we designed a PCR strategy that exploits unique sequences inserted at the sites where coding sequences had been deleted (Figure 3-3B). Using

these primers, we tested the ES cells that were used to create the raDR-GFP mice. These ES cells contain the direct repeat substrate but do not contain full-length EGFP, as expected (Figure 3-3C, left). We then examined primary ear fibroblasts from raDR-GFP mice and isolated autofluorescent and green fluorescent cells using FACS. Analysis of cells that show only autofluorescence (e.g., unrecombined) indicates that Δ3*egfp* and Δ5*egfp* are present, but the full-length EGFP sequence is not (Figure 3-3C, middle). However, green fluorescent cells sorted from the R2 gate carry the full-length EGFP sequence (Figure 3-3C, right). Since many nucleotides need to be transferred in order to restore the deleted regions and thus give rise to a full-length EGFP sequence, we conclude that fluorescent raDR-GFP cells have indeed undergone mitotic HR at the raDR-GFP substrate. It is noteworthy that, depending on the mechanism of recombination, recombinant cells are anticipated to harbor Δ3*egfp*, Δ5*egfp,* or both, in addition to the full-length EGFP sequence (Figure 3-S1).

HR Reporter is Broadly Expressed in raDR-GFP Mice

The *ROSA26* locus has previously been shown to drive ubiquitous expression in the mouse (43). To examine if this is the case for the EGFP recombination substrate in the raDR-GFP mice, we used positive control mice harboring a green fluorescent protein gene at the *ROSA26* locus. Flow cytometry analysis of disaggregated cells from 11 tissues of these mice showed high expression of green fluorescent protein in all tissues examined (Table 3-1). While there is a slight variability among tissues, the universally

strong expression observed in the *ROSA26* positive control suggests recombinant cells can potentially be detected in all examined tissues of the raDR-GFP mouse.

To compare the raDR-GFP and FYDR strains for transgene expression, we examined intact organs and frozen tissue sections from raDR-GFP and FYDR positive control mice. While the FYDR positive control mice were isolated from a recombination event in the germline, which generated mice that express EYFP from the original locus under the original promoter, we have yet to isolate such an event in the raDR-GFP line. Therefore, we used an additional knock-in line expressing a green fluorescent protein from the CAG promoter at the *ROSA26* locus to determine transgene expression (see materials and methods for details). Fluorescence microscopy showed high expression of EYFP in the pancreas of FYDR positive control mice, but low expression in the liver and colon, as expected (Figure 3-4A, upper row). In contrast, expression in the *ROSA26* positive control mice was very strong in all three organs (Figure 3-4A, lower row). Similar results were obtained when comparing expression levels in these organs by flow cytometry (Figure 3-4B). Thus, the broad expression of the HR reporter in raDR-GFP mice enables studies that were not possible with the previous FYDR strain.

Spontaneous HR is Detectable in Various Tissues

High reporter expression in multiple tissues indicates that it is now possible to study HR in those tissues. To measure spontaneous HR, tissues from 10 raDR-GFP mice were disaggregated and analyzed by flow cytometry for EGFP fluorescence. Remarkably, fluorescent recombinant cells were apparent in nearly all tissues (Figure 3-5). As in the

FYDR mice, recombinant cells were detectable in the pancreas. Similar numbers of recombinant cells were observed in the spleen. Significantly lower numbers of recombinant cells were found in the kidney, heart, liver, mammary gland, and colon ($p<0.05$). An even lower frequency was measured in the stomach, and remarkably, almost no fluorescent cells were detected in the brain ($p<0.005$). As we have shown that almost all cells in the brain have the potential to express fluorescent protein (~91% of cells from the *ROSA26* positive control mice were fluorescent), the very low frequency of fluorescent cells in raDR-GFP mice indicates that HR is truly reduced in the brain. This finding is consistent with the fact that HR is active in dividing cells, whereas in the brain, very few cells are mitotically active. Taken together, these are the first data to demonstrate that HR is active in almost all tissues of adult animals.

HR is Detectable *in situ* in the Pancreas, Liver, and Colon

Previous studies show that recombinant fluorescent cells can be detected *in situ* in intact pancreata of FYDR mice as fluorescent foci (39). Importantly, since recombination is a rare event and pancreatic cells do not migrate in tissue, individual fluorescent foci mostly represent independent recombination events (39). Further, *in situ* detection was found to be more sensitive than flow cytometry to detect differences in HR (39). We therefore set out to develop *in situ* detection of recombinant foci in selected tissues of the raDR-GFP mice. We first analyzed pancreata from FYDR mice (Figure 3-6, top row) and raDR-GFP mice (Figure 3-6, second row). At low magnification, the border of the pancreas is apparent and fluorescent foci can be detected. At a higher

magnification, isolated foci can readily be visualized and quantified. To identify the cell type giving rise to fluorescent foci, we analyzed tissue sections by combining fluorescence microscopy and H&E staining to create an overlay. Using this approach, we had previously analyzed 100 foci in the FYDR mice, and we showed that almost all consisted of pancreatic acinar cells (42). Although we have not yet performed an equally exhaustive analysis in raDR-GFP mice, all of the foci analyzed to date are comprised of acinar cells.

Comparing the numbers of recombinant foci in pancreata of FYDR and raDR-GFP mice revealed a higher frequency of HR events in raDR-GFP pancreata (Figure 3-S3, $p<0.005$). This difference may be due to locus effects, small differences in the HR reporter or other factors. Nevertheless, these results indicate that HR is readily detectable in the pancreata of raDR-GFP mice, which prompted us to explore *in situ* detection in other tissues. We found that recombinant foci are detectable within intact liver, and that hepatocytes can give rise to fluorescent recombinant cells (Figure 3-6, third row). We were also able to visualize recombinant cells within the colon (Figure 3-6, bottom row). Interestingly, analysis of frozen sections revealed examples of colonic crypts in which all cells express EGFP, which is consistent with detection of HR in a colonic stem cell (Figure 3-6, bottom row).

Taken together, we have developed *in situ* detection methodology to measure HR in the liver and colon of raDR-GFP mice in addition to the pancreas. *In situ* detection provides increased sensitivity over flow cytometry in addition to reduced sample

processing, and enables analysis of clonal expansion of recombinant cells. Thus, these methods enable rapid and sensitive quantification of HR with smaller cohort sizes.

DNA Damage Induces HR in raDR-GFP Mice

Having developed appropriate detection methods for HR in various tissues, we tested whether DNA damage-induced HR can be detected in raDR-GFP mice. In the course of a separate study using FYDR mice, we have shown that the combination of thyroid hormone (T3) and methylnitrosourea (MNU) is highly recombinogenic in the mouse pancreas (manuscript in preparation). MNU is a model chemical for the S_N1 type alkylating agents which include the chemotherapy drugs procarbazine, dacarbazine and temozolomide (51). To test whether raDR-GFP mice can be used to detect damage-induced HR, we subjected mice to the MNU/T3 combination treatment as described in Materials and Methods, and measured HR in the pancreas using *in situ* detection. We found HR to be significantly higher in MNU/T3 treated pancreata compared to control pancreata (Figure 3-7A, D, $p<0.0005$), demonstrating that raDR-GFP mice can be used to study exposure-induced HR in the pancreas. Remarkably, the increase in HR after this treatment was of the same magnitude in raDR-GFP and FYDR mice despite the different absolute frequencies (Figure 3-S4, $p<0.005$), further validating the raDR-GFP mice for the study of damage-induced HR *in vivo*. In addition to the pancreas, we also tested damage-induced HR in the liver and colon of raDR-GFP mice. *In situ* detection of recombinant foci revealed an induction of HR in these tissues after MNU/T3 treatment (Figure 3-7B,C, Figure 3-S5, $p<0.05$). These results indicate that

the raDR-GFP mouse model makes it possible for the first time to assess the impact of exposures on *de novo* HR events in the liver and colon of adult mice.

Recombinant Cells Accumulate with Age in the Pancreas, Liver, and Colon

Age is an important risk factor for cancer. We previously found that recombinant cells persist in the pancreas and accumulate with age, and the data can be generalized to indicate that the burden of cells harboring genetic changes increases with age (39). We therefore investigated the effect of aging on the numbers of recombinant foci detectable *in situ* in the raDR-GFP pancreas, liver, and colon. As we found in the FYDR mice, recombinant cells increase with age in the pancreata of raDR-GFP mice. The number of recombinant foci in the pancreas was higher at 6 months of age than at 3 months of age, and was further increased at 12 months of age (Figure 3-8A). Measuring HR in the liver and colon of these animals revealed a similar pattern of foci accumulation (Figure 3-8B, C). These data indicate that HR is active in these organs in adult animals and that cells that have undergone HR can persist and accumulate in the tissue. The raDR-GFP mice thus provide a valuable new tool for studying the formation and persistence of recombinant cells in several tissues *in vivo*.

3.5 Discussion

Cancer is a disease of the genome, as mutations in oncogenes and tumor suppressor genes can result in malignant transformation. Thus, an important question in cancer biology is 'what promotes mutagenic alterations in the genome?'. HR is a DNA DSB repair mechanism that is essential for life in vertebrates (11). While HR is generally error-free, misalignments during HR may lead to deleterious sequence rearrangements that can promote cancer. Studies in yeast and in mammalian cells have demonstrated that most carcinogens are recombinogens (16, 34, 52, 53), and sequence changes generated by HR have been found in multiple cancers (20-22). It is therefore important to learn about HR *in vivo*. Toward this end, we previously developed FYDR recombomice, which helped reveal important inducers of HR in the pancreas (40, 41, 48). However, the incomplete expression profile of the HR reporter gene in FYDR mice hampered studies in other organs.

Here we describe the raDR-GFP mouse, a novel HR reporter strain with a broad reporter expression profile. The raDR-GFP mice harbor an EGFP tandem repeat recombination substrate targeted to the *ROSA26* locus, which drives a broad expression of the reporter. The raDR-GFP mouse thus enables studies on HR in the liver, colon, spleen, heart, lung, kidney, stomach, thymus, brain, breast, and pancreas. Indeed, all 11 tissues tested had a strong reporter expression. By enabling the investigation of HR in cancer-prone organs such as the colon and breast, the raDR-GFP mouse is anticipated to yield important insights into the formation of cancer at these sites.

The raDR-GFP recombination substrate was designed to detect all of the major HR pathways. Since both expression cassettes contain a promoter and a polyadenylation signal, either cassette can be a donor or a recipient in a gene conversion event (44). Unequal sister chromatid exchange and replication fork repair at the raDR-GFP substrate may also yield a green fluorescent cell (44). Since the cassettes are arranged with deletions on the outer edges of the coding sequences, single-strand annealing between the repeats will yield a double mutant cassette and no fluorescent signal (44). Fluorescent recombinant cells may be isolated from raDR-GFP mice and subsequently analyzed by PCR or Southern blot to differentiate between HR pathways.

These studies show that nearly all tissues harbor recombinant cells, suggesting that HR is active in nearly all tissues of mammals. Interestingly, the one tissue that had almost no recombinant cells was the brain. Given that HR is active during S and G_2, and that most brain tissue is composed of non-dividing neurons, the extremely low frequency of recombinant cells in the brain is consistent with our understanding of the role of HR during cell division. These studies could provide insight into new avenues for chemotherapy, given a predicted differential dependence of proliferating tumor cells versus largely non-proliferating neurons on HR.

Detection of HR *in situ* is an important feature of the raDR-GFP mice. *In situ* detection has been shown to be more sensitive than flow cytometry in FYDR mice (39), requiring smaller experimental cohorts to detect differences in HR (41). Further, *in situ* detection offers the possibility to differentiate between *de novo* recombination events

and clonal expansion of recombinant cells (39). In tissues with low cell migration, recombinant foci mostly represent independent HR events. This is because HR is very rare, which makes it very unlikely that two neighboring cells in a recombinant focus arose by two separate HR events. On the other hand, if cell migration is low, then clonal expansion of recombinant cells is expected to increase the sizes of foci but not their numbers. Tissue architecture is therefore an important factor in the interpretation of raDR-GFP recombination data and can be visualized in the raDR-GFP model (54, 55). Taken together, the sensitivity of *in situ* detection and the possibility to integrate *de novo* HR, clonal expansion, and tissue architecture make the raDR-GFP mice a valuable tool for delineating the earliest steps of carcinogenesis in different tissues.

There are now many approaches for studying genetic change *in vivo*. The FYDR recombomice and p^{un} mice have proven to detect HR *in situ,* and additional mouse models for detection of HR *in vivo* have recently been developed (DR-EGFP, (56)) or are in development (HPRTdupGFP, Noda laboratory) (48, 56, 57). In addition, there are also mice that have been used to study LOH (*Aprt*$^{+/-}$, *Tk*$^{+/-}$, *Dlb-1* (58-60)) and point mutations/small deletions (*Pig-a*, Muta^{TM}Mouse, Big Blue$^{©}$, Plasmid *lac-z*, *cII*, *Gpt-Δ* (61-66)). LOH studies have been very useful for defining important parameters that lead to loss of genetic information, though extensive additional analysis is required to uncover the underlying mechanisms (15, 67). Importantly, for mouse models that detect point mutations/small deletions, DNA must be isolated and packaged into viral particles that are subsequently used to infect *E. coli* for colony forming assays (66-73). This process is laborious, expensive, slow, and significant expertise is required in order to obtain

reliable data, which together severely limit the utility of these models. In contrast, analysis of recombinant cells within intact raDR-GFP tissue requires minimal expertise, can be performed with standard fluorescent microscopy, and requires much less time (e.g., processing one raDR-GFP tissue takes ~10 minutes for imaging, and ~30 minutes for counting, compared to the many days that are required for methods requiring DNA analysis).

Treatment with a DNA methylating agent resulted in an increase in recombinant foci in the raDR-GFP mouse pancreas, liver, and colon. These results validate the raDR-GFP mice for the study of damage-induced HR in these organs and thus open doors to *in vivo* studies on sequence changes that were previously not possible. Remarkably, the increase in recombinant foci in the pancreas was of the same magnitude as that found using the FYDR mouse. This cross-validation between the FYDR and raDR-GFP strains highlights the specificity and sensitivity of HR detection by repeat substrates *in vivo*. The increase in HR in the liver and colon after DNA methylation damage is consistent with DNA methylating nitrosamines posing a risk factor for colon cancer and possibly liver cancer (74). Thus, the raDR-GFP mice can be used to investigate the effects of DNA damaging agents in a controlled *in vivo* system.

The model agent MNU used in this study is an S_N1 type methylating agent that generates methylated bases such as 3-methyladenine, 7-methylguanine and O^6-methylguanine (75). Several methylating agents creating these lesions are currently used in cancer chemotherapy including temozolomide, which is used to treat metastatic

melanoma and malignant gliomas (76). Importantly, HR contributes to resistance to methylating agents used in the clinic (77). Furthermore, HR induced in healthy tissues during treatment with methylating chemotherapeutics may be linked to the formation of therapy-induced secondary cancers (78). It is therefore of interest to study HR induced by chemotherapeutics both in tumors and in healthy tissue. Because of the broad reporter expression and sensitivity to methylation-induced HR, the raDR-GFP mice can be used to probe how chemotherapy pressures HR in different tissues, and potentially within tumors themselves. Such studies can yield valuable information for getting effective drug concentrations in tumors and also for protecting normal tissues and suppressing chemotherapy-induced cancers.

We have previously shown that the number of recombinant cells in the pancreas increases with age as a result of both the accumulation of *de novo* events and clonal expansion (39). Interestingly, in pancreatic tissue from aged mice, clonal expansion accounts for >90% of the total burden of recombinant cells (79). The observation that cells harboring genetic change accumulate with age is consistent with previous studies showing that point mutations in the liver, colon and heart increase with age (72, 73, 80). Additionally, studies beginning in the 1990s show that mutations in colonic stem cells accumulate with age in humans (81, 82). Here, along with analysis of age-induced recombination in the pancreas of the raDR-GFP mice, we have extended our analysis to include studies of the frequency of recombinant cells in the colon and the liver. For all three tissues there is a very clear accumulation of recombinant cells with age, which is consistent with the observation that point mutations also accumulate in these tissues.

Accumulation was higher in the pancreas and lower in the liver and colon. This difference may reflect the fact that cell turnover is the lowest in the pancreas among these organs. The fact that foci accumulate with age suggests either that the overall recombination rate is higher, or that somatic stem cells acquire sequence changes that persist over time. It will be interesting to differentiate among these possibilities in the future. The observation that recombinant cells accumulate with age demonstrates that this mouse model can be used to study long-term exposures that are believed to either induce or suppress recombination. As such, we anticipate that the raDR-GFP mice will be useful for studies of more environmentally relevant exposures.

In summary, we have generated and characterized raDR-GFP mice, a novel recombination reporter mouse strain with a broad reporter expression. These mice enable the study of tissues that were previously unavailable for studying HR. Further, sensitive *in situ* detection of HR is possible in raDR-GFP pancreas, liver, colon, and potentially in other organs. Treatment with a model alkylating agent induced HR in the raDR-GFP pancreas, liver, and colon, and these tissues also showed an accumulation of recombinant foci with age. Given that multiple mutations must accumulate in order for a normal cell to become neoplastic, the observation that the burden of cells harboring genetic change increases with age contributes to our understanding as to why the risk of cancer increases with age. Furthermore, knowledge about the extent to which different cell types undergo HR is expected to provide insights into the sensitivity of different cell types and tumors to chemotherapeutics whose toxicity is suppressed by HR. Taken together, the raDR-GFP mice have provided new insights into the role of HR *in vivo*, and

they promise to provide a powerful new approach for future studies of genetic, environmental and pharmaceutical-driven HR.

3.6 Acknowledgements

We thank the MIT Division of Comparative Medicine and the Center for Environmental Health Sciences at MIT and J. Kay for technical support and Dr. A. Burds Connor for transgenic services. We also thank Dr. L. Samson and Dr. J. Nickoloff for helpful comments on the manuscript. We acknowledge the Koch Institute Flow Cytometry Facility and the Histology core, particularly G. Paradis, M. Jennings, and M. Griffin. The pROSA26PA and pBigT plasmids were generous gifts from Dr. P. Soriano. This work was primarily supported by National Institutes of Health grant P01-CA026731 (to BPE) with additional support from National Institutes of Health T32 Training Grant in Environmental Toxicology ES007020 (to MRSJ) and a National Science Foundation Graduate Research Fellowship (to MRSJ). Partial support was provided by NIH grants 2-R01-CA079827-05A1 and R33-CA112151-01A2 (to BPE) and from the Kimmel Foundation (to LSC). The Koch Institute Core facilities are supported by NCI CCSG P30-CA14051. The Center for Environmental Health Sciences at MIT is supported by NIEHS P30-ES002109.

3.7 References

1. Helleday T (2003) Pathways for mitotic homologous recombination in mammalian cells. *Mutat Res* 532:103–115.

2. West SC (2003) Molecular views of recombination proteins and their control. *Nat Rev Mol Cell Biol* 4:435–445.

3. McHugh PJ, Spanswick VJ, Hartley JA (2001) Repair of DNA interstrand crosslinks: molecular mechanisms and clinical relevance. *Lancet Oncol* 2:483–490.

4. Friedberg EC (2005) Suffering in silence: the tolerance of DNA damage. *Nat Rev Mol Cell Biol* 6:943–953.

5. Symington LS, Gautier J (2011) Double-strand break end resection and repair pathway choice. *Annu Rev Genet* 45:247–271.

6. van Gent DC, Hoeijmakers JH, Kanaar R (2001) Chromosomal stability and the DNA double-stranded break connection. *Nat Rev Genet* 2:196–206.

7. Rich T, Allen RL, Wyllie AH (2000) Defying death after DNA damage. *Nature* 407:777–783.

8. Ferguson DO, Alt FW (2001) DNA double strand break repair and chromosomal translocation: lessons from animal models. *Oncogene* 20:5572–5579.

9. Pastwa E, Błasiak J (2003) Non-homologous DNA end joining. *Acta Biochim Pol* 50:891–908.

10. Helleday T, Lo J, van Gent DC, Engelward BP (2007) DNA double-strand break repair: from mechanistic understanding to cancer treatment. *DNA Repair (Amst)* 6:923–935.

11. Sonoda E, Hochegger H, Saberi A, Taniguchi Y, Takeda S (2006) Differential usage of non-homologous end-joining and homologous recombination in double strand break repair. *DNA Repair (Amst)* 5:1021–1029.

12. Takata M et al. (1998) Homologous recombination and non-homologous end-joining pathways of DNA double-strand break repair have overlapping roles in the maintenance of chromosomal integrity in vertebrate cells. *EMBO J* 17:5497–5508.

13. Ganesh A, North P, Thacker J (1993) Repair and misrepair of site-specific DNA double-strand breaks by human cell extracts. *Mutat Res* 299:251–259.

14. McKinnon PJ, Burgoyne LA (1985) Altered cellular morphology and microfilament array in ataxia-telangiectasia fibroblasts. *Eur J Cell Biol* 39:161–166.

15. Kolomietz E, Meyn MS, Pandita A, Squire JA (2002) The role of Alu repeat clusters as mediators of recurrent chromosomal aberrations in tumors. *Genes Chromosomes Cancer* 35:97–112.

16. Bishop AJR, Schiestl RH (2002) Homologous Recombination and Its Role in Carcinogenesis. *J Biomed Biotechnol* 2:75–85.

17. Yoshida J, Umezu K, Maki H (2003) Positive and negative roles of homologous recombination in the maintenance of genome stability in Saccharomyces cerevisiae. *Genetics* 164:31–46.

18. Gupta PK et al. (1997) High frequency in vivo loss of heterozygosity is primarily a consequence of mitotic recombination. *Cancer Res* 57:1188–1193.

19. Morley AA, Grist SA, Turner DR, Kutlaca A, Bennett G (1990) Molecular nature of in vivo mutations in human cells at the autosomal HLA-A locus. *Cancer Res* 50:4584–4587.

20. Shammas MA et al. (2009) Dysfunctional homologous recombination mediates genomic instability and progression in myeloma. *Blood* 113:2290–2297.

21. James CD, Carlbom E, Nordenskjöld M, Collins VP, Cavenee WK (1989) Mitotic recombination of chromosome 17 in astrocytomas. *Proc Natl Acad Sci USA* 86:2858–2862.

22. Pal J et al. (2011) Genomic evolution in Barrett's adenocarcinoma cells: critical roles of elevated hsRAD51, homologous recombination and Alu sequences in the genome. *Oncogene* 30:3585–3598.

23. Covo S, Ma W, Westmoreland JW, Gordenin DA, Resnick MA (2012) Understanding the origins of UV-induced recombination through manipulation of sister chromatid cohesion. *Cell Cycle* 11:3937–3944.

24. Latonen L, Laiho M (2005) Cellular UV damage responses--functions of tumor suppressor p53. *Biochim Biophys Acta* 1755:71–89.

25. Gehly EB, Landolph JR, Heidelberger C, Nagasawa H, Little JB (1982) Induction of cytotoxicity, mutation, cytogenetic changes, and neoplastic transformation by benzo(a)pyrene and derivatives in C3H/10T1/2 clone 8 mouse fibroblasts. *Cancer Res* 42:1866–1875.

26. Shimizu RW, Sun JD, Li AP, Newton GJ, Brooks AL (1984) The use of sister-chromatid exchange in Chinese hamster primary lung cell cultures to measure

genotoxicity. *Mutat Res* 130:333–342.

27. Helleberg H et al. (2001) Studies of dose distribution, premutagenic events and mutation frequencies for benzo[a]pyrene aiming at low dose cancer risk estimation. *Mutagenesis* 16:333–337.

28. Bishop AJ, Kosaras B, Sidman RL, Schiestl RH (2000) Benzo(a)pyrene and X-rays induce reversions of the pink-eyed unstable mutation in the retinal pigment epithelium of mice. *Mutat Res* 457:31–40.

29. Schiestl RH (1993) Nonmutagenic carcinogens induce intrachromosomal recombination in dividing yeast cells. *Environ Health Perspect* 101 Suppl 5:179–184.

30. Tikoo S, Sengupta S (2010) Time to bloom. *Genome Integr* 1:14.

31. LaRocque JR et al. (2011) Interhomolog recombination and loss of heterozygosity in wild-type and Bloom syndrome helicase (BLM)-deficient mammalian cells. *Proc Natl Acad Sci USA* 108:11971–11976.

32. Skorokhod OM, Kravchuk IV, Teleheiev HD, Maliuta SS (2006) [Role of Ku protein in normal and cancer cells]. *Ukr Biokhim Zh* 78:5–15.

33. Fu Y-P et al. (2003) Breast cancer risk associated with genotypic polymorphism of the nonhomologous end-joining genes: a multigenic study on cancer susceptibility. *Cancer Res* 63:2440–2446.

34. Reliene R, Bishop AJR, Aubrecht J, Schiestl RH (2004) In vivo DNA deletion assay to detect environmental and genetic predisposition to cancer. *Methods Mol Biol* 262:125–139.

35. Reliene R, Bishop AJR, Li G, Schiestl RH (2004) Ku86 deficiency leads to reduced intrachromosomal homologous recombination in vivo in mice. *DNA Repair (Amst)* 3:103–111.

36. Bishop AJ, Schiestl RH (2001) Homologous recombination as a mechanism of carcinogenesis. *Biochim Biophys Acta* 1471:M109–21.

37. Shao C et al. (2000) Chromosome instability contributes to loss of heterozygosity in mice lacking p53. *Proc Natl Acad Sci USA* 97:7405–7410.

38. Hendricks CA, Engelward BP (2004) "Recombomice": the past, present, and future of recombination-detection in mice. *DNA Repair (Amst)* 3:1255–1261.

39. Wiktor-Brown DM, Hendricks CA, Olipitz W, Engelward BP (2006) Age-dependent accumulation of recombinant cells in the mouse pancreas revealed by in situ

fluorescence imaging. *Proc Natl Acad Sci USA* 103:11862–11867.

40. Wiktor-Brown DM, Sukup-Jackson MR, Fakhraldeen SA, Hendricks CA, Engelward BP (2011) p53 null fluorescent yellow direct repeat (FYDR) mice have normal levels of homologous recombination. *DNA Repair (Amst)* 10:1294–1299.

41. Wiktor-Brown DM, Olipitz W, Hendricks CA, Rugo RE, Engelward BP (2008) Tissue-specific differences in the accumulation of sequence rearrangements with age. *DNA Repair (Amst)* 7:694–703.

42. Wiktor-Brown DM, Hendricks CA, Olipitz W, Rogers AB, Engelward BP (2006) Applications of fluorescence for detecting rare sequence rearrangements in vivo. *Cell Cycle* 5:2715–2719.

43. Soriano P (1999) Generalized lacZ expression with the ROSA26 Cre reporter strain. *Nat Genet* 21:70–71.

44. Jonnalagadda VS, Matsuguchi T, Engelward BP (2005) Interstrand crosslink-induced homologous recombination carries an increased risk of deletions and insertions. *DNA Repair (Amst)* 4:594–605.

45. Shao C et al. (1999) Mitotic recombination produces the majority of recessive fibroblast variants in heterozygous mice. *Proc Natl Acad Sci USA* 96:9230–9235.

46. Ledda-Columbano GM, Perra A, Pibiri M, Molotzu F, Columbano A (2005) Induction of pancreatic acinar cell proliferation by thyroid hormone. *J Endocrinol* 185:393–399.

47. Dopf J, Horiagon TM (1996) Deletion mapping of the Aequorea victoria green fluorescent protein. *Gene* 173:39–44.

48. Hendricks CA et al. (2003) Spontaneous mitotic homologous recombination at an enhanced yellow fluorescent protein (EYFP) cDNA direct repeat in transgenic mice. *Proc Natl Acad Sci USA* 100:6325–6330.

49. Li E, Bestor TH, Jaenisch R (1992) Targeted mutation of the DNA methyltransferase gene results in embryonic lethality. *Cell* 69:915–926.

50. Okabe M, Ikawa M, Kominami K, Nakanishi T, Nishimune Y (1997) "Green mice" as a source of ubiquitous green cells. *FEBS Lett* 407:313–319.

51. Fu D, Calvo JA, Samson LD (2012) Balancing repair and tolerance of DNA damage caused by alkylating agents. *Nat Rev Cancer* 12:104–120.

52. Schiestl RH, Gietz RD, Mehta RD, Hastings PJ (1989) Carcinogens induce intrachromosomal recombination in yeast. *Carcinogenesis* 10:1445–1455.

53. Bishop AJR, Schiestl RH (2003) Role of homologous recombination in carcinogenesis. *Exp Mol Pathol* 74:94–105.

54. Kim KH et al. (2007) Three-dimensional tissue cytometer based on high-speed multiphoton microscopy. *Cytometry A* 71:991–1002.

55. Kwon H-S, Nam YS, Wiktor-Brown DM, Engelward BP, So PTC (2009) Quantitative morphometric measurements using site selective image cytometry of intact tissue. *J R Soc Interface* 6 Suppl 1:S45–57.

56. Kass EM et al. (2013) Double-strand break repair by homologous recombination in primary mouse somatic cells requires BRCA1 but not the ATM kinase. *Proc Natl Acad Sci USA*.

57. Melvold RW (1971) Spontaneous somatic reversion in mice. Effects of parental genotype on stability at the p-locus. *Mutat Res* 12:171–174.

58. Gupta PK et al. (1994) Analysis of in vivo somatic mutations at the APRT locus. *Adv Exp Med Biol* 370:653–656.

59. Dobrovolsky VN, Casciano DA, Heflich RH (1999) Tk+/- mouse model for detecting in vivo mutation in an endogenous, autosomal gene. *Mutat Res* 423:125–136.

60. Vomiero-Highton G, Heddle JA (1995) An assay for loss of heterozygosity in vivo at the Dlb-1 locus. *Mutagenesis* 10:381–384.

61. Bryce SM, Bemis JC, Dertinger SD (2008) In vivo mutation assay based on the endogenous Pig-a locus. *Environ Mol Mutagen* 49:256–264.

62. Gossen JA et al. (1989) Efficient rescue of integrated shuttle vectors from transgenic mice: a model for studying mutations in vivo. *Proc Natl Acad Sci USA* 86:7971–7975.

63. Stiegler GL, Stillwell LC (1993) Big Blue transgenic mouse lacI mutation analysis. *Environ Mol Mutagen* 22:127–129.

64. Dollé ME, Martus HJ, Gossen JA, Boerrigter ME, Vijg J (1996) Evaluation of a plasmid-based transgenic mouse model for detecting in vivo mutations. *Mutagenesis* 11:111–118.

65. Swiger RR et al. (1999) The cII locus in the MutaMouse system. *Environ Mol Mutagen* 34:201–207.

66. Nohmi T et al. (1996) A new transgenic mouse mutagenesis test system using Spi- and 6-thioguanine selections. *Environ Mol Mutagen* 28:465–470.

67. Hsu C-H, Stedeford T (2010) *Cancer Risk Assessment* (Wiley).

68. Thybaud V et al. (2003) In vivo transgenic mutation assays. *Mutat Res* 540:141–151.

69. Hill KA et al. (2004) Spontaneous mutation in Big Blue mice from fetus to old age: tissue-specific time courses of mutation frequency but similar mutation types. *Environ Mol Mutagen* 43:110–120.

70. Stuart GR, Oda Y, Boer JG, Glickman BW (2000) No change in spontaneous mutation frequency or specificity in dietary restricted mice. *Carcinogenesis* 21:317–319.

71. Stuart GR, Oda Y, de Boer JG, Glickman BW (2000) Mutation frequency and specificity with age in liver, bladder and brain of lacI transgenic mice. *Genetics* 154:1291–1300.

72. Ono T et al. (2000) Age-associated increase of spontaneous mutant frequency and molecular nature of mutation in newborn and old lacZ-transgenic mouse. *Mutat Res* 447:165–177.

73. Dollé ME, Snyder WK, Gossen JA, Lohman PH, Vijg J (2000) Distinct spectra of somatic mutations accumulated with age in mouse heart and small intestine. *Proc Natl Acad Sci USA* 97:8403–8408.

74. Kuhnle GGC, Bingham SA (2007) Dietary meat, endogenous nitrosation and colorectal cancer. *Biochem Soc Trans* 35:1355–1357.

75. Wyatt MD, Pittman DL (2006) Methylating agents and DNA repair responses: Methylated bases and sources of strand breaks. *Chem Res Toxicol* 19:1580–1594.

76. Zhang J, Stevens MFG, Bradshaw TD (2012) Temozolomide: mechanisms of action, repair and resistance. *Curr Mol Pharmacol* 5:102–114.

77. Zhang X et al. (2012) Deletion of ku homologs increases gene targeting frequency in Streptomyces avermitilis. *J Ind Microbiol Biotechnol* 39:917–925.

78. Allan JM, Travis LB (2005) Mechanisms of therapy-related carcinogenesis. *Nat Rev Cancer* 5:943–955.

79. Wiktor-Brown DM, Kwon H-S, Nam YS, So PTC, Engelward BP (2008) Integrated one- and two-photon imaging platform reveals clonal expansion as a major driver of mutation load. *Proc Natl Acad Sci USA* 105:10314–10319.

80. Hill KA et al. (2005) Tissue-specific time courses of spontaneous mutation frequency and deviations in mutation pattern are observed in middle to late

adulthood in Big Blue mice. *Environ Mol Mutagen* 45:442–454.

81. Fuller CE, Davies RP, Williams GT, Williams ED (1990) Crypt restricted heterogeneity of goblet cell mucus glycoprotein in histologically normal human colonic mucosa: a potential marker of somatic mutation. *Br J Cancer* 61:382–384.

82. Okayasu I et al. (2006) Significant increase of colonic mutated crypts correlates with age in sporadic cancer and diverticulosis cases, with higher frequency in the left- than right-side colorectum. *Cancer Sci* 97:362–367.

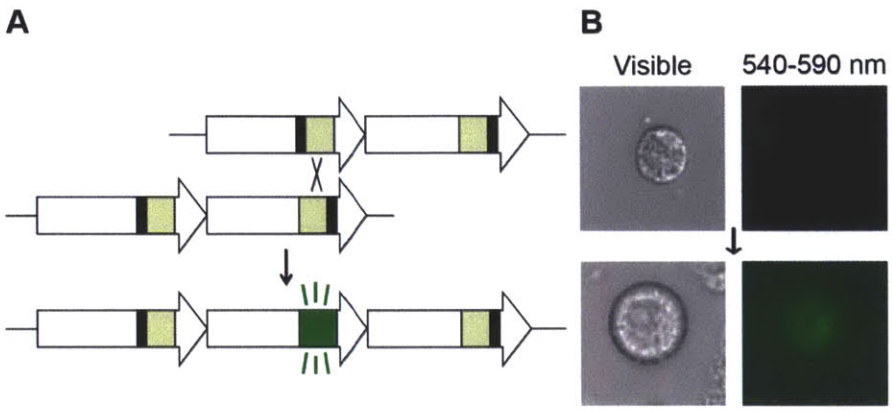

Figure 3-1. Arrangement of raDR-GFP Direct Repeat Transgene and Recombinant raDR-GFP Cells. (A) Sequences in *Δ3egfp* and *Δ5egfp* are represented by two large arrows with emphasis on the coding sequences (green), deleted regions (black). Expression is driven by the chicken β-actin promoter and cytomegalovirus enhancer and each cassette contains a promoter, intron, and poly-adenylation signal. An HR event between the two expression cassettes can restore a full-length EGFP coding sequence, resulting in a fluorescent cell. (B) Images of embryonic stem cells from raDR-GFP mice. Top: unrecombined, Bottom: recombined. Images are pseudocolored green.

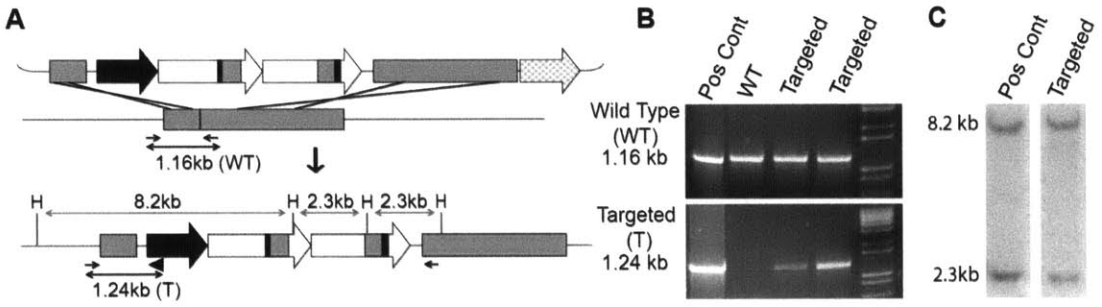

Figure 3-2. Arrangement of the DNA Targeted to the *ROSA26* Locus of raDR-GFP Mice. (A) Diagram of the DNA integrated within the raDR-GFP mice. PCR primers are indicated with arrows and *HindIII* (H) restriction site marked. (B) PCR analysis of targeted clones. (C) Southern analysis of raDR-GFP genomic DNA probed with *EGFP* coding sequence.

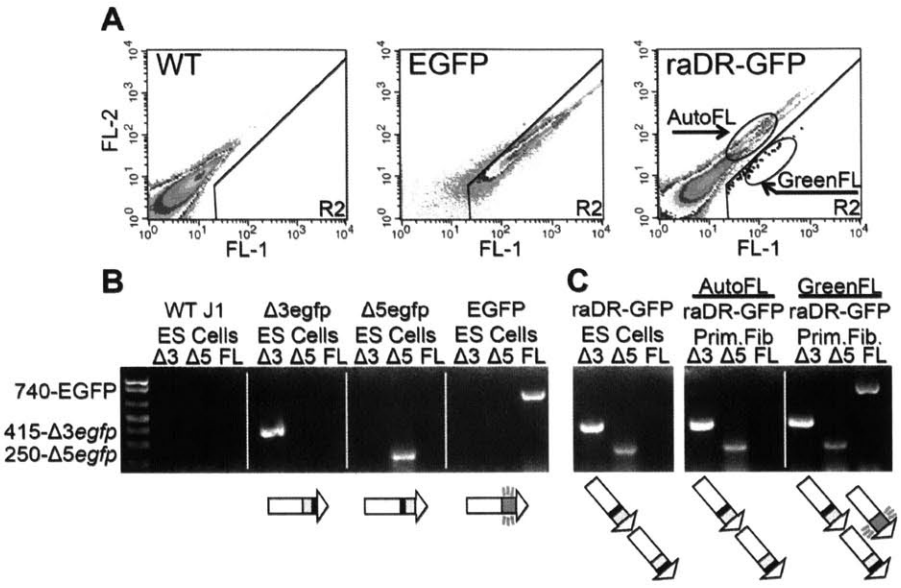

Figure 3-3. Analysis of Cells from raDR-GFP Mice. (A) Flow-cytometry results from fibroblasts from a wild-type mouse, an *EGFP-expressing* mouse, and a raDR-GFP mouse. FL-1 relative fluorescence intensity is 515–545 nm versus FL-2 562–588 nm. For clarity, data for individual cells (dots) have been darkened in the raDR-GFP R2 region. (B) PCR analysis of embryonic stem (ES) cells targeted with individual cassettes. Primers that bind sequences unique to either *Δ3egfp* or *Δ5egfp* yield a 415-bp or 250-bp product respectively. Primers that bind to the full-length EGFP sequence yields a 740-bp product. (C) PCR analysis of un-recombined raDR-GFP targeted embryonic stem cells and raDR-GFP adult fibroblasts. Adult fibroblasts were sorted into autofluorescent and green fluorescent populations with FACS and analyzed by PCR. Green fibroblasts contain the *Δ3egfp*, *Δ5egfp*, and full-length EGFP.

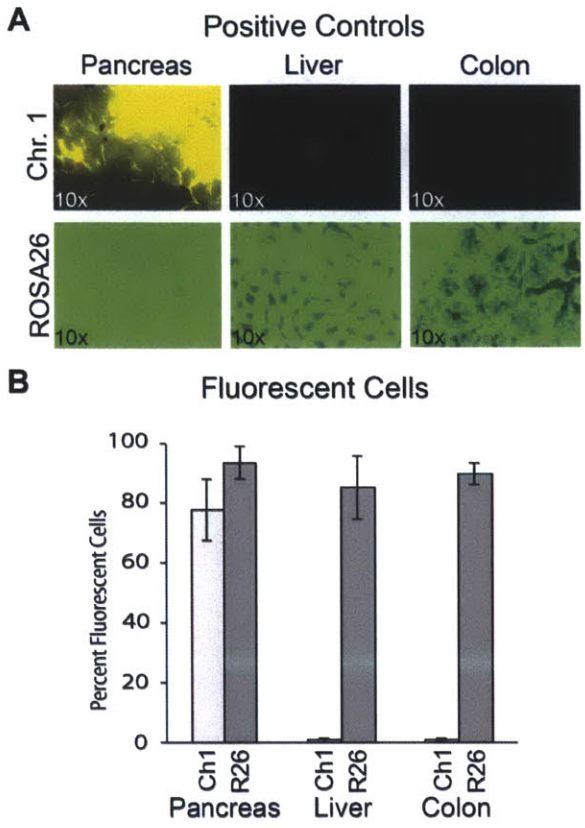

Figure 3-4. Expression of *EGFP* in Various Tissues of Positive Control raDR-GFP Mice. (A) Histological images were collected at 10x. Top row: Chromosome 1 positive control tissues. Bottom row: *ROSA26* positive control tissues. Brightness/contrast for EYFP filtered images was adjusted equivalently all images. EYFP and EGFP fluorescence is pseudocolored. (B) The percentage of cells expressing fluorescent protein in various positive control tissues.

Table 3-1. Recombination Rate and Expression in raDR-GFP C57BL/6 Mice

Tissue	Average Percentage of Fluorescent Cells in 10 raDR-GFP Positive Control Mice ± s.d.
Brain	91 ± 6
Cecum/colon	90 ± 4
Heart	74 ± 18
Kidney	79 ± 9
Liver	86 ± 10
Lung	79 ± 18
Breast	87 ± 9
Pancreas	94 ± 5
Spleen	83 ± 2
Stomach	75 ± 24
Thymus	83 ± 13

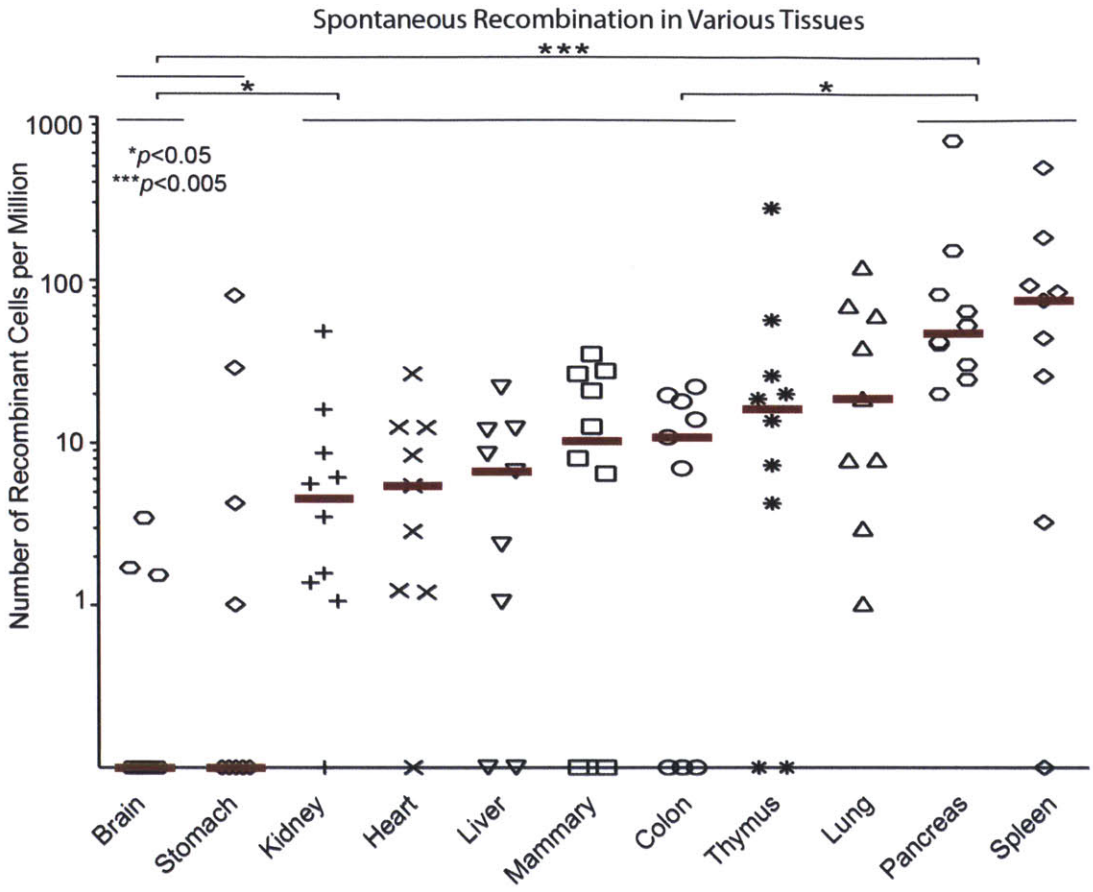

Figure 3-5. Flow Cytometry Detects Spontaneous Recombination in Various Tissues of Heterozygous raDR-GFP Mice (2 mo old). The brain is significantly different than all other organs except for the stomach. The number of recombinant cells per million in the pancreas and spleen are significantly higher than all other organs except for the thymus and lung. The number of recombinant cells per million is reported as Individual data points and medians (n=10).

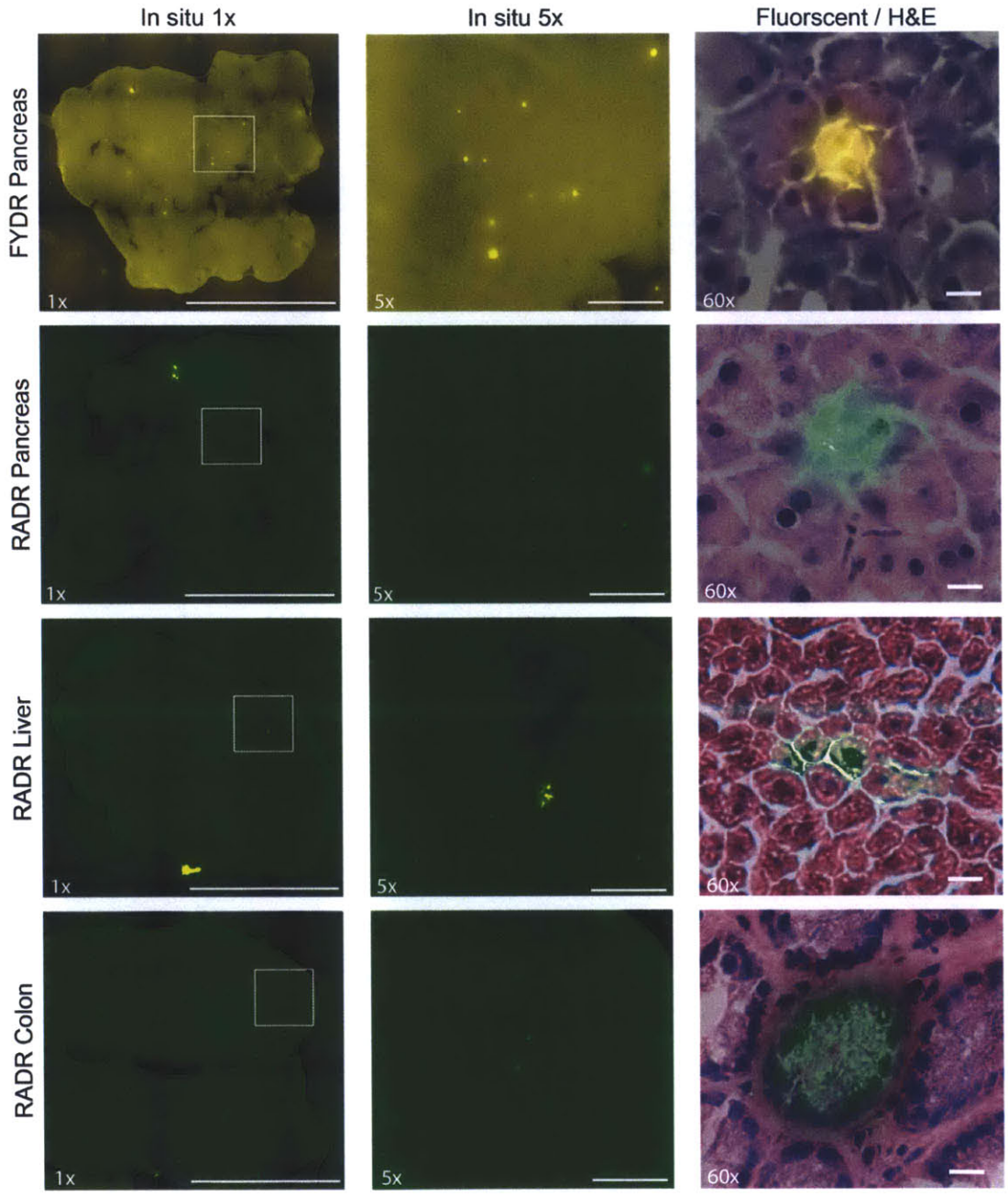

Figure 3-6. Recombinant Foci in Various Tissues of FYDR and raDR-GFP Mice. First column: *In situ* images were collected at 1x (scale = 1cm), Second column: 5x zoom of boxed region of the 1x (scale = 10mm). Brightness and contrast for *in situ* images were adjusted equivalently. Last column: Histological images were collected at 60x. Fluorescence image under EGFP filter (510–560 nm) overlaid with H&E stained section. Brightness/contrast for EGFP filtered images was optimized for each histological section. Fluorescence is pseudocolored.

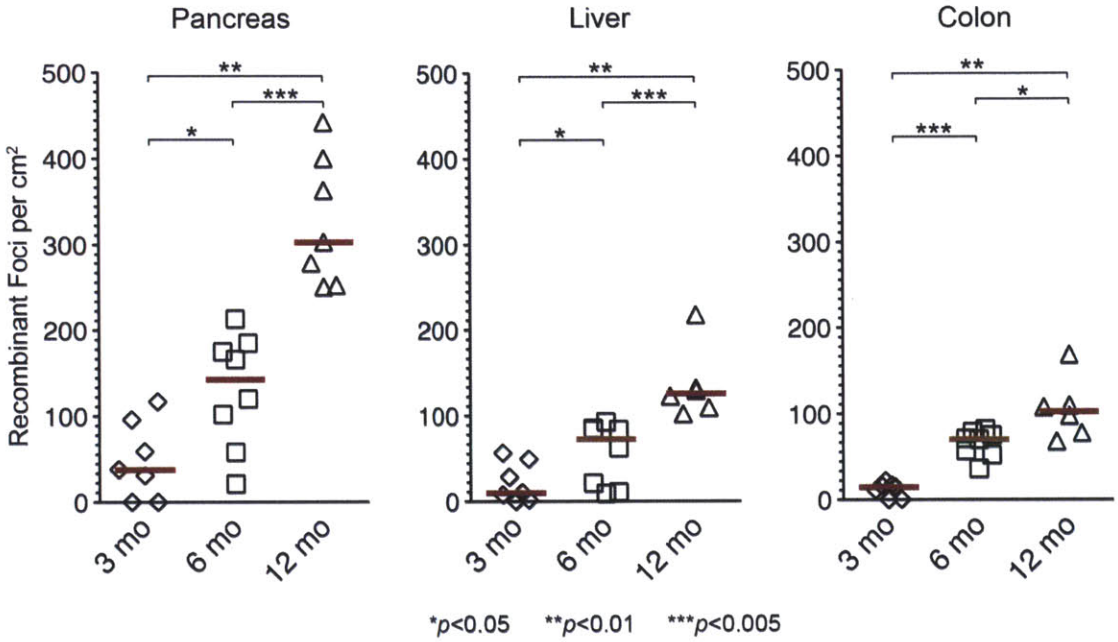

Figure 3-7. Effect of Aging on the Frequency of Recombinant Foci in the Pancreas, Liver, and Colon. Recombinant foci per square cm was detected by *in situ* image analysis of organs from 3 month old, 6 month old, and 12 month old mice. Medians are indicated by red bars.

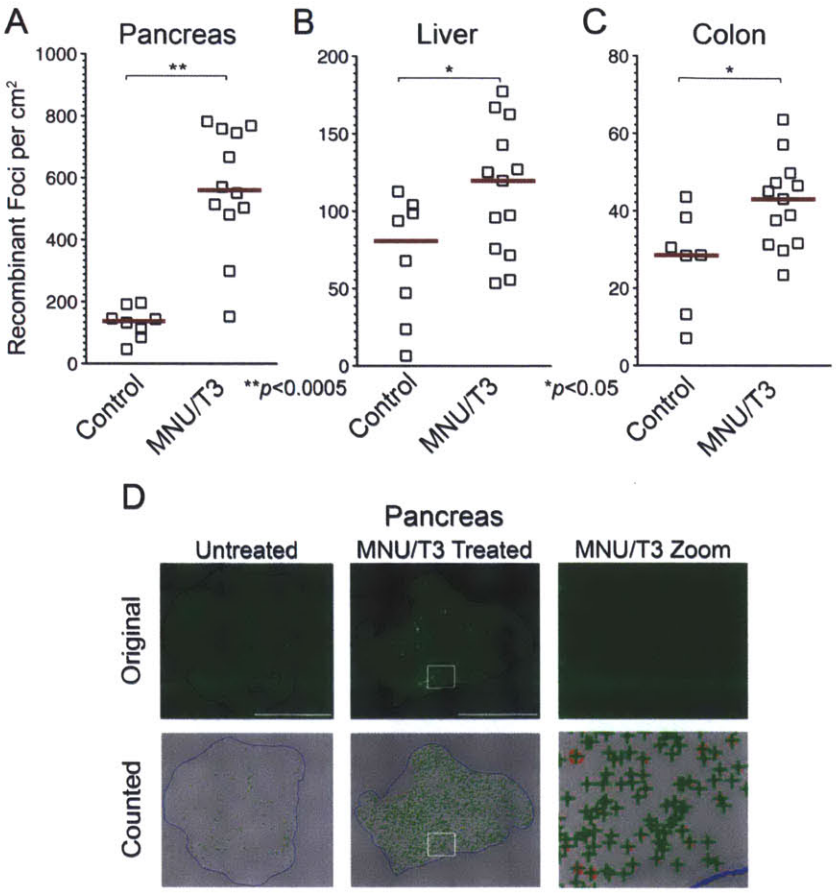

Figure 3-8. Effect of MNU/T3 Treatment on Frequency of Recombinant Cells in the Pancreas, Liver, and Colon. Recombinant foci per square centimeter in the (A) pancreas, (B) liver, and (C) colon show significant increase after treatment with MNU/T3. Medias are indicated by red bars. (D) Compiled images for untreated and treated pancreata with an example of the automatic counting program. Brightness and contrast was adjusted non-linearly to enhance fluorescent foci visibility. Scale = 1 cm. Representative liver and colon images can be found in Figure 3-S5.

Supplemental Figures

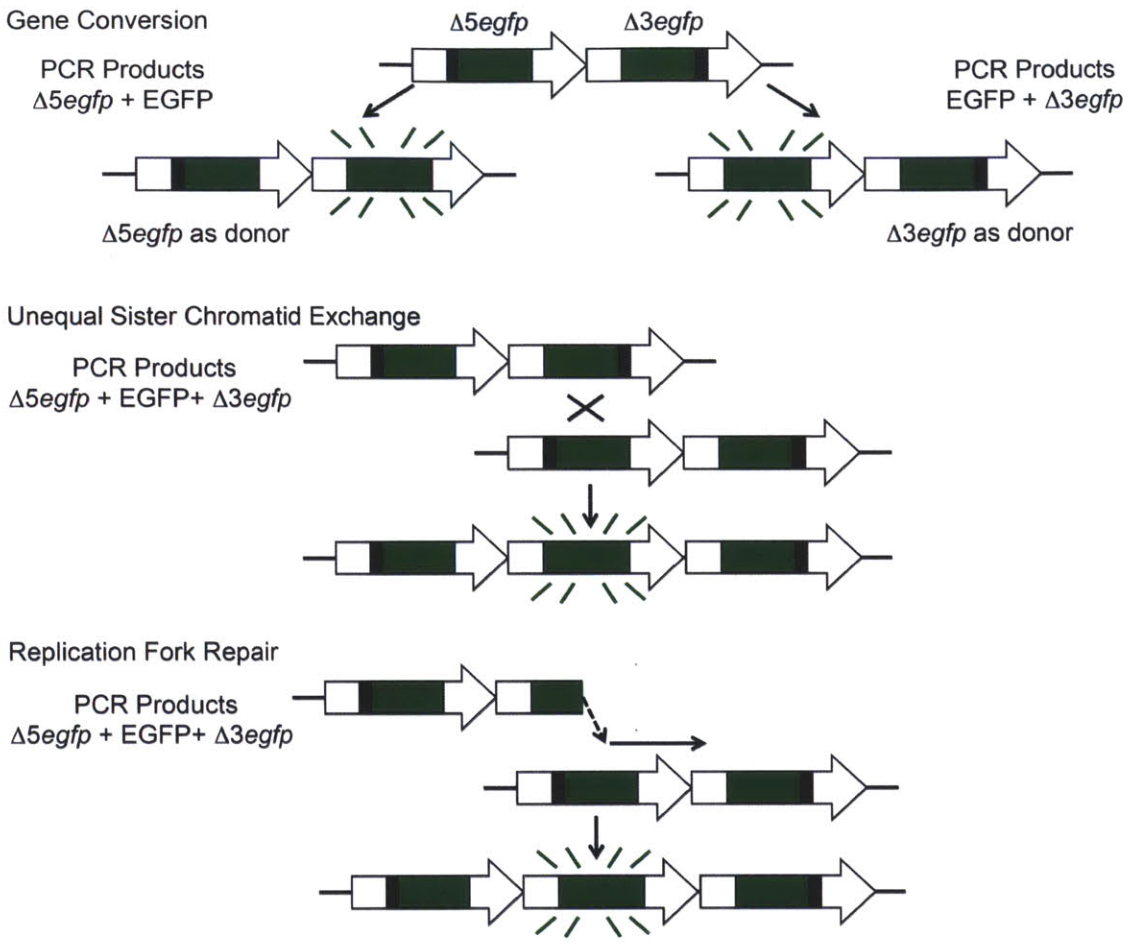

Figure 3-S1. Outline of the Major HR Pathways Resulting in a Fluorescent Cell for the raDR-GFP Construct. Gene conversion without cross-over of flanking sequences. Unequal sister chromatid exchange reconstitutes *EGFP* in one of two daughter cells. Replication fork repair after replication fork breakdown. Single strand annealing (SSA) cannot reconstitute full length *EGFP* in the raDR-GFP construct (not pictured).

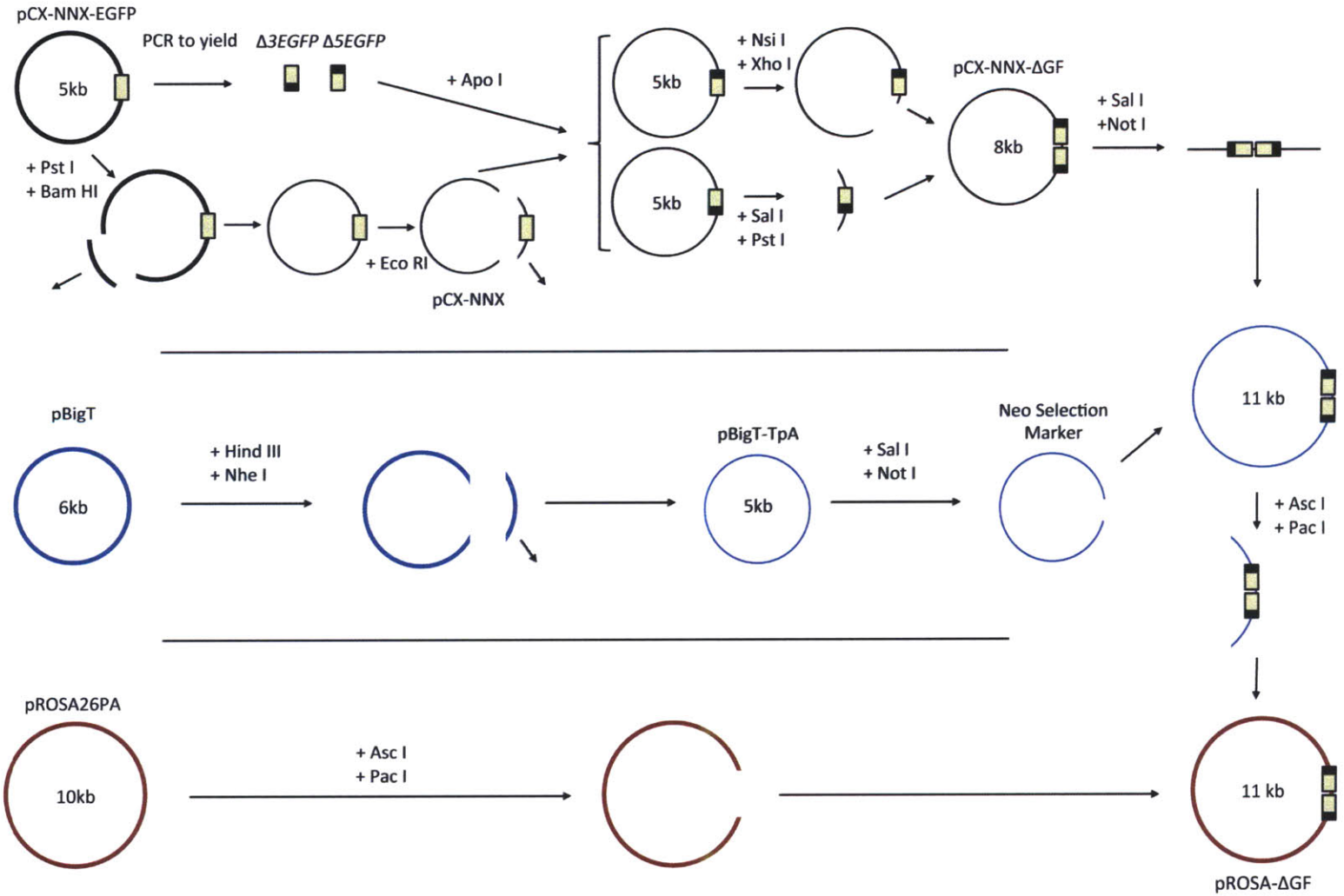

Figure 3-S2. The Δ*3EGFP* and Δ*5EGFP* Cassettes were Created from the pCX-NNX-EGFP Plasmid. A portion of the pCX-NNX-EGFP plasmid is removed with *PstI* and *BamHI* and the EGFP cassette is removed with *EcoRI*. Both the Δ*3egfp* and Δ*5egfp* cassettes are inserted into the PCX backbone to yield pCX-NNX-ΔGF. The pCX-NNX-ΔGF cassette is collected through Sal1 and *NotI* digestion and ligated into a prepared BigT-TpA backbone to confer neomycin resistance. The ΔGF and NEO cassette are harvested and inserted into the pROSA26PA backbone to yield pROSA-ΔGF.

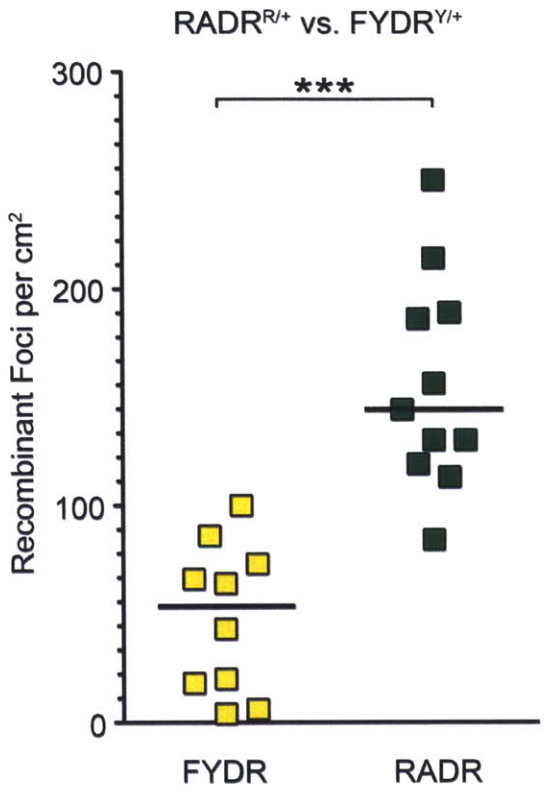

Figure 3-S3. Recombinant Foci per square Centimeter in the Pancreata of FYDR and raDR-GFP Mice. Different locus of incorporation and difference in the transgene contribute to the difference in recombination in heterozygous 2 month-old mice. Medians are indicated by black bars.

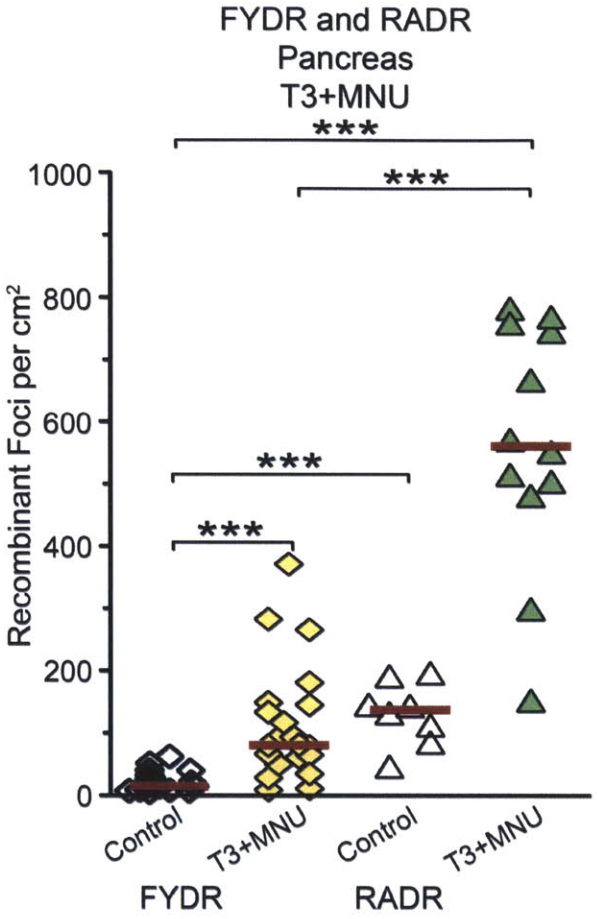

Figure 3-S4. Comparison of the Response to MNU/T3 Treatment in FYDR and raDR-GFP Mice. Both the FYDR and raDR-GFP mice show approximately a 5-fold increase in recombinant foci per square cm. Medians are indicated by red bars.

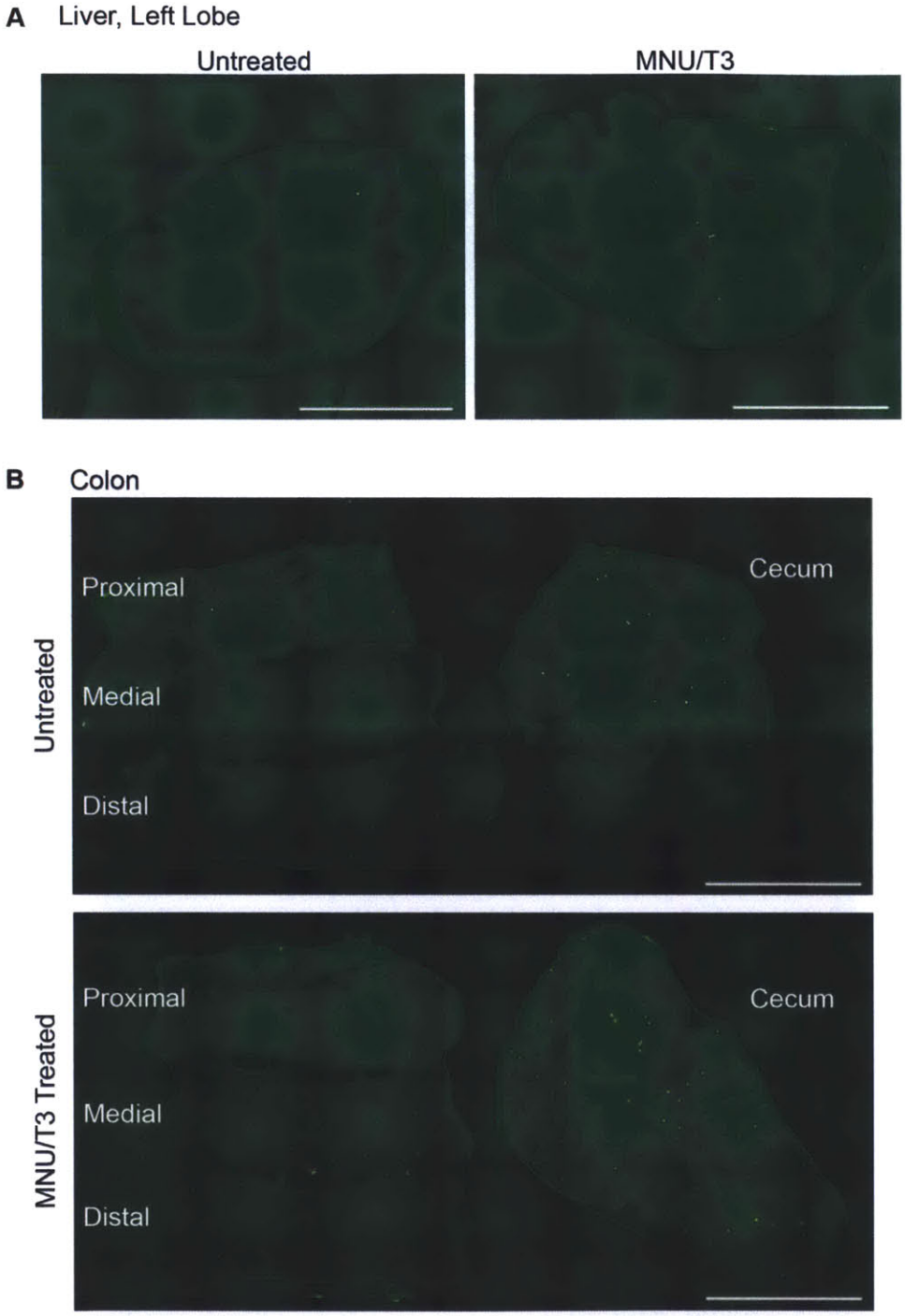

Figure 3-S5. Tissue Response to MNU/T3 Treatment. Representative compiled images of (A) liver and (B) colon response to MNU/T3 treatment. All images were taken with fixed exposure and brightness and contrast were adjusted identically for all images. Images were adjusted non-linearly to increase contrast for publication.

Chapter IV

Studies of Inflammation and its Impact on Homologous Recombination in Proximal and Distal Tissues *in vivo*

Chapter IV

4.1 Abstract

Inflammation is a known risk factor for cancer, but the effects of localized inflammation on distal biological systems are not yet fully-understood. The reactive oxygen nitrogen species resulting from inflammation directly damages DNA, leading us to investigate the role of HR in response to inflammation. We investigated the effects on HR in the pancreas of FYDR mice with long-term DSS-induced inflammation of the colon, but did not see any effect, leading us to explore a model that is susceptible to inflammation. Experimental *Rag2*$^{-/-}$ animals lack mature T- and B-cells, which leads to a predilection for inflammation, and we saw that unchallenged *Rag2*$^{-/-}$ *IL10*$^{-/-}$ *raDR-GFP*$^{R/+}$ mice, which are also deficient in an anti-inflammatory cytokine, showed a significant increase in recombinant foci in the pancreas when compared with unchallenged WT mice, leading us to further investigate the effects of induced inflammation. Examination of HR in raDR-GFP mice with long-term (10 week) *Helicobacter hepaticus* infection showed no consistent change locally in the colon, or distally in the pancreas or liver. An unexpected but significant decrease in the number of recombinant foci was seen in the liver in addition to a decrease in the total number of recombinant cells in the colon. Longer duration studies (20 week) of *Helicobacter trogontum* infection also show no detectable change in the level of homologous recombination in the colon, pancreas, or liver. Other studies have shown damage coupled with proliferation synergistically

increases HR; therefore the lack of a consistent HR response in these infection studies may reflect the temporal separation of DNA damage and proliferation as a response to inflammation *in vivo*, possibly as a mechanism to prevent DNA damage in proliferating cells. Further study of exposure-induced HR is necessary to understand the implications of environmentally-induced inflammation on DNA repair.

4.2 Introduction

Chronic Inflammation Increases Cancer Risk

Chronic inflammation induces carcinogenesis and may increase the susceptibility of predisposed individuals to cancer (1-3). As an example, patients with IBD, including ulcerative colitis (UC), and Crohn's disease have a 3- to 5-fold increase in risk of developing colorectal cancer over the general population, with some reporting a 19-fold increase in risk with extensive UC (4-6). Inflammation associated with human immune system activation by parasitic, viral, and bacterial infections have contributed to cancer in the bladder (7), liver (8), and stomach (9), in addition to other tissues (1, 10-14). Induction of chronic inflammation by *Helicobacter pylori* infection has been shown to cause gastric cancer in humans (15-17). Furthermore, non-infectious, environmentally induced inflammation has been implicated in a number of other cancers affecting the lung, liver, esophagus, and pancreas (18-20). Samson and colleagues illustrated the danger of inflammation in a two-step model of carcinogenesis that is initiated by inflammation-induced DNA damage and further promoted by an inflamed microenvironment conducive to cellular proliferation (1-3, 21). We hypothesize that cancer associated with *H. pylori* and other infections is the result of inflammation-induced DNA damage and associated proliferation.

Inflammation Induces DNA Damage Through ROS and RNS

The mechanistic link between inflammation and cancer begins with the production of nitric oxide (NO), superoxide ($O_2^{\bullet-}$) and other reactive oxygen and nitrogen species (ROS, RNS) by neutrophils and macrophages of the innate immune system (4-6, 22). In the case of bacterial infection, the initial biological insult causes cells to release cytokine and chemotactic signals that recruit other immune cells and mediate infected cell death (7, 22, 23). The high levels of NO produced by macrophages not only interfere with normal cell-signaling but also react with $O_2^{\bullet-}$ and oxygen to produce a plethora of DNA damaging nitrogen species that can cause the deamination, oxidation, or halogenation of DNA nucleobases in addition to causing the formation of DNA adducts (8, 21, 22, 24, 25). Meira, *et al.*, showed that repeated bouts of dextran sulfate sodium (DSS) induced colitis, which, while not directly damaging DNA, did result in increased εdA, εdC, and 8oxoG lesions as a result of the chemically-induced inflammation, and that tumorgenesis was dependent on a DNA damage initiating event (9, 21).

Bacterial Infection Induces Tumorgenesis

In addition to causing inflammation in the stomach, *H. pylori* infection is a known human carcinogen that results in increased in 8oxoG lesions in the gastric mucosae (1, 10-14, 26, 27). Similarly, analogous infections with *Helicobacter hepaticus* in mice cause a variety of inflammation-induced genomic lesions that result in colitis and hepatitis in a

number of immunodeficient mice (e.g. *Rag2*$^{-/-}$ and/or *IL10*$^{-/-}$ animals). In fact, infection of *Rag2*$^{-/-}$ mice has shown to cause malignant invasive colorectal cancer (15-17, 28, 29) and these lesions resembled neoplasia in human IBD patients (18-20, 30), showing a clear link between bacterial infection an carcinogenesis.

To create a hospitable niche for long-term infection of the gastrointestinal tract, *H. pylori* produces CagA and VacA that helps the invading bacteria evade the host response (9). *H. hepaticus* also produces a similar protein, cytolethal-distending toxin (CDT), that enables chronic infection and causes cell cycle arrest with eventual cell death (31, 32). A subunit of CDT enters the nucleus inducing DNA damage, including DSBs, with its DNaseI-like degradation of DNA (33). *In vitro* studies of cell lines treated with CDT indicates cell cycle arrest in G_1 or G_2, or direct apoptosis depending on cell type (34-36). Notably, human intestinal epithelial cell lines treated with CDT have shown to arrest primarily in G_2 and DNA DSBs cause cell cycle arrest in G_2 (33, 37-39). Thus, CDT may be the DNA damage-initiating factor that leads to tumorgenesis in response to bacterial infection and associated inflammation.

Surprisingly, the distal inflammatory effects of *H. hepaticus* infection of the colon induced mammary adenocarcinoma in *APC*$^{Min/+}$ mice, which are susceptible to spontaneous intestinal neoplasia (10, 40). As the pancreas and liver are much closer to the colon spatially and systemically than mammary tissue, we hypothesized that infection in the colon would also induce damage in these systems. In addition to dangerous mispairings and mutations, this damage or the attempt to repair this damage

may lead to replication fork breakdown during mitosis and result in deletions, duplications, or translocations as a consequence of HR (41, 42).

Innate and Adaptive Immunity

Inflammation related to *H. hepaticus* infection also seems to be linked with its production of CDT, suggesting an interaction between the host immune system and the invading bacteria (39). The immune system is responsible for the inflammatory response to bacteria, viral, or foreign body threats. Mature B and T lymphocytes within the mammalian adaptive immune system are able to recognize pathogens *in vivo* through V(D)J rearrangement of genes recognizing variable domains of immunoglobulin (Ig) or T cell receptor (TCR) molecules that are unique to each type of bacteria (43). While the V(D)J recombination process involves a complex coordination of numerous enzymes, the RAG2 protein is necessary for mature T and B lymphocyte development and adaptive immunity (44). *Rag2*$^{-/-}$ mice are left with innate immunity consisting of a variety of leukocytes: mast cells, natural killer cells, eosinophils, basophils, macrophages, neutrophils, and dendritic cells that are responsible for the initial response of inflammation and provide a physical or chemical barrier to prevent the spread of infectious agents (45). The innate immune response also recruits and primes the specialized adaptive immune response and then subsides. Since the adaptive immune response is unavailable in *Rag2*$^{-/-}$ mice, the inflammatory based innate immune response is thought to be constitutively active in the face of parasitic, viral, or bacterial infections (10, 45-47). The increased susceptibility to inflammation of *Rag2*$^{-/-}$ mice

marks it as an ideal model to study the effects of infection-induced inflammation and damage on HR.

4.3 Materials and Methods

Experimental Animals

All experiments involving animals were performed according to protocols approved by the Institutional Animal Care and Use Committee at Massachusetts Institute of Technology and animals were housed in static microisolator cages in Association for Assessment and Accreditation of Laboratory Animal Care-approved facilities.

Female *Xrcc1*$^{floxp/floxp}$ *FYDR*$^{Y/Y}$ mixed-background littermates on the FVB background were split into DSS treated and control cohorts. In these mice, *Xrcc1* is flanked by floxp sites, but the *Xrcc1*$^{floxp/floxp}$ *FYDR*$^{Y/Y}$ mice do not contain a cre expression cassette. Thus, these homozygous FYDR mice are effectively wild-type.

To examine the effect of systemic inflammation on spontaneous HR events, we compared the pancreata of 6-8 week old *raDR-GFP*$^{R/+}$ with *Rag2*$^{-/-}$ *IL10*$^{-/-}$ *raDR-GFP*$^{R/+}$ mice on the 129 S6 background. All mice are housed in the same barrier animal facility with *Rag2*$^{-/-}$ *IL10*$^{-/-}$ *raDR-GFP*$^{R/+}$ mice receiving autoclaved food, water, and bedding.

Litters of *Rag2*$^{-/-}$ mice (129S6/SvEvTac-*Rag2*^{tm1Fwa}) (29) harboring the *raDR-GFP*$^{R/+}$ and *gpt-Δ* reporter were split into infection and control cohorts with equal numbers of males and females in each group. Uninfected mice were housed in a barrier facility free of known murine *Helicobacter* species, viruses, *Salmonella* species, *Citrobacter rodentuim*, ecto- and endoparasites.

Chronic DSS Exposure

Treated *XRCC1*$^{floxp/floxp}$ *FYDR*$^{Y/Y}$ mice were removed from normal water and provided water containing 2.5% dextran dodecyl sulfate (DSS, Sigma) *ad libidum* (n=5); control animals remained on regular water throughout the experiment (n=7). Six- to eight-week old mice received water with DSS for 5 days, followed by 16 days of regular water, for 8 cycles. Following the last DSS treatment, pancreata from these mice were harvested 9 days after being returned to normal water.

Experimental *H. hepaticus* Inoculation

H. hepaticus (strain 3B1, no. 51449; ATCC, Rockville, MD) was grown as described under microaerobic conditions on blood agar plates and collected into sterile freeze media (48). A total of 41 experimental *Rag2*$^{-/-}$ *raDR-GFP*$^{R/R}$ animals 6-8 weeks of age received 0.2 ml freezing medium (n=19) or freshly prepared *H. hepaticus* inoculum (total organism dose of 10^8 CFU, n=22) via gastric gavage every other day for 3 doses. Two weeks later, the mice received a second round of 3 doses every other day for a total of 6 doses. Prior to dosing, all *H. hepaticus* samples were examined via gram stain

to ensure >85% of the bacteria were in the spirochete form (virulent form). Mice were euthanized with carbon dioxide and tissues were harvested at 10 weeks post infection (w.p.i.) utilizing standard necropsy procedures. Feces were collected upon necropsy and analyzed by PCR using *H. hepaticus*-specific primers to verify infection (49).

Experimental *H. trogontum* Inoculation

H. trogontum (no. 700114; ATCC, Rockville, MD) was grown as described under microaerobic conditions on agar plates and collected into sterile freeze media (48). Litters of *Rag2*$^{-/-}$ *raDR-GFP*$^{R/+}$ mice were split into treated and untreated cohorts and were dosed at 6 to 8 weeks of age with 2×10^7 *H. trogontum* organisms (treated, n=11) or freezing media (untreated, n=9) twice over 5 days by oral gavage. Mice were euthanized with carbon dioxide and necropsied at time points between 15 and 20 w.p.i based on progressive evidence of bloody feces, dehydration, and weight loss in *H. trogontum* infected mice. Feces were collected 2 w.p.i and upon necropsy and analyzed by PCR using *H. trogontum*-specific primers to verify infection.

Fluorescent Foci Imaging

Upon harvest, tissues were placed in ice cold 0.01% soybean trypsin inhibitor (Y-9008 Sigma-Aldrich) until imaging. The lumen of the colon and cecum was incised and the laid open. The colon and cecum were gently shaken in RT PBS for 30 sec. and the surface gently irrigated with PBS to remove contents. The left lobe of the liver was harvested for recombinant cell analysis. For recombinant foci analysis, pancreata were

imaged as described previously (50, 51). Briefly whole organs were compressed to 0.5 mm and imaged using a fixed exposure time with a Nikon 80i microscope (1x objective). Composite images covering the surface of each tissue were taken with TRITC filter (Excitation: 540/25nm, Emission: 605/55 mn) and FITC (Excitation: 500/20 nm, Emission: 535/30 nm) and DAPI (Excitation: 360/20, Emission: 460/25). The Nikon Elements software associated with the Nikon80i camera was used to automatically pseudocolor black and white images.

The brightness and contrast of each experimental set of images was adjusted identically using Adobe Photoshop CS3 (Adobe Systems, San Jose, CA). Counting of foci in the pancreata and livers was performed with in-house developed counting software that also calculated the surface area of each organ, while foci in the colon was counted manually in a blinded fashion and area was determined manually by tracing the outline in ImageJ. After imaging, tissues were returned to ice cold 0.01% soybean trypsin inhibitor if processed for flow cytometry.

Fluorescent Cell Analysis by Flow Cytometry

Tissues were minced in 5 ml 2 mg/ml collagenase V in Hank's Buffered Salt Solution (C-9263 Sigma) using a GentleMacs Dissociator (Miltenyi Biotec, Auburn, CA). Tissue and collagenase solutions were incubated at 37°C for 45 min and shaken at approximately 150 cycles per minute. The samples were triturated and filtered through a 70 μm filter into 10 ml DMEM with 20% FBS on ice (Atlanta Biologicals, Lawrenceville, GA). Cells were pelleted at 1500 rpm for 10 minutes and resuspended in OptiMEM

(31985-062 GIBCO) and passed through a cell strainer filter for flow cytometry analysis (Falcon).

Histological Evaluation

Formalin-fixed tissues were embedded in paraffin, cut at 5 μm, and stained with hematoxylin and eosin for further analysis. A pathologist blinded to the identity of each sample scored the tissue for inflammation, lesions, and morphology. The ascending colon was scored on a scale of 0 to 4 with ascending severity (0, none; 1, minimal; 2, mild; 3, moderate; and 4, severe) as described (10).

Statistical Evaluation of Data

Fluorescent cell frequency follows a non-normal distribution, thus difference in fluorescent foci per square centimeter was calculated using a two-tailed Mann-Whitney test for both flow cytometry and foci data. Medians of non-parametric recombinant cell foci data are reported.

4.4 Results

A Pro-Inflammatory Environment Induces Recombination

To investigate effect of an inflamed environment on HR, we compared HR in the pancreas of 8 week-old pro-inflammatory *raDR-GFP*$^{R/+}$ mice deficient in both RAG2 and IL10 (n=10) and age-matched wild-type counterparts (n=7). The inflamed environment led to a significant increase in the number of fluorescent foci per square centimeter as seen in Figure 4-1 (39 vs 219, $p<0.0005$), showing that HR increases in response to systemic inflammation.

Chemically Induced Inflammation Does Not Induce Distal HR

To explore the result of distal damage as a result of a localized infection, we first investigated the effect of DSS-induced chronic inflammation in the colon on the distal site of the pancreas. At this time the raDR-GFP mice were not available so we utilized the FYDR mice to visualize HR in the pancreas. Previous pilot studies by Dr. Susan Erdman indicated pre-neoplastic lesions in the pancreas of *H. hepaticus* infected mice as seen in Figure 4-2, further motivating our study of HR in the pancreas in response to infection or inflammation in the colon. The animals in the DSS treated cohort (n=5) showed clear signs of colitis (ie, diarrhea, thickened colon, and in one animal, toxic mega colon), while the control cohort (n=7) showed no gross abnormalities. The number of fluorescent foci per square centimeter showed no change when comparing the two groups as seen in Figure 4-3 (11 vs 11, $p=0.92$), suggesting that previously observed

pancreatic lesions in the pancreata of *H. hepaticus* infected *Rag2*$^{-/-}$ mice are not solely induced by inflammation and that the immune system response may play a role in initiation of damage.

H. hepaticus Infection Does Not Lead to a Detectable Change in HR *in vivo*

In order to determine if the biological insult of *H. hepaticus* or *H. trogontum* infection would lead to an increase in HR, we examined HR in the colon, liver, and pancreas of homozygous raDR-GFP mice deficient in RAG2. While *H. hepaticus* is known to cause lower bowel inflammation and colon cancer (12), and did increase inflammation in the colon in this study as seen in Figure 4-4, it does not appear to increase HR in the colon. Examination of the number of fluorescent foci per square centimeter in the colon shows no detectable difference in HR between the infected and uninfected cohorts as seen in Figure 4-5 (20 vs 19, p=0.66). Surprisingly, the median number of recombinant cells per million determined by flow cytometry significantly decreased in the colons of *H. hepaticus* infected mice (69 vs 23, p=0.02).

While previous infection of RAG2 deficient mice with *H. hepaticus* has resulted in visible pre-neoplastic lesions in the pancreas (Figure 4-2), we again saw no difference in either the number of fluorescent foci per square centimeter (374 vs 347, p=0.54) or the total number of recombinant cells per million (103 vs 153, p=0.45) as seen in Figure 4-6. Surprisingly, as seen in Figure 4-7, there are significantly more fluorescent foci per square centimeter in the livers of uninfected mice when compared with infected mice (40 vs 25, p=0.048). This difference was not observed in the total number of fluorescent

cells per million (16 vs 11, p=0.98). Though the number of animals in the control and infected cohort was of appropriate size, 19 and 22 respectively, the distribution of recombinant foci per square centimeter and fluorescent cells per million indicates that these populations have a large overlap. These inconsistent results indicate that though pre-neoplastic lesions are potentially forming, detectable HR has not increased at 10 w.p.i.

H. trogontum Infection Does Not Lead to a Detectable Change in HR

Though inflammation increased and pathological changes were apparent in histological sections of *H. hepaticus* infected mice at 10 w.p.i., we recognize that chronic infections occur on a longer time scale. Therefore, we infected *RAG2*$^{-/-}$ *raDR-GFP*$^{R/+}$ mice with *H. trogontum*, an alternative, but potentially more virulent species of *Helicobacter* and harvested at approximately 20 w.p.i. or earlier at the onset of morbidity. Though the incubation time of the infection was nearly twice that of the *H. hepaticus* infected mice, we detected no change in HR locally in the colon (19 vs 24, p=0.36) or distally in the pancreas (224 vs 154, p=0.54), and liver (16 vs 19, p=0.20). These mice developed severe colitis resulting in bloody stools and dehydration, with some mice requiring euthanasia before 20 w.p.i. As with the *H. hepaticus* infected mice, there was again no detectable change in the level of HR locally or distally.

4.5 Discussion

Chronic infection has been causally linked with local tumorgenesis not only in mice, but also in humans (9, 12). Erdman and colleagues have shown that infection of C57BL/6 *Apc*$^{Min/+}$ with *H. hepaticus* also promotes mammary tumors (10). Though CDT clearly damages host genomic DNA *in vitro*, it is unclear if CDT causes cell-cycle arrest and subsequent death before or after DNA replication *in vivo*. Initial data showed pre-neoplastic lesion development in the pancreas in response to *H. hepaticus* infection in the colon, leading us to explore the impact of inflammation and infection on genomic integrity with our FYDR and raDR-GFP mice.

The significant increase in recombinant foci in pancreata of unchallenged raDR-GFP$^{R/+}$ vs. *IL10*$^{-/-}$ *Rag2*$^{-/-}$ *raDR-GFP*$^{R/+}$ mice indicate a significant increase in HR in an inflamed environment. IL10 primarily acts as an anti-inflammatory cytokine that inhibits the secretion of pro-inflammatory cytokines by monocytes or macrophages of the innate immune system (52, 53). Studies examining the role of IL10 show it reduces severity in chemically induce pancreatitis, and may reduce the expression of TNF-α (54, 55). Therefore, in the absence of IL10, it is likely that systemic inflammation is increased. Infection studies in *IL10*$^{-/-}$*Rag2*$^{-/-}$ mice show a rapid and extreme progression of infection pathology (56); therefore, further studies to examine the combined effect of RAG2 and IL10 deficiencies in response to infection offer an opportunity to better understand the importance of IL10 and inflammation on DNA damage and HR in local and distal tissues.

Examination of HR in the pancreas of wild-type FYDR mice after DSS-induced colitis indicated no increase in HR. While this study was small, there was no indication that chemically-induced inflammation causes DSB inducing DNA damage repaired via HR in a nearby tissue in wild-type FYDR mice. As the pre-neoplastic pancreatic lesions observed in preliminary data were the result of infection, these data suggested that inflammation might not bear sole responsibility for the damage, even though the findings of Erdman, *et al.*, indicate colitis and subsequent tissue remodeling in *Rag2*$^{-/-}$ mice infected with *H. hepaticus* is largely the result of NO produced by macrophages, and is greatly reduced with iNOS inhibitors (25). These data warranted further study of the effects of *H. hepaticus*-induced colitis on HR locally and distally.

While we examined the effects of DSS-induced inflammation in immune competent animals of a mixed background, we utilized RAG2 deficient animals in the 129 background to establish sustained *H. hepaticus* and *H. trogontum* infections (23). While *H. hepaticus* infection has been shown to induce DNA damage through the inflammatory cascade and CDT (23, 33), it does not appear to cause an increase in HR in the colon at 10 w.p.i. Since CDT induces cell cycle arrest and subsequent cell death, the lack of a response to infection may be the result of damaged cells undergoing apoptosis rather than repair in response to DNA damage. *H. trogontum*, on the other hand, does not produce CDT, thus DNA damage may be the result of ROS and RNS due to inflammation (57).

The absence of a consistent effect on HR in response to *H. hepaticus* and *H. trogontum* infection may be a result of the length of infection. Though Dedon and coworkers saw an increase in colitis and hepatitis at 10 w.p.i., with *H. hepaticus* infection, they discovered that εdA and εdC lesions had decreased with infection (23). At 20 w.p.i. with *H. hepaticus*, colitis and hepatitis were present, but the ε-adducts had returned to baseline levels while the incidence of 5-Cl-dC, dI, and Sp adducts increased (23). Furthermore, they discovered that genes related to DSB repair were down-regulated in the colon at both 10 and 20 w.p.i. (23). Even though we did not observe a change in HR in *H. trogontum* infected animals at 20 w.p.i., a longer infection course with *H. hepaticus* may cause the accumulation of more DSBs through CDT exposure and induction of more recombination events, thereby presenting a more damaging environment to the genome that necessitates HR repair.

On the other hand, though cells exposed to CDT incur DSBs, CDT also induces cell cycle arrest and subsequent cell death. It is possible that the majority of cells afflicted with CDT-induced recombinogenic DNA damage underwent apoptosis before analysis at 10 w.p.i. *In vitro* studies of CDT showed cells grew in size and died within five days (38). Though, if destined for apoptosis, these damaged cells would not contribute to later tumorgenesis. Knowing the extent of DSBs and HR in response to *H. hepaticus* infection may yield further understanding of the risks associated with chronic infection. Therefore, a shorter incubation time may prove the ideal time (1 w.p.i.) to visualize DNA damage repair in the raDR-GFP *H. hepaticus* infected mice.

Ongoing work in our laboratory has shown that temporally distinct bouts of DNA damage and proliferation does not induce a marked increase in HR in the pancreas of FYDR mice, but rather that simultaneous DNA damage coupled with proliferation is necessary to induce an increase in HR (Kiraly, manuscript in preparation). The inflamed environment of the *IL10*$^{-/-}$ *Rag2*$^{-/-}$ *raDR-GFP*$^{R/+}$ mice resulted in an increase in HR, which may be due to the presence of chronic inflammation during early development and growth when many cells are dividing, providing a scenario whereby inflammation is inducing DNA damage in a proliferative environment. This first result led us to expect an increase in HR in response to environmentally induced inflammation since infection with *Helicobacter* species has been linked with cancer. *H. hepaticus* is reported to initiate DSBs directly through CDT (33), which may act as the DNA damage initiating event which, when coupled with inflammation, leads to tumorgenesis. Alternatively, ROS and RNS resulting from *H. hepaticus* or *H. trogontum* infection-induced inflammation may provide the initiating damage. We had anticipated infection with either CDT producing *H. hepaticus* or non-producing *H. trogontum*, would induce DNA damage and proliferation in response to colitis. Histologically, there is evidence of hyperproliferation with infection (Figure 4-4B), but surprisingly, no increase in HR in response to either infection. This may indicate that the initiating DNA damage is being repaired by another pathway or that sufficient damage has not yet accrued at 10 w.p.i. in the *H. hepaticus* infection or at 20 w.p.i. in the *H. trogontum* infection to yield a detectable difference. In the case of the *H. hepaticus* infection, it is possible that cells are damaged shortly after infection, but quickly apoptose due to CDT damage. Alternatively, the production of

DNA damaging ROS and RNS may be temporally distinct from tissue remodeling and proliferation *in vivo*. As inflammation is a conserved response to many different stimuli *in vivo*, the separation of the production of DNA-damage inducing chemicals and proliferation to protect against unintentionally induced mutations may be ideal. Nonetheless, inflammation remains a potent risk for tumorgenesis. Further studies of various length infections with *H. hepaticus* and *H. trogontum* or other bacterium coupled with further work examining the role of DNA damage alongside chemically-induced inflammation may elucidate the mechanisms of the risk associated with environmentally-induced inflammation.

4.6 Acknowledgements

The work described in this chapter was performed in collaboration with Dr. Susan E. Erdman and several members of the Engelward laboratory and the Wogan Laboratory. Jennifer E. Kay, Elizabeth A. Rowland, and Danielle N. Chow and the author all contributed to collection of the harvest and analysis of these data. Dr. Dushan Nawoda Wadduwage, Dr. Vijay Ray Singh, and Dr. Peter So created the program to automatically count foci in the liver and pancreas. Jennifer Kay and Elizabeth Rowland were responsible for determining the recombinant foci per square centimeter in the colon of *H. hepaticus* and *H. trogontum* infected mice, respectively.

Thanks are due to Dr. Leona D. Samson and Dr. Amy Wu for assistance with initiating the DSS exposure experiment. The author extends special thanks to Erin Turowski and Dr. Orsola Kiraly for thoughtful discussion and to Dr. Susan E. Erdman and Dr. Thoefilos Poutahidis for interpretation and scoring of histological sections.

Dr. Susan E. Erdman and Dr. James G. Fox graciously provided founder mice deficient in Rag2 or IL10. Special thanks Tatiana Levkovitch and Jessica Lakritz of the Erdman Laboratory for technical expertise in infection of experimental animals and Christian Kaufman and Lenzie Cheaney of the Fox Laboratory for assistance in inoculating and harvesting the *H. trogontum* infected mice. The author is also grateful to Dr. Susan E. Erdman, Dr. Gerald N. Wogan, Dr. Leona D. Samson, Dr. John M. Essigmann, and Dr. James G. Fox for helpful suggestions in planning experiments and preparing this text.

4.7 References

1. Shacter E, Weitzman SA (2002) Chronic inflammation and cancer. *Oncology (Williston Park, NY)* 16:217–26– 229– discussion 230–2.

2. O'Byrne KJ, Dalgleish AG (2001) Chronic immune activation and inflammation as the cause of malignancy. *Br J Cancer* 85:473–483.

3. O'Byrne KJ, Dalgleish AG (2001) Infection and cancer. *Lancet* 358:156.

4. Group UCSW (2013) United States Cancer Statistics: 1999–2009 Incidence and Mortality Web-based Report. ... *Prevention*.

5. Harpaz N, Polydorides AD (2010) Colorectal Dysplasia in Chronic Inflammatory Bowel Disease: Pathology, Clinical Implications, and Pathogenesis.

6. Gillen CD, Walmsley RS, Prior P, Andrews HA, Allan RN (1994) Ulcerative colitis and Crohn's disease: a comparison of the colorectal cancer risk in extensive colitis. *Gut* 35:1590–1592.

7. Badawi AF, Mostafa MH, Probert A, O'Connor PJ (1995) Role of schistosomiasis in human bladder cancer: evidence of association, aetiological factors, and basic mechanisms of carcinogenesis. *Eur J Cancer Prev* 4:45–59.

8. Imperial JC (1999) Natural history of chronic hepatitis B and C. *J Gastroenterol Hepatol* 14 Suppl:S1–5.

9. Blaser MJ (2000) Linking Helicobacter pylori to gastric cancer. *Nat Med* 6:376–377.

10. Rao VP et al. (2006) Innate immune inflammatory response against enteric bacteria Helicobacter hepaticus induces mammary adenocarcinoma in mice. *Cancer Res* 66:7395–7400.

11. Hanahan D, Weinberg RA (2011) Hallmarks of cancer: the next generation. *Cell* 144:646–674.

12. Fox JG, Ge Z, Whary MT, Erdman SE, Horwitz BH (2011) Helicobacter hepaticus infection in mice: models for understanding lower bowel inflammation and cancer. *Mucosal Immunol* 4:22–30.

13. Ohshima H, Tatemichi M, Sawa T (2003) Chemical basis of inflammation-induced carcinogenesis. *Arch Biochem Biophys* 417:3–11.

14. Balkwill F, Mantovani A (2001) Inflammation and cancer: back to Virchow? *Lancet* 357:539–545.

15. Farrell RJ, Peppercorn MA (2002) Ulcerative colitis. *Lancet* 359:331–340.

16. Asaka M, Takeda H, Sugiyama T, Kato M (1997) What role does Helicobacter pylori play in gastric cancer? *Gastroenterology* 113:S56–60.

17. Ebert MP, Yu J, Sung JJ, Malfertheiner P (2000) Molecular alterations in gastric cancer: the role of Helicobacter pylori. *Eur J Gastroenterol Hepatol* 12:795–798.

18. Roy S, Bagchi D, Raychaudhuri SP (2012) *Chronic Inflammation* (CRC Pressl Llc).

19. Wingo PA et al. (1999) Annual report to the nation on the status of cancer, 1973-1996, with a special section on lung cancer and tobacco smoking. *J Natl Cancer Inst* 91:675–690.

20. Itzkowitz SH, Yio X (2004) Inflammation and cancer IV. Colorectal cancer in inflammatory bowel disease: the role of inflammation. *Am J Physiol Gastrointest Liver Physiol* 287:G7–17.

21. Lisiane B Meira JMBSLGC-WLBPDBBHRABRCAM-EJLMDBSPCDJGFLDS (2008) DNA damage induced by chronic inflammation contributes to colon carcinogenesis in mice. *J Clin Invest* 118:2516.

22. Lonkar P, Dedon PC (2011) Reactive species and DNA damage in chronic inflammation: reconciling chemical mechanisms and biological fates. *Int J Cancer* 128:1999–2009.

23. Mangerich A et al. (2012) Infection-induced colitis in mice causes dynamic and tissue-specific changes in stress response and DNA damage leading to colon cancer. *Proc Natl Acad Sci USA* 109:E1820–9.

24. Wiseman H, Halliwell B (1996) Damage to DNA by reactive oxygen and nitrogen species: role in inflammatory disease and progression to cancer. *Biochem J* 313 (Pt 1):17–29.

25. Erdman SE et al. (2009) Nitric oxide and TNF-alpha trigger colonic inflammation and carcinogenesis in Helicobacter hepaticus-infected, Rag2-deficient mice. *Proc Natl Acad Sci USA* 106:1027–1032.

26. Baik SC et al. (1996) Increased oxidative DNA damage in Helicobacter pylori-infected human gastric mucosa. *Cancer Res* 56:1279–1282.

27. Tardieu D et al. (2000) The COX-2 inhibitor nimesulide suppresses superoxide and 8-hydroxy-deoxyguanosine formation, and stimulates apoptosis in mucosa

during early colonic inflammation in rats. *Carcinogenesis* 21:973–976.

28. Erdman SE et al. (2003) CD4(+)CD25(+) regulatory lymphocytes require interleukin 10 to interrupt colon carcinogenesis in mice. *Cancer Res* 63:6042–6050.

29. Erdman SE et al. (2003) CD4+ CD25+ regulatory T lymphocytes inhibit microbially induced colon cancer in Rag2-deficient mice. *Am J Pathol* 162:691–702.

30. Engle SJ et al. (2002) Elimination of colon cancer in germ-free transforming growth factor beta 1-deficient mice. *Cancer Res* 62:6362–6366.

31. Smith JL, Bayles DO (2006) The contribution of cytolethal distending toxin to bacterial pathogenesis. *Crit Rev Microbiol* 32:227–248.

32. Pratt JS, Sachen KL, Wood HD, Eaton KA, Young VB (2006) Modulation of host immune responses by the cytolethal distending toxin of Helicobacter hepaticus. *Infect Immun* 74:4496–4504.

33. Lara-Tejero M, Galán JE (2002) Cytolethal distending toxin: limited damage as a strategy to modulate cellular functions. *Trends Microbiol* 10:147–152.

34. Johnson WM, Lior H (1988) A new heat-labile cytolethal distending toxin (CLDT) produced by Campylobacter spp. *Microb Pathog* 4:115–126.

35. Johnson WM, Lior H (1988) A new heat-labile cytolethal distending toxin (CLDT) produced by Escherichia coli isolates from clinical material. *Microb Pathog* 4:103–113.

36. Cortes-Bratti X, Karlsson C, Lagergård T, Thelestam M, Frisan T (2001) The Haemophilus ducreyi cytolethal distending toxin induces cell cycle arrest and apoptosis via the DNA damage checkpoint pathways. *J Biol Chem* 276:5296–5302.

37. Ward JD, Barber LJ, Petalcorin MI, Yanowitz J, Boulton SJ (2007) Replication blocking lesions present a unique substrate for homologous recombination. *EMBO J* 26:3384–3396.

38. Liyanage NPM et al. (2010) Helicobacter hepaticus cytolethal distending toxin causes cell death in intestinal epithelial cells via mitochondrial apoptotic pathway. *Helicobacter* 15:98–107.

39. Young VB et al. (2004) In vitro and in vivo characterization of Helicobacter hepaticus cytolethal distending toxin mutants. *Infect Immun* 72:2521–2527.

40. Powell SM et al. (1992) APC mutations occur early during colorectal

tumorigenesis. *Nature* 359:235–237.

41. Shaw CJ, Lupski JR (2004) Implications of human genome architecture for rearrangement-based disorders: the genomic basis of disease. *Hum Mol Genet* 13 Spec No 1:R57–64.

42. Agmon N, Pur S, Liefshitz B, Kupiec M (2009) Analysis of repair mechanism choice during homologous recombination. *Nucleic Acids Res* 37:5081–5092.

43. Voet D, Pratt CW, Voet JG (2012) *Principles of Biochemistry* (John Wiley & Sons).

44. Shinkai Y et al. (1992) RAG-2-deficient mice lack mature lymphocytes owing to inability to initiate V(D)J rearrangement. *Cell* 68:855–867.

45. Erdman SE, Poutahidis T (2010) Roles for inflammation and regulatory T cells in colon cancer. *Toxicol Pathol* 38:76–87.

46. Badoual C et al. (2009) Revisiting the prognostic value of regulatory T cells in patients with cancer. *J Clin Oncol* 27:e5–6– author reply e7.

47. Erdman SE et al. (2010) Unifying roles for regulatory T cells and inflammation in cancer. *Int J Cancer* 126:1651–1665.

48. Fox JG et al. (1994) Helicobacter hepaticus sp. nov., a microaerophilic bacterium isolated from livers and intestinal mucosal scrapings from mice. *J Clin Microbiol* 32:1238–1245.

49. Ge Z et al. (2005) Cytolethal distending toxin is essential for Helicobacter hepaticus colonization in outbred Swiss Webster mice. *Infect Immun* 73:3559–3567.

50. Wiktor-Brown DM, Hendricks CA, Olipitz W, Engelward BP (2006) Age-dependent accumulation of recombinant cells in the mouse pancreas revealed by in situ fluorescence imaging. *Proc Natl Acad Sci USA* 103:11862–11867.

51. Wiktor-Brown DM, Hendricks CA, Olipitz W, Rogers AB, Engelward BP (2006) Applications of fluorescence for detecting rare sequence rearrangements in vivo. *Cell Cycle* 5:2715–2719.

52. Bain CC et al. (2013) Resident and pro-inflammatory macrophages in the colon represent alternative context-dependent fates of the same Ly6C(hi) monocyte precursors. *Mucosal Immunol* 6:498–510.

53. Harden LM et al. (2013) Interleukin-10 modulates the synthesis of inflammatory mediators in the sensory circumventricular organs: implications for the regulation of fever and sickness behaviors. *J Neuroinflammation* 10:22.

54. Kusske AM, Rongione AJ, Ashley SW, McFadden DW, Reber HA (1996) Interleukin-10 prevents death in lethal necrotizing pancreatitis in mice. *Surgery* 120:284–8– discussion 289.

55. Van Laethem JL et al. (1995) Interleukin 10 prevents necrosis in murine experimental acute pancreatitis. *Gastroenterology* 108:1917–1922.

56. Lee C-W et al. (2007) Wild-type and interleukin-10-deficient regulatory T cells reduce effector T-cell-mediated gastroduodenitis in Rag2-/- mice, but only wild-type regulatory T cells suppress Helicobacter pylori gastritis. *Infect Immun* 75:2699–2707.

57. Whary MT et al. (2006) Rapid onset of ulcerative typhlocolitis in B6.129P2-IL10tm1Cgn (IL-10-/-) mice infected with Helicobacter trogontum is associated with decreased colonization by altered Schaedler's flora. *Infect Immun* 74:6615–6623.

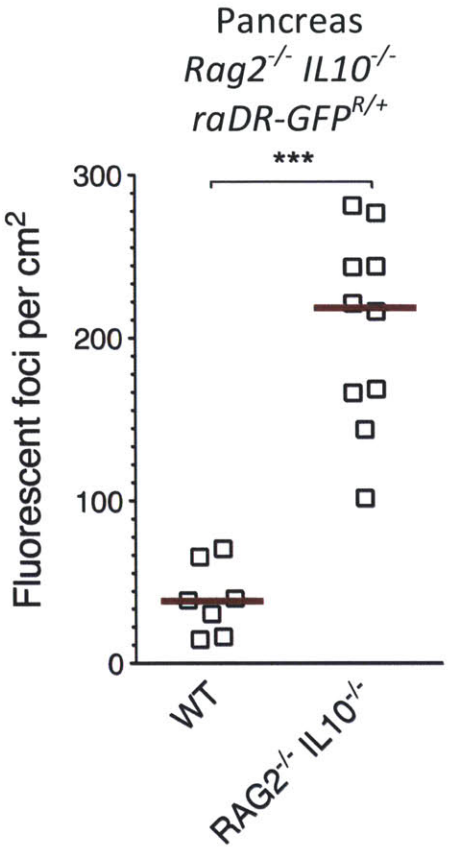

Figure 4-1. Spontaneous HR Increases in Pancreata of *RAG2$^{-/-}$IL10$^{-/-}$raDR-GFP$^{R/+}$* Mice. The absence of anti-inflammatory cytokine IL-10 and mature T- and B-lymphocytes leads to increased HR.

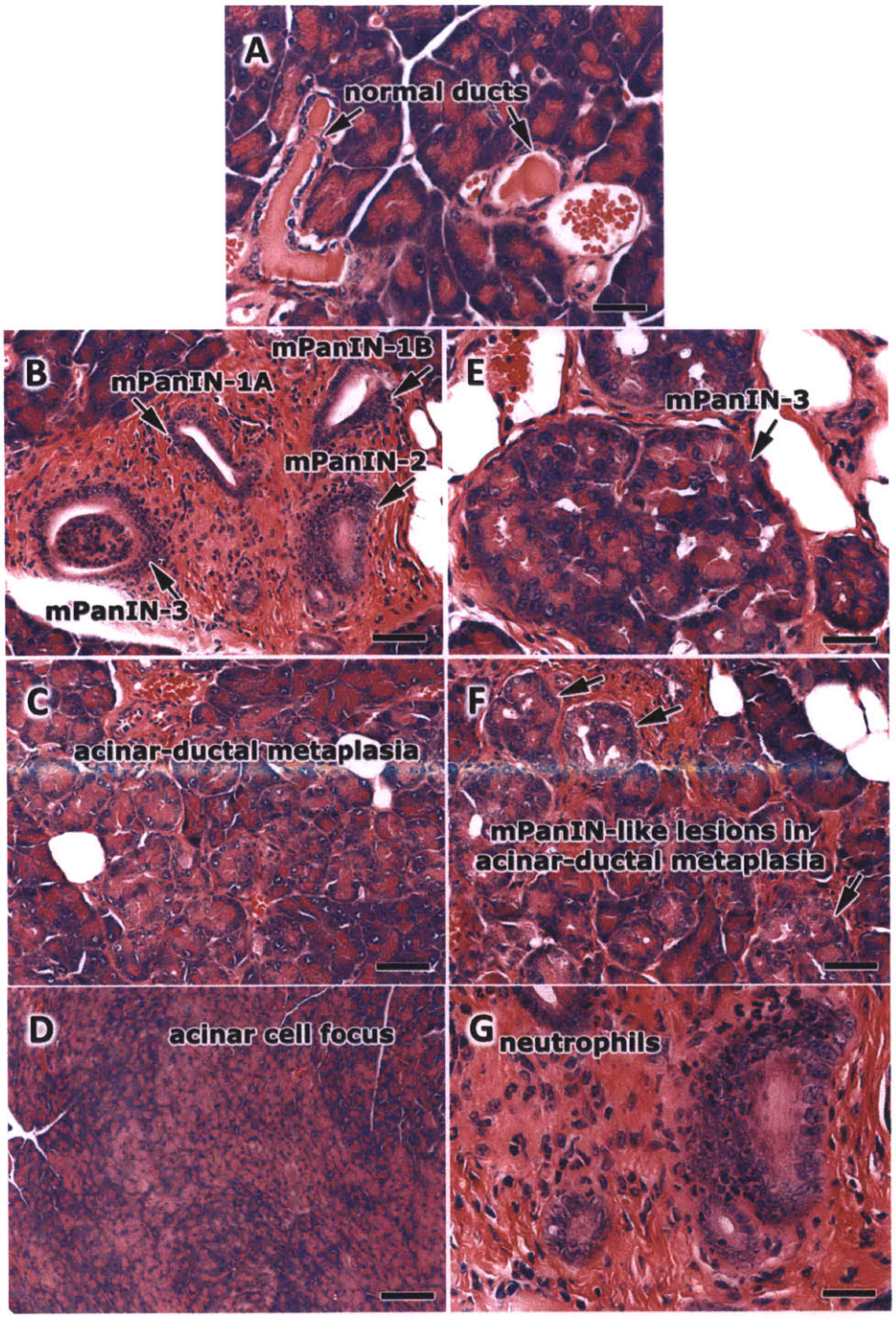

Figure 4-2. Histology of the Pancreas of *H. hepaticus* Infected Mice. (A) Normal pancreatic ducts are compared with (B) pre-neoplastic lesions (mPanINs), (C) acinar to ductal metaplasia, and (D) an acinar cell focus. (E) Increased magnification of a PanIN, (F) mPanIN-like lesions present in acinar-ductal metaplasia, and (G) higher magnification of mPanIN-2 in (B) showing neutrophil infiltrations. Tissues from mice were harvested 20 w.p.i., fixed, and stained with H&E.

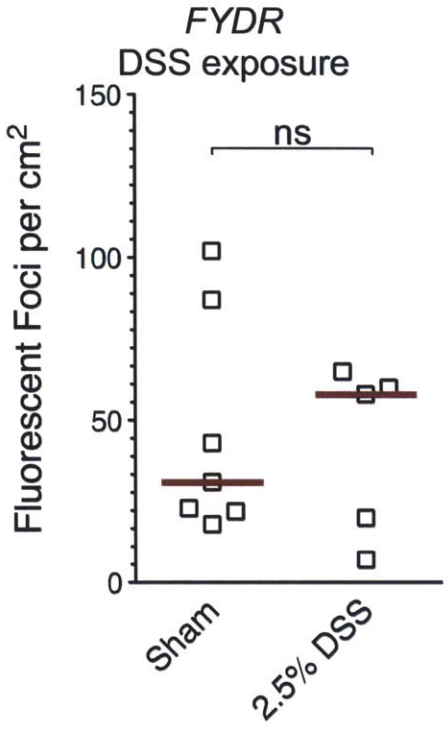

Figure 4-3. DSS-induced Colitis Has No Apparent Impact on Distal HR. Mice received 8 cycles of 2.5% DSS water and showed no significant change in the frequency of HR in the pancreas.

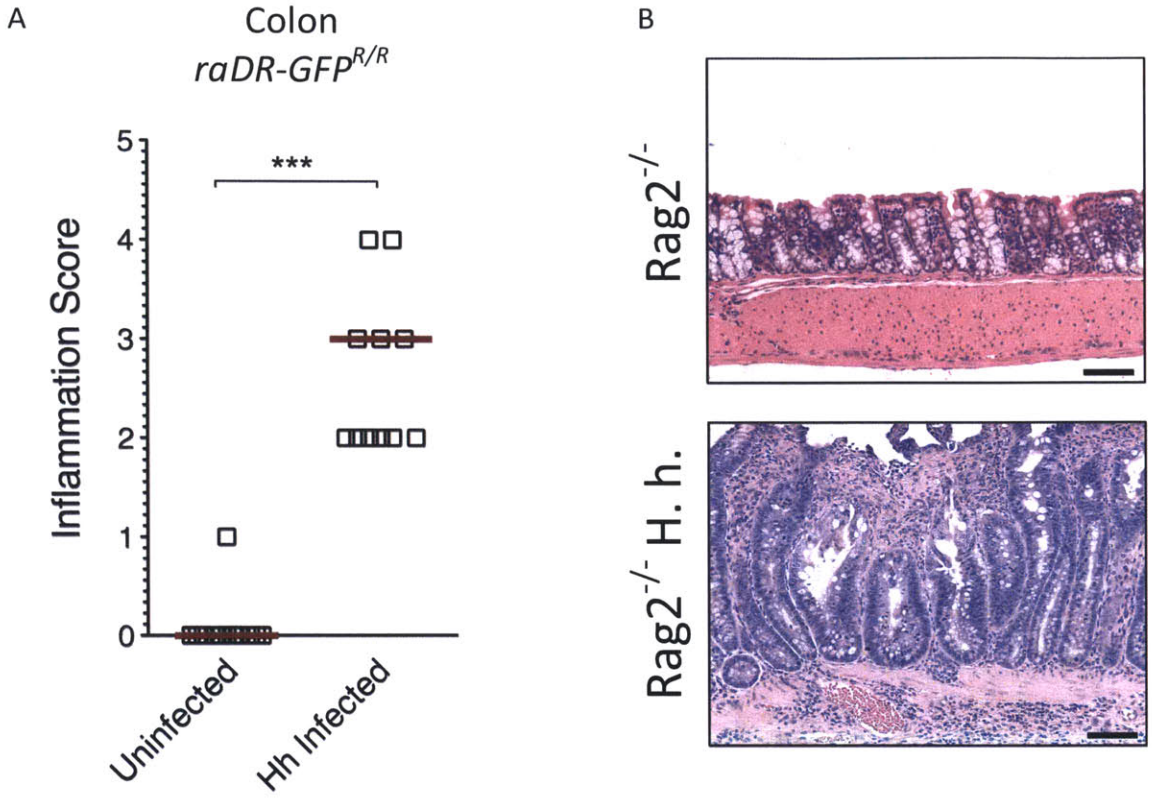

Figure 4-4. Inflammation Increased in the Colon Following *H. hepaticus* Infection. raDR-GFP mice were infected with *H. hepaticus* and harvested 10 w.p.i. (A) Inflammation score increased with infection, with (B) aberrant crypt morphology.

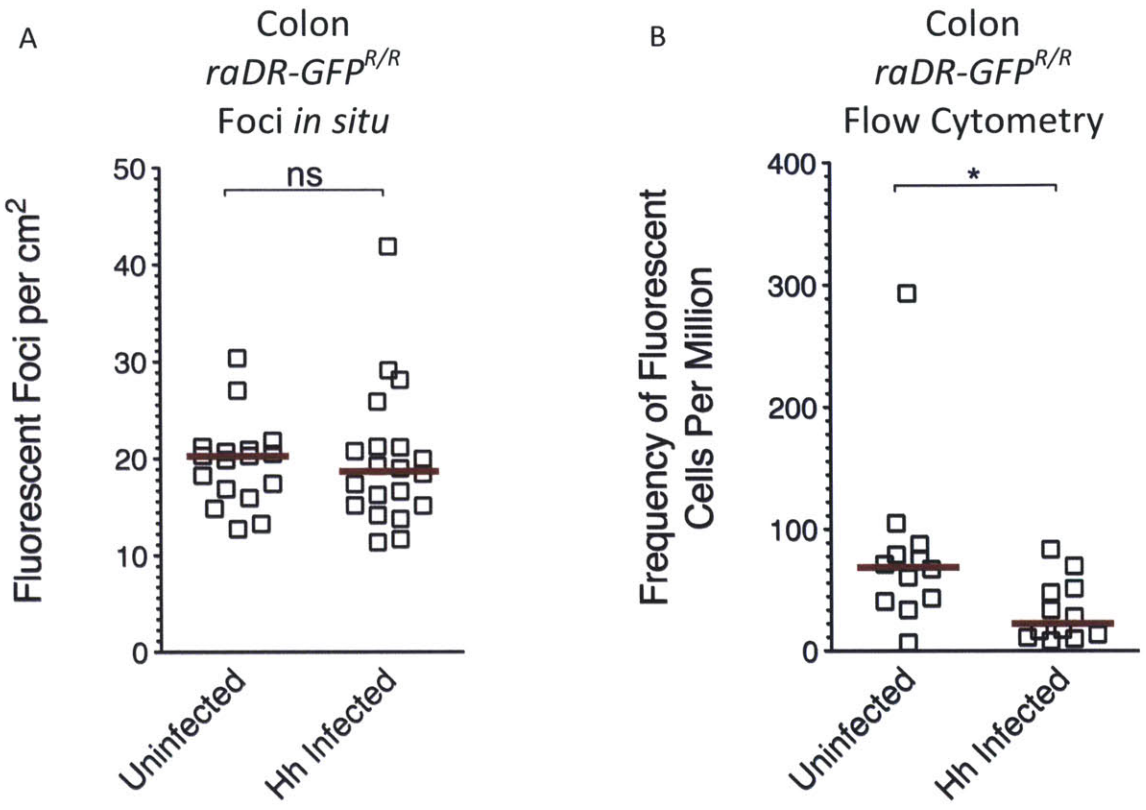

Figure 4-5. HR in the Colon Following *H. hepaticus* Infection. raDR-GFP mice were infected with *H. hepaticus* and harvested 10 w.p.i. No significant change in (A) the number of fluorescent foci per square centimeter in the colon, but (B) the frequency of fluorescent cells per million showed a statistically significant decrease.

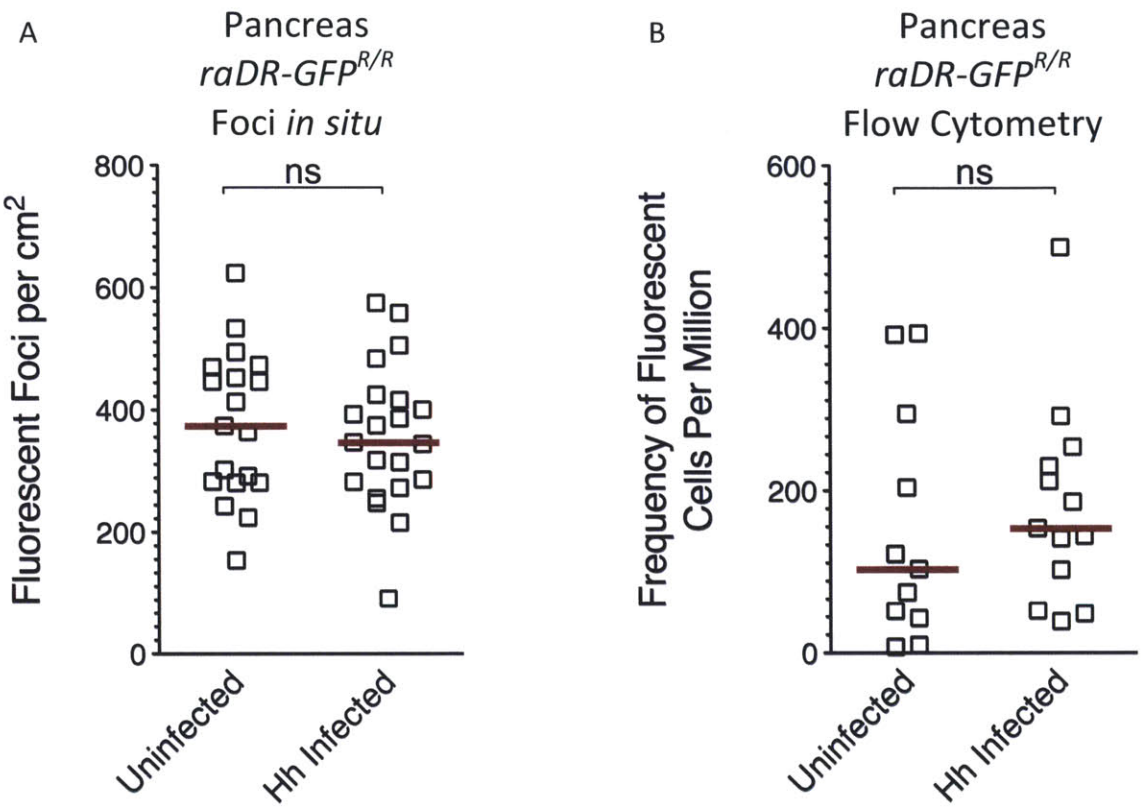

Figure 4-6. HR in the Pancreas Following *H. hepaticus* Infection. raDR-GFP mice were infected with *H. hepaticus* and harvested 10 w.p.i. No significant change in (A) the number of fluorescent foci per square centimeter or (B) the frequency of fluorescent cells per million was seen in the pancreas.

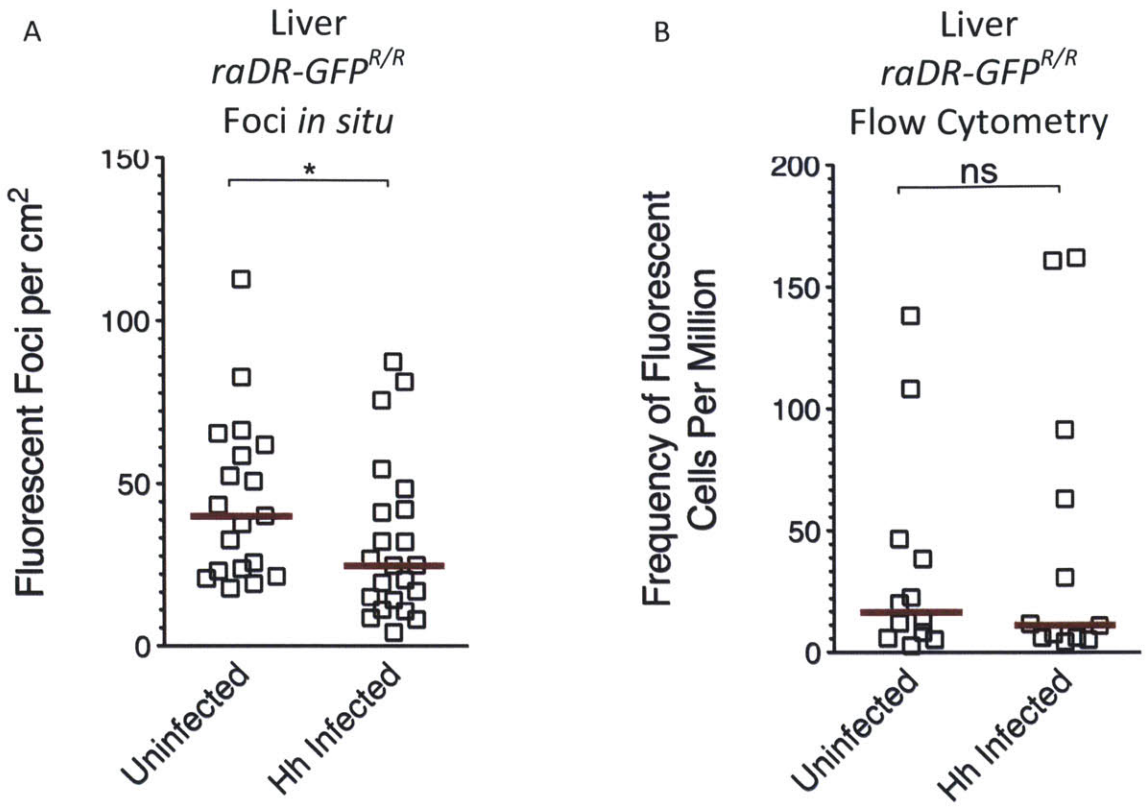

Figure 4-7. HR in the Liver Following *H. hepaticus* Infection. raDR-GFP mice were infected with *H. hepaticus* and harvested 10 w.p.i. (A) A statistically significant decrease in the number of fluorescent foci per square centimeter was observed in the liver, though there was no change in (B) the frequency of fluorescent cells per million.

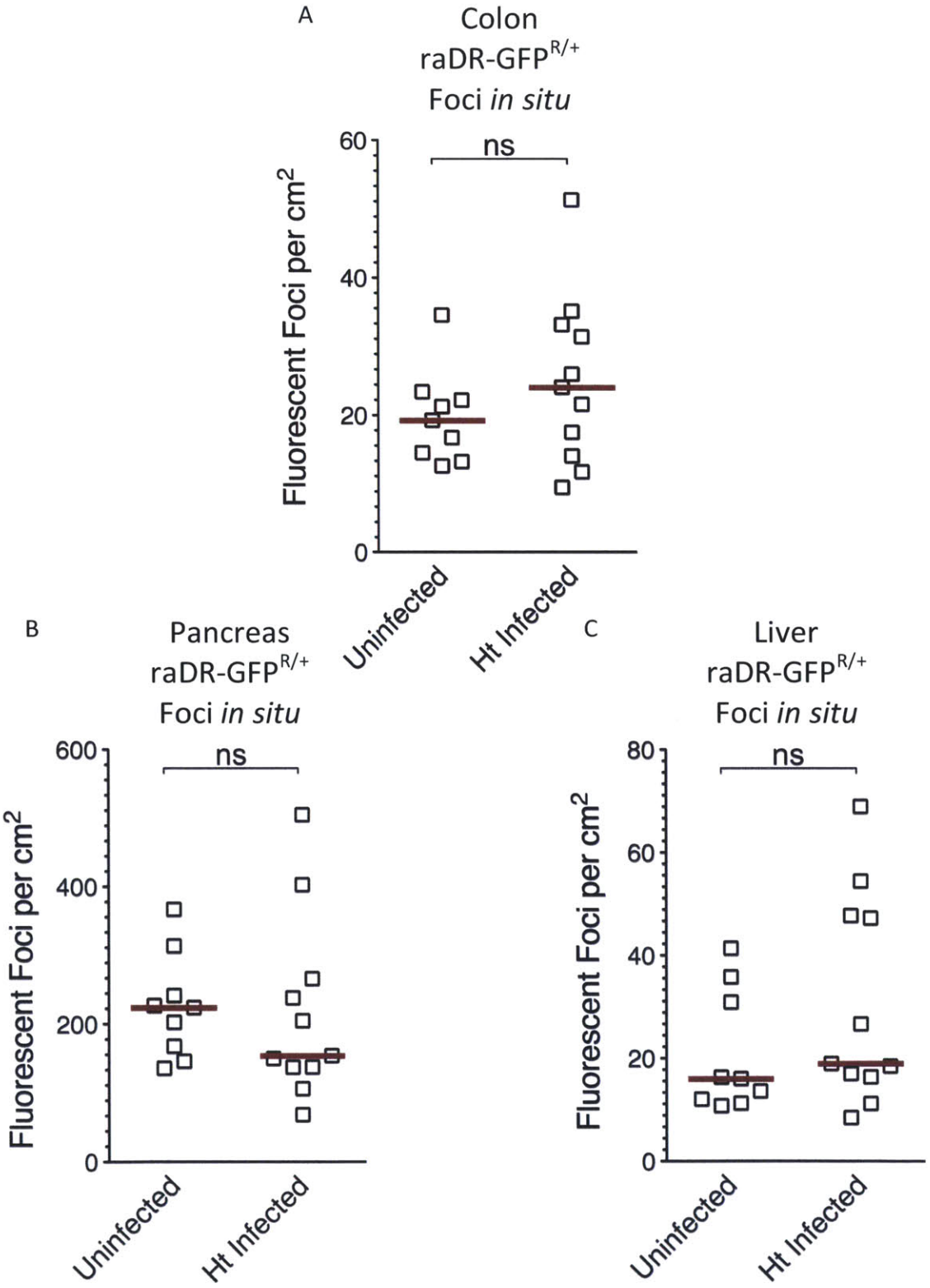

Figure 4-7. HR in the Colon, Pancreas, and Liver Following *H. trogontum* Infection. raDR-GFP mice were infected with *H. trogontum* and harvested 20 w.p.i. No significant change in the number of fluorescent foci per square centimeter was observed in the (A) colon, (B) pancreas, or (C) liver.

Chapter V

Conclusions and Future Work

Chapter V

5.1 Conclusions and Future Work

Homologous recombination plays a vital role in the repair of spontaneous and exposure-induced DSBs and replication fork breakdown events, but over- or under-utilization of HR can lead to genomic instability. Many genetic, tissue-specific, and environmental factors that either suppress or induce HR are known to contribute to cancer risk. For this thesis, we have exploited the FYDR mice for studies of exposure-induced HR, as well as created a new mouse model, the raDR-GFP mice, and used this new model to learn about HR *in vivo*.

One of the most important advantages of a mouse model is that it can be crossed with other mice that harbor deficiencies in genes of interest, enabling the study of the impact of those genes on HR in multiple tissues *in vivo* for the first time. To better understand the interplay among DSB repair pathways, we crossed the FYDR mice with mice that carry defects in HR-independent DSB processing. Specifically, we investigated impact of a deficiency in NHEJ by crossing the $Ku^{-/-}$ mice with FYDR mice. Our findings showing increased homology directed repair is consistent with previous *in vitro* studies showing that loss of one DSB repair pathway (NHEJ) can put pressure on another (HR). We also showed that a deficiency in MMEJ protein ERCC1 also results in an increase in HR in the pancreata of FYDR mice, suggesting the possibility that this little-studied, alternative double-strand break repair pathway may modulate the frequency of HR.

These data illustrate the importance of NHEJ and MMEJ in spontaneous DNA damage repair, and show that HR can compensate for the absence of these pathways *in vivo*.

Studies of genetic and environmental factors that modulate susceptibility to HR in mammals have historically been hampered by an inability to study multiple cell types and tissues. In this work, we have described the development of the transgenic raDR-GFP mice that are engineered for the detection of HR events in primary somatic cells in a wide variety of tissues *in vivo* and *in vitro*. This mouse builds on the foundation of previous mouse models that detect genetic mutations, but offers significant improvements in usability, time, and extent of tissues available. Most other mouse models for detecting sequence changes, such as the *gpt-Δ* mouse, requires that DNA harvested from tissues be packaged and delivered to bacteria for colony counting assays. These assays are costly, require significant technical expertise, and can take weeks to complete. The raDR-GFP mouse, on the other hand, effectively overcomes these technical and economical challenges as recombinant cells in raDR-GFP mice can be visualized with standard fluorescence microscopy or other readily available fluorescence detecting techniques such as flow cytometry. In addition, while other models, such as the $Aprt^{+/-}$ and $Tk^{+/-}$ mice, require somatic cells to be cultured *in vitro* before analysis, the raDR-GFP mouse allows for direct analysis of recombinant cells, including cell types that do no grow *in vitro*, such as hepatocytes. Moreover, although the FYDR and p^{un} mice enable *in vivo* analysis of HR, they are limited by incomplete expression of their respective reporters. In contrast, all raDR-GFP tissues examined exhibit high expression

of the positive control transgene, without the sex-linked expression difference seen in the pancreata of FYDR mice.

In addition to detecting HR in the pancreas, we have also developed techniques to visualize individual homologous recombination events *in situ* in the liver and colon. While we examined the total number of spontaneously recombinant cells in other tissues by flow cytometry, we are confident that additional imaging techniques can be developed to visualize homologous recombination *in situ* in other tissues. Ongoing work in our laboratory in collaboration with Dr. Tim Ragan of TissueVision is focused on visualizing recombinant cells *in situ* in 3D utilizing the TissueCyte 1000.

The development of methods to visualize recombinant cells *in situ* in the liver and colon has enabled us to study the effects of endogenous and exogenous cancer risks in these tissues. Since age is an important risk factor for a number of different cancers, particularly for pancreatic, liver, and colorectal cancer, we examined the change in the number of recombination events in these tissues with age. We saw a significant increase in the number of recombinant cells in each of these tissues, suggesting that HR is active throughout adulthood in each of these tissues. Each of these tissues shows similar levels of raDR-GFP transgene expression, but a higher frequency of recombinant pancreatic foci compared to hepatic and colonic foci implies a difference in the frequency of HR among these tissues, which may be linked to the longevity of recombinant cells and their progeny.

In addition to spontaneous HR, we also investigated the potential for the raDR-GFP mice to detect exposure-induced HR. By repeating the treatment regime of mitogenic thyroid hormone and alkylating agent MNU optimized for study of HR in the pancreas of FYDR mice on raDR-GFP mice, we showed that the colon and liver are also susceptible to and can be used to study alkylation damage-induced HR. Drug development is often halted by liver toxicity. Thus, detection of HR in the liver with the raDR-GFP mouse enables relatively rapid detection of long-lasting genotoxic effects that may take significantly longer to manifest into physiologically relevant changes.

Previous studies have shown that inflammation in the colon can lead to increased risk of cancer in distal tissues (1, 2). We therefore asked whether or not inflammation in the colon can impact genomic stability at distal sites. We did not observe distal changes in recombination in the pancreas after long-term DSS-induced colitis in FYDR mice. Since the raDR-GFP mice make it possible to study HR in the colon, we are currently collaborating with the Samson Laboratory to determine if acute DSS-induced colitis coupled with AOM-initiated DNA damage affects recombination in the colon. Furthermore, our preliminary studies of bacterially-induced inflammation does not appear to increase HR locally in the colon or distally in the liver or pancreas. On the other hand, chronic inflammation due to RAG2 and IL10 deficiencies result in a higher rate of HR in raDR-GFP animals. The increased level of systemic inflammation due to the loss of anti-inflammatory cytokine IL10 may lead to more spontaneous recombinogenic DNA damage. Therefore, it is likely that the raDR-GFP reporter is capable of identifying inflammation-induced damage, even though we did not see local

or distal increases in inflammation-induced damage with *H. hepaticus* infection at 10 w.p.i. or *H. trogontum* infection at 20 w.p.i. Further studies in our laboratory are planned to examine the potential recombinogenic effects of *H. hepaticus* infection after a dramatically shorter (1 week) or longer (20 weeks) incubation and may yield a better understanding of the initiation and progression of DNA damage in response to bacterially induced inflammation.

We recognize the balance of the gut microbiome may be affected by a variety of external pathogens, thus we are in the process of experiments to examine the effect of *H. trogontum* on HR in *Rag2*$^{-/-}$*gpt-Δ* and *Rag2*$^{-/-}$*IL10*$^{-/-}$*gpt-Δ* mice in collaboration with the laboratories of Dr. Susan Erdman, Dr. Gerald Wogan, Dr. James Fox, and Dr. John Essigmann (MIT). *H. trogontum* does not produce CDT, and offers an alternative model of infection progression to examine infection-induced DNA damage. Further work in collaboration with Dr. Susan Erdman exploring the use of probiotics to mitigate pathogenic infection and associated DNA damage has the potential to lead to the use of probiotics in diet to prevent DNA damage and related diseases in humans.

The ability to detect DNA damage-induced recombination in multiple tissues enables exploration into the underlying mechanisms by which genes and environment modulate the risk of cancer. Furthermore, many chemotherapeutics damage the DNA of rapidly dividing cancer cells, making the raDR-GFP model potentially valuable for studies of chemotherapy induced HR both in target cells and in normal tissues that are at risk for secondary cancers. Taken together, the raDR-GFP mice open doors to a wide array of

studies that are hoped to both enhance our fundamental understanding of HR as well as provide new insights into factors that modulate genomic stability.

5.2 References

1. Rao VP et al. (2006) Innate immune inflammatory response against enteric bacteria Helicobacter hepaticus induces mammary adenocarcinoma in mice. *Cancer Res* 66:7395–7400.

2. Rao VP, Poutahidis T, Fox JG, Erdman SE (2007) Breast cancer: should gastrointestinal bacteria be on our radar screen? *Cancer Res* 67:847–850.